KLOE memo # 256
October 2001

# Measurement of $BR(K_S \to \pi e \nu)$

T.Spadaro,
Università di Roma "La Sapienza"

C.Gatti
Università di Pisa e sez. I.N.F.N.

**Abstract**

This memo is devoted to a detailed description of the method used to measure the $BR(K_S \to \pi e \nu)$ using a sample of 17 pb$^-$1 collected in the year 2000. The selection algorithm as well as the methods applied to estimate the involved efficiencies are discussed.

# Contents

# 1 Introduction

The physical interest of the decay $K_S \to \pi e \nu$ is related to the test of the CPT (and indirect CP) symmetry [1], through charge asymmetry measurements. Besides, the $\Delta S = \Delta Q$ rule can be tested measuring the branching ratio. Assuming

$$\Gamma\left(K_S \to \pi e \nu\right) = \Gamma\left(K_L \to \pi e \nu\right),$$

a condition implied by the $\Delta S = \Delta Q$ rule and the CPT symmetry, and using the values of $BR\left(K_L \to \pi e \nu\right)$ and $\tau_S/\tau_L$ from ref [2], the expected value of the branching ratio is obtained:

$$BR\left(K_S \to \pi e \nu\right) = (6.70 \pm 0.07) \times 10^{-4} \tag{1}$$

The violation of the rule is parametrized in terms of the ratio of amplitudes:

$$x = \frac{A\left(\overline{K}^0 \to \pi^- e^+ \nu_e\right)}{A\left(K^0 \to \pi^- e^+ \nu_e\right)} \tag{2}$$

A measurement of the absolute branching ratio inclusive of both lepton charges with a precision better than $\sim 2\%$ could put an error on Re$x$ at a competitive level with respect to the present knowledge ($\delta\mathrm{Re}x = 6 \times 10^{-3}$ [3]). This last statement is clarified in detail in appendix A. The statistical accuracy needed corresponds to $\sim 2000$ observed events, *i.e.,* $\sim 70$ pb$^{-1}$ of acquired data with the present selection algorithm, as can be seen in figure 1.

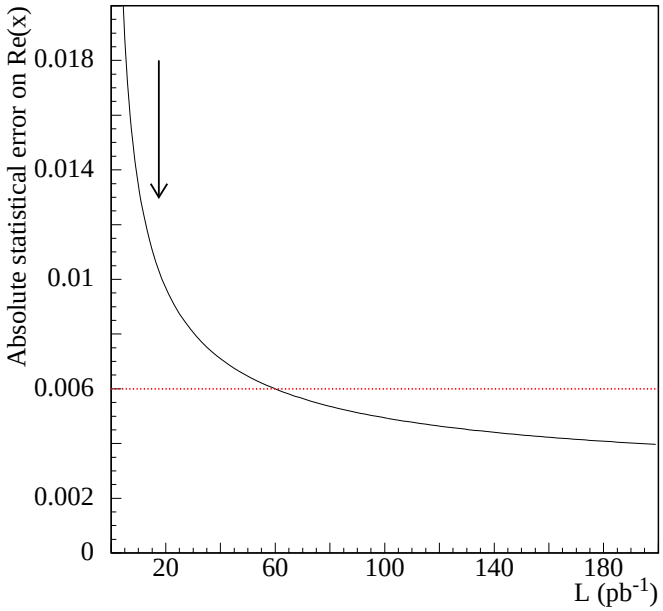


Figure 1: Statistical error on Re$x$, as a function of the integrated luminosity $L$. The arrow indicates the statistics used in the present analysis. The horizontal line represents the present experimental error, dominated by a measurement of the CPLEAR collaboration [3].

At present (March 2002) only one measurement of the branching ratio has been performed, by the CMD-2 Collaboration at VEPP-2M [4]:

$$BR\left(K_S \to \pi e \nu\right) = (7.2 \pm 1.4) \times 10^{-4}, \tag{3}$$

obtained with 75$\pm$13 observed events counted after the subtraction of 8.6$\pm$2.2 background events.

### 1.1 Method of the measurement

In KLOE $K_S$ decays are tagged efficiently by the identification of a $K_L$ interaction in the calorimeter, the so called "$K_L$ crash"; this idea can be actually be exploited thanks to the exceptional timing performance of the calorimeter and to the fact that the $K_L$ beam is almost monochromatic, with a velocity as low as $0.2c$. The typical $K_{\rm crash}$ event is shown in Fig. 2.

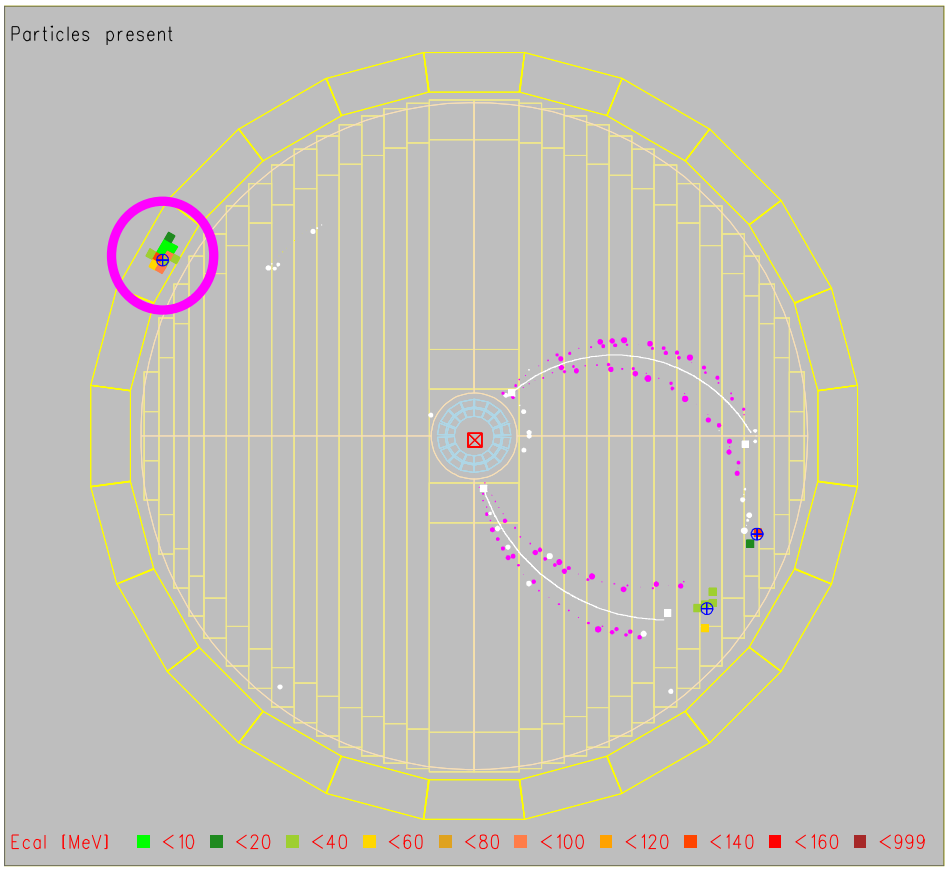


Figure 2: A typical $K_S$ selected event: the $K_S$ is tagged identifying a $K_{\rm crash}$ cluster in the calorimeter.

Even if this tag maximizes the spatial separation of the kaons, this condition does not necessarily imply that the $K_S$ tagging efficiency is independent of the $K_S$ decay mode. The tag bias, which depends ultimately on the method used to fix the "time zero" of the event (Sec. 2), has been therefore carefully considered (Sec. 6.4).

The basic scheme of the measurement is to select the "signal" ($K_S \to \pi e \nu$) and "normalization" ($K_S \to \pi^+\pi^-$) events starting from a selected sample of $K_S$-tagged events, output of the $K_{\rm crash}$ algorithm [5, 6] (briefly described in Sec. 2).

Let $N^{\pi e\nu}$ ($N^{\pi\pi}$) be the number of events identified as $K_S \to \pi e \nu$ ($K_S \to \pi^+\pi^-$) in a given sample of $K_{\rm crash}$-tagged events. In order to be identified, a $K_S \to \pi e \nu$ ($K_S \to \pi^+\pi^-$) event has to be triggered, has to satisfy the cuts of the $K_{\rm crash}$-tagging (a golden-$t_0$ cluster and a $K_{\rm crash}$-cluster have to be found), and those of a selection algorithm. Hence, the global efficiency $\varepsilon_{\rm tot}^{\pi e\nu(\pi\pi)}$ of these requirements has to be estimated, in order to obtain

from the number of observed events $N^{\pi e\nu}$ ($N^{\pi\pi}$) the $T^{\pi e\nu}$ ($T^{\pi\pi}$) truly produced events:

$$N^{\pi e\nu(\pi\pi)} = \underbrace{\mathcal{L}\sigma_\phi \mathrm{BR}(\phi \to \mathrm{K_S K_L}) \times \mathrm{BR}[\mathrm{K_S} \to \pi e\nu(\pi^+\pi^-)]}_{T^{\pi e\nu(\pi\pi)}} \times \varepsilon_{\mathrm{tot}}^{\pi e\nu(\pi\pi)} \tag{4}$$

The integrated luminosity $\mathcal{L}$ and the cross section of production $\sigma_\phi \mathrm{BR}(\phi \to \mathrm{K_S K_L})$ exactly cancel out in the calculation of the ratio of the number of events observed in the two $K_S$ channels, allowing the measurement of the ratio of branching fractions:

$$\frac{N^{\pi e\nu}}{N^{\pi\pi}} = \frac{\mathrm{BR}(\mathrm{K_S} \to \pi e\nu)}{\mathrm{BR}(\mathrm{K_S} \to \pi^+\pi^-)} \times \frac{\varepsilon_{\mathrm{tot}}^{\pi e\nu}}{\varepsilon_{\mathrm{tot}}^{\pi\pi}} \tag{5}$$

Since the branching ratio for $K_S \to \pi^+\pi^-$ is known with a relative accuracy of $4 \times 10^{-3}$, while the statistical error in the number of observed semileptonic decays is at the level of $5 \times 10^{-2}$, this is practically a measurement of the branching ratio for $K_S \to \pi e\nu$.

The total efficiencies $\varepsilon_{\mathrm{tot}}$ are expressed as a product of efficiencies of the single requirements. These, in turn, have to be calculated as conditional probabilities, given the previous cuts. In order to simplify the efficiency estimation, the sequence of the cuts (all put in logical-AND) can be reordered. In the chosen scheme, the total efficiencies are expressed as follows:

$$\varepsilon_{\mathrm{tot}}^{\pi e\nu} = \varepsilon_{\mathrm{crash}}(E_{\mathrm{cut}}) \cdot \varepsilon_{\mathrm{sele}}^{\pi e\nu} \cdot \varepsilon_{\mathrm{T0trg}}^{\pi e\nu} \cdot \varepsilon_{\mathrm{TOF}}^{\pi e\nu} \cdot \varepsilon_{\mathrm{tag}}^{\pi e\nu} \cdot \varepsilon_{\mathrm{FILFO}}^{\pi e\nu} \cdot \varepsilon_{\mathrm{veto}}^{\pi e\nu} \tag{6}$$

where:

- the efficiency $\varepsilon_{\mathrm{crash}}(E_{\mathrm{cut}})$ for the $K_L$ to produce a $K_{\mathrm{crash}}$-cluster with energy greater than $E_{\mathrm{cut}} = 100$ MeV is independent on the particular $K_S$ decay mode and cancels out in the ratio of efficiencies of equation (5);
- the efficiency $\varepsilon_{\mathrm{sele}}^{\pi e\nu}$ of the selection algorithm (described in Sec. 3) is calculated given the $K_{\mathrm{crash}}$-tag, as discussed in Sec. 6. This is also estimated as a product of the probabilities to satisfy the various cuts: DC preselection (discussed in Sec. 6.1), extrapolation to the calorimeter surface, and track-to-cluster association (Sec. 6.2):

$$\varepsilon_{\mathrm{sele}}^{\pi e\nu} = \varepsilon_{\mathrm{DCpre}} \cdot \varepsilon_{\mathrm{Extrap}} \cdot \varepsilon_{\mathrm{TCA}} \tag{7}$$

- the $t_0$ and trigger ($t_0$-given) efficiency $\varepsilon_{\mathrm{T0trg}}^{\pi e\nu}$ are calculated for the selected events (Sec. 6.2). The KLOE trigger [7] uses both calorimeter and chamber information. **For the present analysis, the trigger relies entirely on calorimeter information (events triggered by the drift chamber only are rejected.) Two local energy deposits in the calorimeter above threshold (**50 MeV **on the barrel,** 150 MeV **on the end-caps) are required.**
- The probability $\varepsilon_{\mathrm{TOF}}$ to satisfy the cuts on the time of flight (described in Sec. 3.3) is estimated as discussed in Sec. 6.3;
- the ratio of tagging efficiency corrections $R_{\mathrm{tag}}^{\pi e\nu/\pi\pi} = \varepsilon_{\mathrm{tag}}^{\pi e\nu}/\varepsilon_{\mathrm{tag}}^{\pi\pi}$, specific of the $t_0$-estimate of each $K_S$-channel is estimated as discussed in Sec. 6.4;
- the corrections $\varepsilon_{\mathrm{FILFO}}^{\pi e\nu}$ due to the FILFO [8] machine background rejection algorithm and $\varepsilon_{\mathrm{veto}}^{\pi e\nu}$ due to the cosmic-ray trigger veto [7] will be discussed in Secs. 6.5 and 6.6 respectively.

The estimates of these efficiencies involve the use of data control samples, which are selected as discussed in Sec. 5.

An analogous expression has been used for the normalization sample:

$$\varepsilon_{\rm tot}^{\pi\pi} = \varepsilon_{\rm crash}(E_{\rm cut}) \cdot \varepsilon_{\rm sele}^{\pi\pi} \cdot \varepsilon_{\rm T0trg}^{\pi\pi} \cdot \varepsilon_{\rm tag}^{\pi\pi} \cdot \varepsilon_{\rm FILFO}^{\pi\pi} \cdot \varepsilon_{\rm veto}^{\pi\pi} \tag{8}$$

The methods used to estimate these efficiencies are discussed in detail in [9]. The resulting efficiency is used in Sec. 7.

### 1.2 Data sample

Data of the KLOE year 2000 running period have been used, after the official reconstruction [10, 11] had runned and classification algorithm had divided events in different "streams" [12]. The signal has been selected from the main $K_S$-tag sample represented by the *kcrash* stream [5, 6]. Other data subsamples were extensively used for the various efficiency estimates, in particular events from the *kltag* [13], the *ksneut* [14], and $\rho\pi$ [15] streams. Details about the event reconstruction and classification algorithms are given in the cited references.

Since the standard KLOE *ntuple*-production was used, the analyzed dataset represents the 70% of the year 2000 statistics ($\approx 17$ pb$^{-1}$). These data were then divided in four subsamples, as reported in Tab. 1, in order to check the stability of the detection and selection efficiencies.

| Running period | Range of runs | Integrated luminosity |
|---|---|---|
| 15/07 $\rightarrow$ 05/08 | 14075 $\rightarrow$ 14678 | 3.53 pb$^{-1}$ |
| 30/10 $\rightarrow$ 15/11 | 16211 $\rightarrow$ 16712 | 6.15 pb$^{-1}$ |
| 15/11 $\rightarrow$ 24/11 | 16713 $\rightarrow$ 17010 | 3.90 pb$^{-1}$ |
| 24/11 $\rightarrow$ 06/12 | 17011 $\rightarrow$ 17249 | 3.92 pb$^{-1}$ |
| Total | | 17.5 pb$^{-1}$ |

Table 1: Year 2000 data samples used for the present analysis.

## 2 $K_S$ tagging

In KLOE roughly 50% of the produced $K_L$'s reach the calorimeter before decaying. The fraction of $K_L$ decays in a fiducial volume

$$30 \text{ cm} \leq \sqrt{x^2+y^2} \leq 180 \text{ cm} \ ; \ |z| \leq 150 \text{ cm}$$

is roughly of 30%, while $\sim 12\%$ is the probability that the $K_L$ decays before reaching the drift chamber volume:

$$\sqrt{x^2+y^2} \leq 25 \text{ cm}$$

Moreover, total angular momentum conservation of the spin-1 $\phi$ meson determine the angular distribution of the produced kaons:

$$\frac{{\rm d}N}{{\rm d}\Omega} \propto \sin^2\theta,$$

where $\theta$ is the angle of the $K_{S,L}$ momentum in the $\phi$ rest frame with respect to the beam axis. The small $\phi$ boost only slightly affects the angular distribution; so the previous relation roughly applies to the laboratory, too. The probability that a $K_L$ reaches the barrel calorimeter before decaying is so a factor of 1.18 higher than that to reach the end-cap.

The $K_L$ is the slowest particle produced in the interaction point (IP) that can reach the calorimeter before decaying; charged kaons, in fact, lose a relevant fraction of their energy traversing the materials, have a mean decay length of $\sim 90$ cm, and reach the calorimeter with small probability. Since the emitted $K_L$'s are almost monochromatic ($p \sim 110\,\mathrm{MeV}$), the identification of the $K_L$ interaction ("$K_{\mathrm{crash}}$") in the calorimeter can be performed using the time-of-flight of the energy deposit. The measurement of calorimeter times is described in the following section.

### 2.1 The reconstruction of calorimeter times

For each calorimeter cell, the coordinate $z$ along the fiber direction and the arrival time $t$ are related to the measured times $T$ (in TDC counts) at the $A, B$ sides:

$$z = \frac{v}{2} \times \left[ \left( t^{\mathrm{A}} - t_0^{\mathrm{A}} \right) - \left( t^{\mathrm{B}} - t_0^{\mathrm{B}} \right) \right] \tag{9}$$

$$t = \frac{t^{\mathrm{A}} - t_0^{\mathrm{A}}}{2} + \frac{t^{\mathrm{B}} - t_0^{\mathrm{B}}}{2} - \frac{L}{2v} - t_0^G \tag{10}$$

$$t^{\mathrm{A,B}} = c^{\mathrm{A,B}} \times \left( T^{\mathrm{A,B}} - T_{\mathrm{p}}^{\mathrm{A,B}} \right) \tag{11}$$

where:

- the constants $c^{\mathrm{A,B}}$ convert TDC counts to ns;
- $T_{\mathrm{p}}^{\mathrm{A,B}}$ are the delays of the entire electronic chains up to the preamplifiers;
- $L$ is the total module length along the fiber direction;
- $v$ is the velocity of the light in the fibers;
- $t_0^{\mathrm{A,B}}$ are the fine corrections to the time offsets;
- finally $t_0^G$, the event global time offset, is common to all the channels and depends on the trigger formation time with respect to the real $e^+e^-$ interaction time.

The signal from the first level trigger (FL) is distributed to the Calorimeter TDC boards, and acts as the common *Start* for all channels. The signals coming from the photomultipliers, after discrimination, undergo a fixed delay $\delta_{\mathrm{cable}}$ and finally give the *Stop* to the TDC channels. The measured time counted by the TDC can then be written as:

$$T = \underbrace{t^{\mathrm{TOF}} + t^{\mathrm{fiber}} + t^{\mathrm{zero}} + \delta_{\mathrm{cable}}}_{Stop} - \underbrace{t^{\mathrm{FL}}}_{Start} \tag{12}$$

where

$t^{\mathrm{TOF}}$ is the time of flight of the particle entering in the calorimeter;
$t^{\mathrm{fiber}}$ is the time needed for the light to reach the calorimeter side;
$t^{\mathrm{zero}}$ includes all the delay from the input to the photomultiplier, to the input to the TDC;
$t^{\mathrm{FL}}$ is the arrival time of the signal from the first level trigger.

The global time offset of the event, $t_0^G$, is given by:

$$t_0^G = \delta_{\mathrm{cable}} - t_{\mathrm{FL}} \tag{13}$$

This quantity has to be estimated event by event and subtracted from all calorimeter times, as in Eq. (10). **In order not to introduce a contribution to the time resolution coming from the $t_0^G$ estimation, the distribution of the first level trigger is synchronized to a high accuracy with the signal of the DAΦNE radiofrequency.**

For collisions events *the time zero of the event is correlated with a bunch crossing*; this is not true in general in a cosmic-ray event. Hence, for collision events the trigger formation time is an integer multiple of the bunch crossing period $T_{\rm bunch}$:

$$t^{\rm FL} = n_{\rm b} \times T_{\rm bunch} \tag{14}$$

The integer $n_{\rm b}$ has to be estimated after event reconstruction, as explained in the following section.

### 2.2 Selection of the $K_{\rm crash}$ cluster

The value of cluster times is used for the calculation of the $K_L$ velocity (see below), so it is necessary to explicitly define an algorithm to fix the global event offset ($t_0^G$). The first requirement imposed is that the global $t_0$ has to be fixed by a "golden $t_0$ cluster", defined as the first cluster in time satisfying:

$$E_{\rm CL} > 50 \text{ MeV AND } \sqrt{x_{\rm CL}^2 + y_{\rm CL}^2} > 60 \text{ cm} \tag{15}$$

This cut is imposed in order to minimize the probability that the $t_0$-cluster is actually an accidental from machine background. If no cluster satisfies this requirement, the event is rejected. The time of flight of a prompt photon is assumed for the $t_0$-cluster:

$$t_{\rm t0}^{\rm TOF} = \frac{\sqrt{x_{\rm CL}^2 + y_{\rm CL}^2 + z_{\rm CL}^2}}{c} = \frac{|\mathbf{r}_{\rm CL}|}{c} \tag{16}$$

The global-$t_0$ is then related to the fixed delay $\delta_{\rm cable}$ of the signals coming from the calorimeter TDC's, to the time of the $t_0$-cluster $t_{\rm t0CL}$, and to its $\gamma$-time-of-flight:

$$t_0^G = \delta_{\rm cable} - \text{Nint}\left[\frac{t_{\rm t0}^{\rm TOF} - t_{\rm T0CL} + \delta_{\rm cable}}{T_{\rm bunch}}\right] \times T_{\rm bunch} \tag{17}$$

where "Nint" stands for the nearest integer and $T_{\rm bunch} = 2.715\,$ns is the nominal inter-bunch time spacing. This offset is subtracted from the times of all calorimeter cells.

The bias of the requirement of Eq. (15) for signal and normalization events and the bias induced by the different $t_0$ estimates are discussed in Secs. 6.2, 6.4.

The logical scheme of the $K_{\rm crash}$ tagging algorithm [5, 6] is shown in figure 3. For each cluster on the barrel, not associated to any track, the "cluster-velocity" $\beta = r_{\rm CL}/cT_{\rm CL}$ is calculated and "boosted" in the $\phi$ rest frame:

$$\beta^* = \frac{\sqrt{\langle\beta_\phi\rangle^2 + \beta^2 + 2\langle\beta_\phi\rangle\beta\cos\alpha}}{1 + \langle\beta_\phi\rangle\beta\cos\alpha} \tag{18}$$

where the nominal values for the c.m. energy $\sqrt{s}$ and for the $\phi$ momentum $\vec{p}_\phi$ ($\sim -13\,$MeV) are used to calculate the $\phi$ velocity $\langle\beta_\phi\rangle$ and the angle $\cos\alpha$ between cluster direction and $\phi$ momentum. The clusters which satisfy the cuts:

$$E_{\rm CL} > 100 \text{ MeV AND } 0.195 \le \beta^* \le 0.2475 \tag{19}$$

are called $K_{\rm crash}$-clusters. In order to reject the background due to low-energy cosmic rays, a cut is imposed on the number $N_{\rm cc}$ of adjacent barrel columns with an energy above 7 MeV:

$$N_{\rm cc} \le 5 \tag{20}$$

Events with at least one $K_{\rm crash}$-cluster surviving this cosmic-ray rejection cut are selected as $K_S$-tagged.

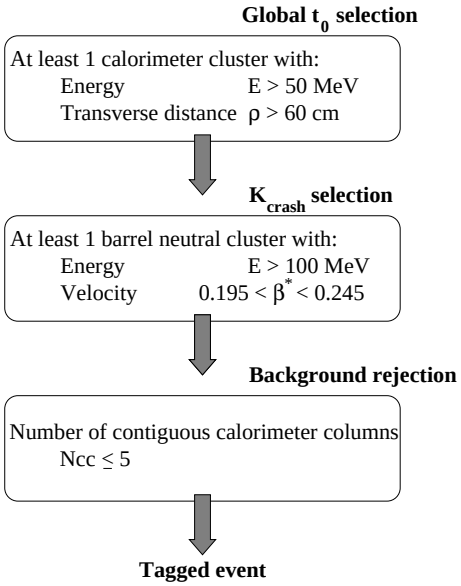


Figure 3: $K_{\rm crash}$ algorithm logic scheme.

## 3 Selection algorithm for $K_S \to \pi e \nu$ events

A sketch of the typical signal event that we want to select is shown in figure 4. Starting from a $K_S$-tagged event, a "drift chamber (DC) preselection" is applied. A vertex close to the IP, reconstructed from two oppositely charged tracks is required. $K_S \to \pi^+\pi^-$ decays constitute the main background for the identification of $K_S \to \pi e \nu$ events, with a rate larger by a factor of $10^3$. A cut is then applied, using the track momenta extrapolated to the vertex, in order to reject the $K_S \to \pi^+\pi^-$ invariant mass peak [16] (next section).

Particle identification is obtained through a time-of-flight (TOF) technique implemented as follows. Both tracks are extrapolated toward the calorimeter and are geometrically associated to calorimeter clusters (Sec. 3.2). The pion-electron particle identification is then obtained by comparing measured cluster times and expected flight times. The expected flight times are calculated by using different mass hypotheses [17] (Sec. 3.3).

The extrapolation of the tracks toward the calorimeter is actually an acceptance cut. This requirement also allows safe estimates of the probability for having a golden-$t_0$ cluster [this is imposed at the streaming level, Eq. (15)] and a valid trigger. These points are discussed in Sec. 6.2.

At this stage of the analysis, the main background to the identification of $K_S \to \pi e \nu$ events is constituted by $K_S \to \pi^+\pi^-$ events in which one or both $K_S$ pions decays in flight to a muon. In order to estimate and subtract the contribution from this background, events are kinematically closed at the $K_S$ vertex. The missing energy and momentum are calculated using the $K_{\rm crash}$-tag information. For a signal event, in which a neutrino is also emitted, missing momentum and missing energy have to be equal. The difference between the missing momentum and missing energy is used to subtract the residual background (Sec. 3.4).

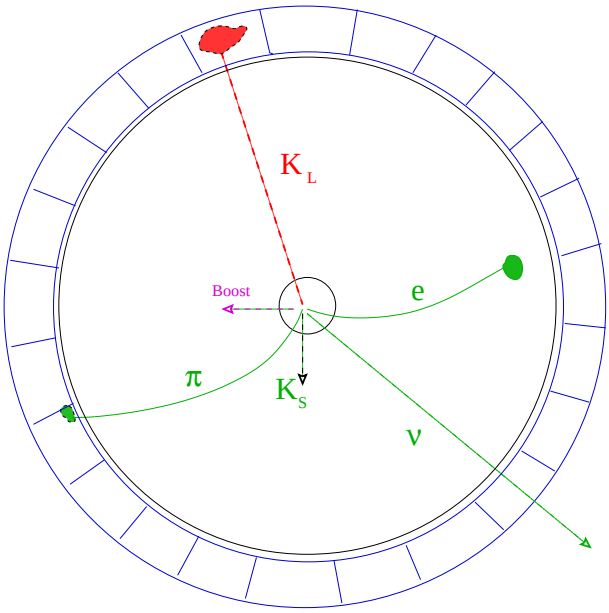


Figure 4: A sketch of the transverse view of a typical selected event. The $K_S$ is tagged by identifying a $K_{\rm crash}$ cluster (at the top). The $K_S$ "drift chamber preselection" requires two tracks connected to a vertex close to the IP. Loose cuts on the vertex kinematics are also applied. Both tracks are then extrapolated toward the calorimeter and associated to calorimeter clusters. Finally, the event is kinematically closed: the neutrino momentum-energy is calculated by using the $K_{\rm crash}$-cluster direction (dashed line), the $\phi$ boost (dashed arrow), and the momenta at the vertex.

### 3.1 Drift chamber (DC) preselection of the events

In a $K_{\rm crash}$-tagged event, vertices reconstructed from two oppositely charged tracks and located in a cylindrical volume centered around the interaction point

$$\rho_{\rm v} = \sqrt{x_{\rm v}^2 + y_{\rm v}^2} < 4 \text{ cm AND } |z_{\rm v}| < 10 \text{ cm}$$

are considered. Events with exactly one of such vertices are retained. The first hit of each track has to lie within the cylindrical volume

$$\rho_{\rm first} = \sqrt{X_{\rm first}^2 + Y_{\rm first}^2} \leq 40 \tag{21}$$

The invariant mass $M_{\pi\pi}$ in the pion-pion hypothesis and the $K_S$ momentum $P_{\rm S}$ in the $\phi$ rest frame are calculated, the latter using a non relativistic approximation [13]:

$$\mathbf{P}_{\rm S} = \mathbf{P}_1 + \mathbf{P}_2 - \mathbf{P}_\phi \times M_{K0}/\sqrt{s} \tag{22}$$

In order to reject the $K_S \to \pi^+\pi^-$ invariant mass peak, a cut is applied in the $P_{\rm S} \otimes M_{\pi\pi}$ plane. The definition of this cut is shown in figure 5, where the distributions from $K_S \to \pi e\nu$ and $K_S \to \pi^+\pi^-$ Monte Carlo events are plotted. The signal efficiency associated with this cut is around 87% due to the rejection of the region around the $K^0$ mass, in which $K_S \to \pi e\nu$ and $K_S \to \pi^+\pi^-$ events overlap. Background events surviving this cut are mainly $K_S \to \pi^+\pi^-$ decays, either with pion tracks badly reconstructed, or with one pion decaying to a muon before entering the drift chamber. In the latter case, the vertex is reconstructed from a pion and a muon track and the invariant mass $M_{\pi\pi}$ is lower than the $K^0$ mass.

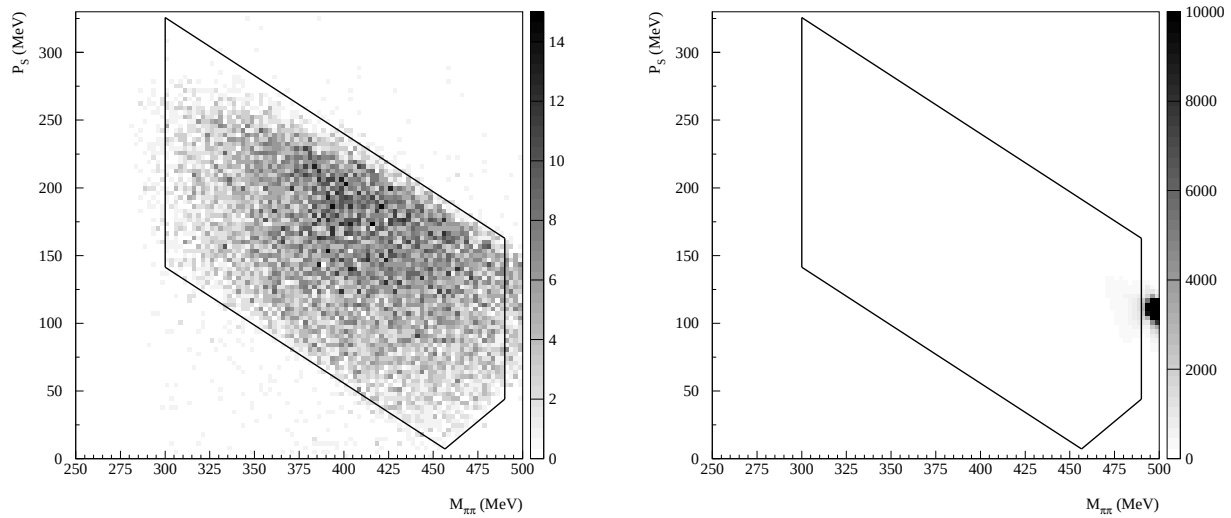


Figure 5: The "DC preselection" cut applied in the plane of the $K_S$ momentum in the $\phi$ rest frame ($P_{\rm S}$) vs. the invariant mass ($M_{\pi\pi}$) is shown for $K_S \to \pi e\nu$ (left) and $K_S \to \pi^+\pi^-$ (right) Monte Carlo events. The region within the solid line is retained. The two distributions are not normalized to the same number of events.

### 3.2 Track to cluster association (TCA)

Both tracks connected to the selected vertex are extrapolated toward the calorimeter surface, using the algorithm described in the next section. In order to reject spiralizing tracks, for which the Monte Carlo simulation is not reliable, the tracks re-entering the internal DC wall at some point along the extrapolated path are rejected. In addition, in order to select events with higher probability of having a $K_S$ golden-$t_0$ cluster [Eq. (15)], a cut is imposed on the transverse position $\rho_{\rm extrap} = \sqrt{x^2_{\rm extrap} + y^2_{\rm extrap}}$ of each track-impact point. Events in which *two* tracks are identified as $\pi \to \mu\nu$ in flight decays (i.e., both tracks belong to the *Kink* category: see the next section), or in which a track is connected to a secondary vertex not well reconstructed (i.e., belongs to the *Other* category), are rejected. These acceptance cuts are summarized by the conditions below:

$$\text{No forward impact on the DC internal wall} \tag{23a}$$

$$\rho_{\rm extrap} \geq 60 \text{ cm} \tag{23b}$$

$$\text{Both tracks of the } \textit{Golden} \text{ or } \textit{Kink} \text{ categories. } \textit{Kink-Kink} \text{ events are rejected.} \tag{23c}$$

The association to calorimeter clusters (TCA) is then performed by cutting on the transverse distance $d_{\rm TRA}$ between cluster centroids and the track direction of incidence. The distribution of $d_{\rm TRA}$ is shown in figure 6, for $\pi^+$ and $\pi^-$ tracks. A cluster is associated to a track if it lies within a 100 cm sphere centered around the track-impact point and satisfies the following condition:

$$d_{\rm TRA} \leq 30 \text{ cm} \tag{24}$$

Among all the clusters associated to a track, the one with highest energy is used for time of flight identification purposes. Again, both tracks are required to be associated to at least one EmC cluster. In the next section, the algorithm used to extrapolate tracks

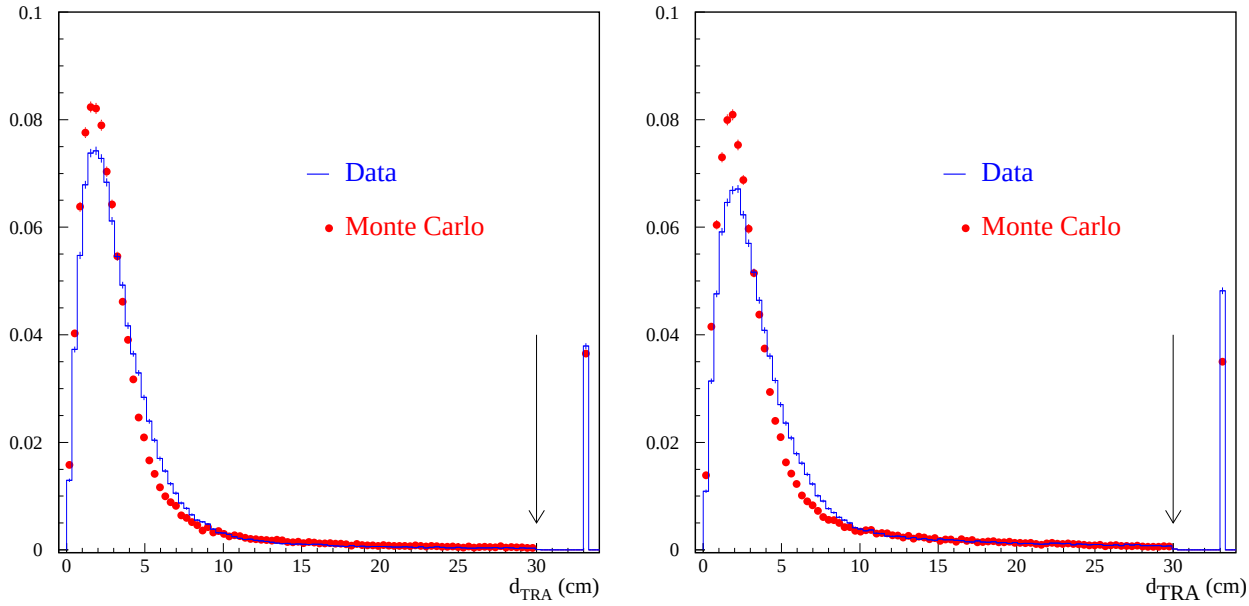


Figure 6: The distributions of the transverse distance $d_{\rm TRA}$ between track direction of incidence and closest candidate cluster are shown for $\pi^+$ (left) and $\pi^-$ (right) tracks, from data (solid line) and Monte Carlo (solid circles) $K_S \to \pi^+\pi^-$ events (tracks incident on barrel). The association cut [Eq. (24)] is indicated by the arrow. Both distributions are normalized and there is one entry per track extrapolated to the EmC. The single bins at $d_{\rm TRA} > 30$ cm are populated by events either with no cluster within a 100 cm sphere centered around the track-impact point, or with no cluster with $d_{\rm TRA} \leq 30$ cm. Hence, their height corresponds to the inefficiency of the association.

coming from the IP toward the calorimeter surface is described; this also takes care of in flight decays $\pi \to \mu\nu$ (in the DC volume) and of the presence of erroneously split tracks. The tuning of the cuts of the extrapolation algorithm is also discussed, since it has an impact on the effectiveness of the comparison between data and Monte Carlo efficiencies.

*3.2.1 Extrapolation of a track from IP to the calorimeter surface*

For each track connected to the vertex, possible secondary vertices (and tracks) are searched for in the outgoing direction: tracks with more than one secondary vertex are rejected. These secondary vertices either are due to real in flight decays $\pi \to \mu\nu$, or are "fake" vertices.[1)] In order to distinguish fake secondary vertices from real $\pi \to \mu\nu$ kinks, the missing momentum $P_{\rm miss}$, the squared mass $M_{\rm d}^2$ of the daughter particle, and the number of hits $N_{\rm H}$ belonging to the secondary track are calculated:

$$\mathbf{P}_{miss} = \mathbf{P}_{in} - \mathbf{P}_{out} \tag{25}$$

$$M_d^2 = \left(\sqrt{P_{in}^2 + M_\pi^2} - P_{miss}\right)^2 - P_{out}^2 \tag{26}$$

The mass $M_d^2$ is obtained under the hypothesis of an incoming pion and massless missing particle; this variable, plotted in the left panel of figure 7 for $K_S$ tracks from $K_S \to \pi^+\pi^-$

[1)] In turn, these are due either to the fact that multiple track segments corresponding to a single real track are output by the pattern recognition algorithm, or to an incorrect response of the "kink-finder" algorithm. This algorithm performs a dedicated search for $\pi \to \mu\nu$ decays in the chamber, using the trend in the track-hit residuals as a function of the hit progression [20].

selected events, clearly peaks around $M_\mu^2$, signaling the presence of reconstructed $\pi \to \mu\nu$ kinks.

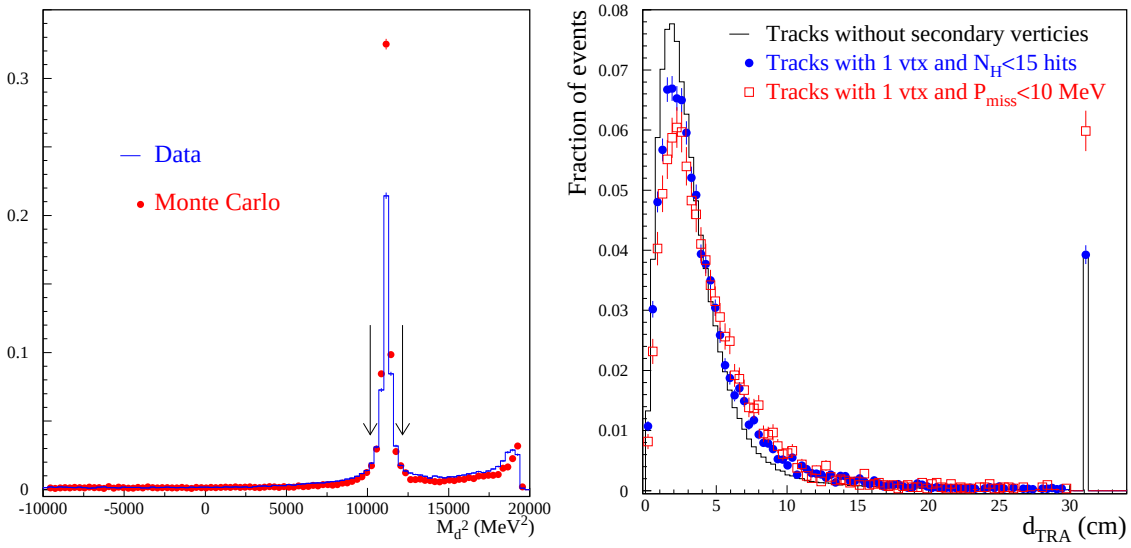


Figure 7: The distribution of the squared mass of a daughter particle is shown in the left panel for data (solid line) and Monte Carlo (circles) pion tracks in $K_S \to \pi^+\pi^-$ events. Both distributions are normalized. The *kink* category is defined as the region within the arrows, corresponding to $\pi \to \mu\nu$ decays. The distribution of the transverse distance $d_{\rm TRA}$ between the track impact direction and the closest candidate cluster is shown in the right panel, for $K_S \to \pi^+\pi^-$ events of Summer 2000 ($\pi^+$ tracks incident on barrel). The distribution for tracks having no secondary vertices [category 1(a) in the text] is compared with that for tracks having one secondary with $P_{\rm miss} < 10$ MeV [1(b)] or else with $N_{\rm H} < 15$ hits [1(c)]. All the plots are normalized to one and, as above, the height of the single bin at $d_{\rm TRA} > 30$ cm represents the inefficiency of the track-to-cluster association.

On the contrary, if the missing momentum $P_{\rm miss}$ at the vertex is small or if the secondary track has few associated hits, the vertex is probably a fake. This can be seen by extrapolating *the first track segment* to the calorimeter and comparing the TCA efficiency for tracks with:

(a) no secondary vertex,
(b) one secondary vertex with missing momentum $P_{\rm miss} < 10$ MeV,
(c) one secondary vertex with a secondary track of $N_{\rm H} < 15$ hits.

As can be seen in the right panel of figure 7, the efficiencies for categories (a) and (c) are compatible within the errors, while category (b) is slightly more inefficient. In the following, cases (a), (b), and (c) are merged into a single topological category. Even if there is a 2% difference between the efficiency for category (b) and those for categories (a) and (c), the small population of category (b) (see table 2) allows the associated systematic error to be neglected.

In order to perform the extrapolation to the calorimeter and the subsequent association to clusters, the tracks are divided into three categories, defined as follows:

1. *Golden* Three cases are actually merged:
   1.(a) No secondary vertex, or

1.(b) One secondary with

$$P_{\rm miss} < 10 \text{ MeV} \tag{27}$$

1.(c) One secondary with

$$N_{\rm H} < 15 \text{ hits} \tag{28}$$

These tracks are extrapolated to the calorimeter using the first track segment.

2. *Kink* One secondary vertex with squared mass of the daughter particle around the muon squared mass $M_\mu^2$:

$$\left|M_{\rm D}^2 - M_\mu^2\right| < 1000 \text{ MeV}^2 \tag{29}$$

These tracks are extrapolated to the calorimeter using the second track segment, due to the muon.

3. *Other* Not belonging to the first two categories, rejected.

The extrapolation is performed through an offline [2] analytic calculation [3].

The probability that tracks from $K_S \to \pi e\nu$ decay are assigned to categories 1 or 2 (rejecting the 2-2 case) is estimated using both $K_L \to \pi e\nu$ data and $K_S \to \pi e\nu$ Monte Carlo events (Sec. 6.2). In order to allow an effective comparison of data and Monte Carlo efficiencies, the cut values have been tuned using $K_S \to \pi^+\pi^-$ data and Monte Carlo events. The probability of creating a secondary fake vertex is indeed different for data and Monte Carlo events [4]. Hence the cut values of Eqs. (27) and (28) have been chosen in order to minimize the differences between the data and Monte Carlo populations of the three categories, without significantly changing the TCA efficiency of each sub-category for real data. After this tuning, the populations of the three categories for data and Monte Carlo event samples are listed in table 2. In this manner, data and Monte Carlo estimates

| Category | Data Population | MC Population |
|---|---|---|
| *Golden(a)* | 86.6% | 89.7% |
| *Golden(b)* | 1.2% | 0.6% |
| *Golden(c)* | 4.6% | 1.7% |
| *Golden* | 92.4% | 92.0% |
| *Kink* | 5.0% | 5.8 |
| *Other* | 2.6% | 2.2 |

Table 2: Populations of the track categories used for the extrapolation to the calorimeter, for data and Monte Carlo $K_S \to \pi^+\pi^-$ events. The three sub-categories that compose the *Golden* category are also separately listed.

of the efficiency $\varepsilon_{\rm categ}$ for having both tracks from a $K_S \to \pi e\nu$ decay belonging to the

[2] At present, information on the point of impact of the tracks to the calorimeter are only available for tracks associated to clusters by the official algorithm [19], while for efficiency studies it is mandatory to have such information for every track. Moreover, tracks producing a secondary vertex at the last hit side are never extrapolated, while this would be needed if the vertex is recognized to be a fake.

[3] In doing this calculation, the calorimeter geometry is taken from the data base, and the magnetic field is assumed axial and uniform.

[4] The kink-finder algorithm, which is responsible for half of the fake vertices in data, has been tuned on the Monte Carlo. The probability that a track is incorrectly split is therefore lower in the Monte Carlo than in real data. Also, the resolution on $M_{\rm D}^2$ from real $\pi \to \mu\nu$ decays (figure 7) is better for Monte Carlo than for data.

*Golden* or *Kink* categories can be safely compared. This point is discussed in detail in Sec. 6.2.5. The agreement between the data and Monte Carlo efficiencies seen in table 4 confirms the effectiveness of this tuning.

### 3.3 Time of flight (TOF) particle identification

The TOF particle identification aims at rejecting the residual $K_S \to \pi^+\pi^-$ background, which is mainly constituted by events with $\pi \to \mu\nu$ decays before the drift chamber wall, and also at identifying $\pi^\pm$ and $e^\mp$ tracks. The difference $\delta t$ between the measured time of the associated cluster ($T_{\rm CL}$) and the expected time of flight is calculated under a mass hypothesis:

$$\delta t\,(M_x) = T_{CL} - \frac{L}{c\beta(M_x)}\ ;\ \beta(M_x) = \frac{P}{\sqrt{P^2 + M_x^2}}$$

where $L$ is the total length of the flight path (from the vertex to the calorimeter) and $M_{\rm x}$ is the assumed particle mass: the values obtained with electron and pion masses have to be compared. If the track is a *Kink*, when applying the pion hypothesis the time of flight is calculated using the following formula [5)]:

$$\delta t\,(M_\pi) = T_{CL} - \frac{L_1}{c\beta(M_\pi)} - \frac{L_2}{c\beta(M_\mu)}$$

where $L_{1(2)}$ is the length of the first (second) track segment. A T0-independent variable is obtained by subtracting the $\delta t$ values for the two tracks: the variable

$$D\delta t\,(\pi\pi) = \delta t\,(M_\pi)_1 - \delta t\,(M_\pi)_2 \tag{30}$$

is expected to be around zero for a pair of pion tracks. Hence, the following cut is applied to reject the pion-pion hypothesis:

$$|D\delta t\,(\pi\pi)| > 1.5 \text{ ns} \tag{31}$$

For events surviving this cut, the pion and electron assignments are tested, using the variables

$$D\delta t\,(e_1\pi_2) = \delta t\,(M_e)_1 - \delta t\,(M_\pi)_2 \tag{32}$$

$$D\delta t\,(e_2\pi_1) = \delta t\,(M_e)_2 - \delta t\,(M_\pi)_1 \tag{33}$$

If the pair of tracks is actually due to an electron and a pion, one of the two variables above should be around zero, while the other has to be away from zero. So the applied cut is:

$$\{|D\delta t\,(e_2\pi_1)| < 1 \text{ ns AND } D\delta t\,(e_1\pi_2) > 3 \text{ ns}\} \text{ OR } 1 \leftrightarrow 2 \tag{34}$$

The distribution of $D\delta t\,(e_1\pi_2)$ vs $D\delta t\,(e_2\pi_1)$ is shown in figure 8.

[5)] At present the fact that a track is identified as a *Kink* is not used in the particle identification.

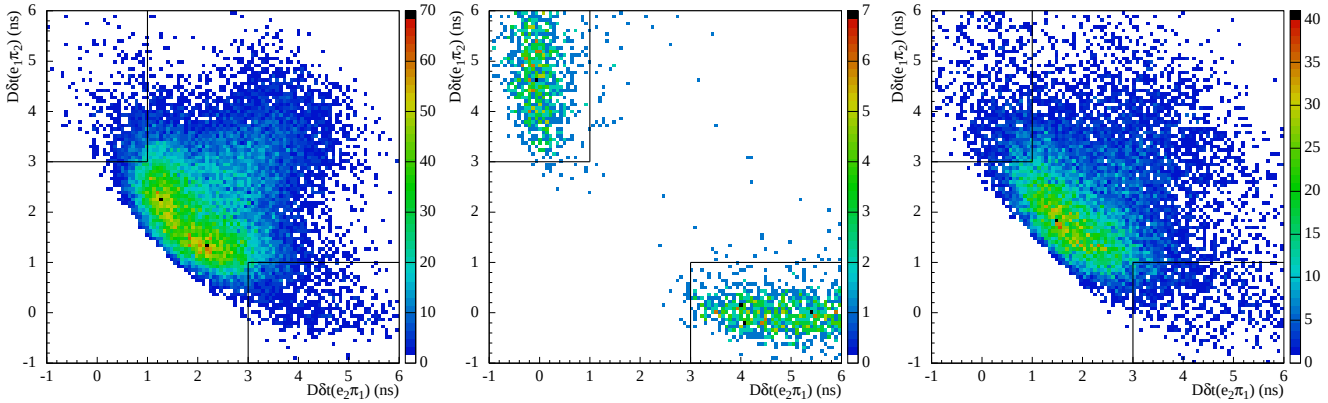


Figure 8: Distribution of the time differences D$\delta$t of Eqs. (32), (32) in the $e\pi$ vs $\pi e$ mass hypotheses, for Monte Carlo events with $K_S \to \pi^+\pi^-$ (left) and $K_S \to \pi e\nu$ (center) decays, and for November 2000 data (right). The regions within the solid lines are selected as signal.

### 3.4 Estimate of the number of signal events

In the end, events are kinematically closed at the $K_S$ vertex. For this pourpose, the $K_L$ momentum $\mathbf{P}_{\rm L}$ is calculated using the direction of the $K_{\rm crash}$ cluster. The $\phi$ boost $\mathbf{P}_\phi$ and the c.m. energy $\sqrt{s}$ are measured run by run in Bhabha events, and are averaged over homogeneous groups of runs. Using the angle $\alpha$ between $\mathbf{P}_\phi$ and the direction $\hat{\mathbf{n}}$ of the $K_{\rm crash}$ cluster [6)], the $K_L$ momentum $P_{\rm L}$ is estimated. The $K_S$ momentum $\mathbf{P}_{\rm S}$ is obtained again from the $\phi$ boost, and the missing momentum at the $K_S$ vertex is finally calculated using the $K_S$ track momenta extrapolated to the vertex ($\mathbf{p}_{1,2}$):

$$\mathbf{P}_{\rm miss} = \mathbf{P}_{\rm S} - \mathbf{p}_1 - \mathbf{p}_2 \; ; \; \mathbf{P}_{\rm S} = \mathbf{P}_\phi - P_{\rm L} \cdot \hat{\mathbf{n}} \tag{35}$$

The missing energy is calculated according to the mass assignments derived from the TOF identification [the cut in Eq. (34)]:

$$E_{\rm miss}\,(\pi e) = \sqrt{\mathbf{P}_{\rm S}^2 + M_K^2} - \sqrt{\mathbf{p}_1^2 + M_\pi^2} - \sqrt{\mathbf{p}_2^2 + M_e^2} \tag{36}$$

The difference $E_{\rm miss}(\pi e) - P_{\rm miss}$ is expected to be around zero if the missing particle is actually massless. It is shown in the left panel of Fig. 9, where the whole year 2000 data set of table 1 has been used. Events above 30 MeV are due to residual $K_S \to \pi^+\pi^-$ background events, as can be seen comparing the distributions for Monte Carlo events with $K_S \to \pi e\nu$ (center) and $K_S \to \pi^+\pi^-$ (right) decays. The distribution from real data is then fit with a linear combination of the two Monte Carlo *histograms* of figure 9. This outputs directly the number of signal events in the range of the fit. The finite Monte Carlo statistics is taken into account in the calculation of the likelihood function, as explained in ref. [21]. The result obtained for the entire year-2000 data sample is shown in figure 10 (left). In order to check the stability of the yield estimate, this procedure has been also applied separately on the four data subsamples defined in table 1. The result is shown in table 3 and in the right panel of figure 10, in which the number of observed signal events has been normalized to the integrated luminosity (estimated from radiative Bhabha events with a total fractional error of $\sim 1\%$). The result is stable within the statistical error.

[6)] Between all cluster satisfying $K_{\rm crash}$ requirements, that with the higher $\beta^*$ is chosen.

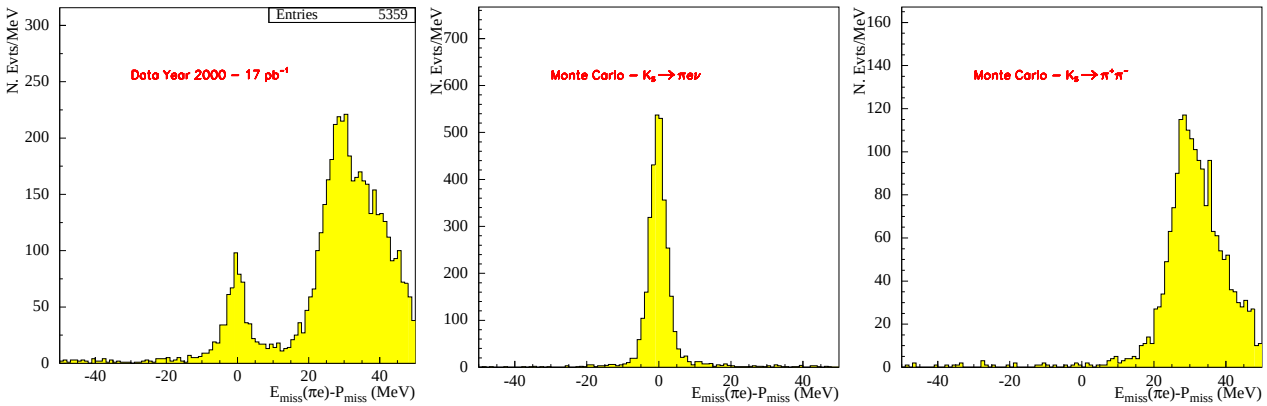


Figure 9: Difference between the missing energy and the missing momentum at the $K_S$ vertex, $E_{\rm miss}(\pi e) - P_{\rm miss}$, from $\sim 17$ pb$^{-1}$ of data integrated during year 2000 (left panel), and from Monte Carlo events of $K_S \to \pi e \nu$ (center), $K_S \to \pi^+\pi^-$ (right) decays.

| Period | Luminosity | Nobs | Nobs/pb |
|---|---|---|---|
| July-August 15/7→5/8 | 3.53 pb$^{-1}$ | $113 \pm 12$ | $32.2 \pm 3.3$ |
| October-November 30/10→15/11 | 6.15 pb$^{-1}$ | $242 \pm 17$ | $39.3 \pm 2.8$ |
| November 15/11→24/11 | 3.90 pb$^{-1}$ | $133 \pm 13$ | $34.1 \pm 3.3$ |
| November-December 24/11→6/12 | 3.92 pb$^{-1}$ | $151 \pm 13$ | $38.3 \pm 3.4$ |
| Year 2000 15/7→6/12 | 17.5 pb$^{-1}$ | $624 \pm 30$ | $35.7 \pm 1.7$ |

Table 3: Summary of the results for the observed number of events.

## 4 Selection of the normalization sample

In this section, the selection of the normalization sample of $K_S \to \pi^+\pi^-$ decays is briefly summarized. For a detailed discussion of the selection and of the methods used to estimate the related efficiency, see [9].

The selection of $K_S \to \pi^+\pi^-$ events is based on the identification of both the $K_S$ pion tracks, mainly obtained by applying topological requirements with very loose kinematical cuts. Since the possible background due to charged modes other than $K_S \to \pi^+\pi^-(\gamma)$ (semileptonic $K_S$ decays and $K_S \to \pi^0\pi^0$ decays in which a $\pi^0$ undergoes a Dalitz pair decay, $\phi \to K^+K^-$ decays) amounts to few $10^{-3}$, these cuts are sufficient to select a clean sample of $K_S \to \pi^+\pi^-$ decays.

In a $K_{\rm crash}$-tagged event, all of the tracks starting close to the drift chamber wall are considered: the first hit is required to be within the cylindrical volume:

$$\rho_{\rm first} = \sqrt{X^2_{\rm first} + Y^2_{\rm first}} \leq 40 \qquad (37)$$

This means that the track has to start by one of the five innermost layers of the chamber. An acceptance cut is also imposed on the polar angle $\theta_{\rm trk}$ of the momentum, which is required to be in the range:

$$30^\circ \leq \theta_{\rm trk} \leq 150^\circ$$

The tuning of these preliminary cuts has been performed in order to simplify the implementation of the correction due to the track-reconstruction efficiency. Using the cuts listed above, this correction reduces to a constant independent on the pion track momentum (see Fig. 20).

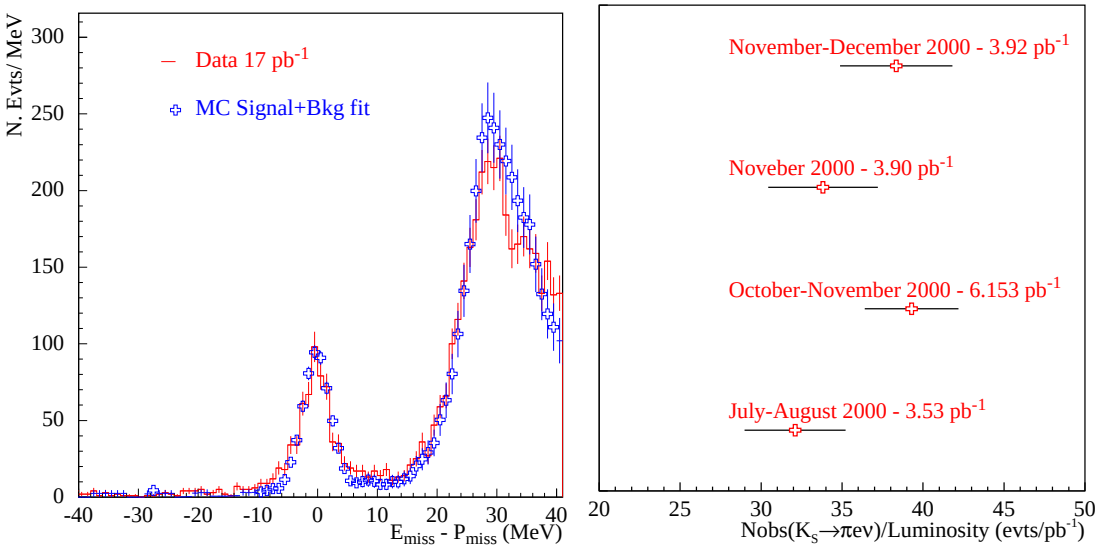


Figure 10: Left: $E_{\rm miss}(\pi e) - P_{\rm miss}$ distributions for data. The fit with a linear combination of the Monte Carlo signal and background histograms is superimposed. Right: number of observed events normalized to the estimated luminosity in the four data subsamples defined in table 1.

All of the considered tracks are then extrapolated at the point of closest approach to the origin (PCA). The beam-transverse ($\rho_{\rm PCA} = \sqrt{X^2_{\rm PCA} + Y^2_{\rm PCA}}$) and beam-longitudinal ($Z_{\rm PCA}$) distances of closest approach are then calculated. The applied cut

$$\rho_{\rm PCA} \leq 4 \text{ cm AND } |Z_{\rm PCA}| \leq 10 \text{ cm}$$

aims at rejecting the tracks of machine-background events, which mostly originate from the quadrupoles. These tracks have small values of $\rho_{\rm PCA}$, but are away in $|Z_{\rm PCA}|$ (by $\sim 40$ cm).

The pion tracks are extrapolated toward the calorimeter using the algorithm described in Sec. 3.2. In order to reject spiralizing tracks, and to select events with higher probability of having a $K_S$ golden-T0 cluster [Eq. (15)], the cuts of Eqs. (23a) and (23b) are applied.

At least a pair of tracks of opposite curvatures, completely disconnected one from each other, satisfying all of the previous cuts, is required. A loose cut on the momentum $P_{\rm trk}$ of the selected tracks is finally applied, in order to reject the small background due to $\phi \to K^+K^-$ decays (around 100 MeV) and residual machine-background events (above 300 MeV):

$$120 \text{ MeV} \leq P_{\rm trk} \leq 300 \text{ MeV} \tag{38}$$

The selection efficiency is defined as the probability that, *given the* $K_{\rm crash}$*-tag*, at least two tracks of opposite charge coming from the IP are selected, at least a golden-$t_0$ cluster is found, and the event is triggered.

The track-selection efficiency has been estimated in two steps. First the track reconstruction efficiency is extracted directly from data samples of $K_S \to \pi^+\pi^-$ with a $K_{\rm crash}$-tag, as a function of the track transverse momentum and polar angle; then, the efficiency profiles are used to correct the Monte Carlo simulation and the data-tuned Monte Carlo is used to calculate the efficiency of the track-selection. The radiation

of the soft photons in the final state is taken into account in the efficiency estimate, $\varepsilon^{\pm}_{\rm sele} = 0.576 \pm 0.001_{\rm stat} \pm 0.001_{\rm syst}$. Events selected as $K_S \to \pi^+\pi^-$ can be considered fully inclusive of all photons emitted in the final state ($K_S \to \pi^+\pi^-(\gamma)$ events).

The $t_0$ and trigger efficiencies have been estimated using two methods: directly from data using $K_L \to \pi^+\pi^-\pi^0$ -tagged data samples, and tuning the Monte Carlo simulation with data-extracted efficiencies. The result is $\varepsilon_{\rm t0TRG} = 0.976 \pm 0.003$.

The total average efficiency for the selection of $K_S \to \pi^+\pi^-$ events is then:

$$\boxed{\varepsilon^{\pi\pi}_{\rm tot} = 0.5622 \pm 0.0022_{\rm tot}} \tag{39}$$

# 5 Selection of data control samples

In this section the selection of the control samples used for the efficiency estimates is described. Different methods are used to extract the efficiencies, relying on different control samples. On the one hand, $K_L \to \pi e\nu$ decays before the DC wall have exactly the same kinematics as the signal, the only difference being the fact that, unlike in the case of $K_S \to \pi e\nu$ decays, $K_L$ vertices are almost uniformly distributed within the DC wall. This sample, tagged by $K_S \to \pi^+\pi^-$ decays as explained in Sec. 5.1, allows a direct-from-data estimate of the probabilities for having both $K_S$ tracks associated to EmC clusters (TCA), for having at least a golden-T0 cluster (T0), for giving a valid trigger, and for satisfying the time of flight cuts defined in Sec. 3.3.

On the other hand, it is possible to extract from other data samples *single-particle* efficiencies which are used to weight Monte Carlo $K_S \to \pi e\nu$ events. A copious sample of pions coming from the IP is selected (Sec. 5.2) in order to extract the probabilities for a $\pi^+$, $\pi^-$, $\mu^+$, or $\mu^-$ entering the calorimeter to give an associated cluster (TCA), a golden-$t_0$ cluster, and a fired trigger sector. The same efficiencies for $e^{\pm}$ are extracted from a sample of $K_L \to \pi e\nu$ decays before the DC wall, selected as described in Sec. 5.3.

Finally, another $K_L \to \pi e\nu$ sample, *selected in $K_S \to \pi^0\pi^0$ events without requiring the $K_L$-vertex reconstruction* (Sec. 5.4), allows an estimate of the vertex efficiency (Sec. 6.1).

In the following subsections, the selection criteria used to obtain the various control samples are illustrated.

## 5.1 $K_L \to \pi e\nu$ prompt decays in $K_S \to \pi^+\pi^-$ events

These $K_L$ decays are selected among events in which a $K_S \to \pi^+\pi^-$ decay is identified by the *ks2pi* algorithm [13]. We look for two tracks of opposite charge coming from the IP with a reconstructed vertex inside the $K_S$ "fiducial volume", $\rho \leq 4$ cm and $|Z| \leq 8$ cm. A tighter cut is applied here on the $K_S$ invariant mass and the $K_S$ momentum in the $\phi$ rest frame:

$$\begin{array}{ccccc} 490 \text{ MeV} & \leq & M_{\pi\pi} & \leq & 506 \text{ MeV} \\ 50 \text{ MeV} & \leq & P_{\rm S} & \leq & 170 \text{ MeV} \end{array} \tag{40}$$

The $K_L$ momentum $\mathbf{P}_{\rm L}$ is then estimated as follows:

$$\mathbf{P}_{\rm L} = \mathbf{P}_\phi - \mathbf{p}_1 - \mathbf{p}_2$$

where $\mathbf{p}_{1,2}$ are the momenta of the $K_S$ tracks and $\mathbf{P}_\phi$ is the $\phi$ boost. For the selected events, the vertices reconstructed before the DC wall

$$|z_{\rm v}| \leq 25 \text{ cm AND } \sqrt{x_{\rm v}^2 + y_{\rm v}^2} \leq 24 \text{ cm}, \tag{41}$$

from two oppositely charged tracks, and lying in a 26° cone around the estimated $\hat{\mathbf{P}}_{\rm L}$ direction are considered ("$K_L$-candidate" vertices). The main backgrounds for the $K_L \to \pi e\nu$ identification are $K_L \to \pi\mu\nu$, $K_L \to \pi^+\pi^-$ , and $K_L \to \pi^+\pi^-\pi^0$ decays, and the charged decays of $K_S$'s which are regenerated in the beam pipe or in the chamber inner wall.

In order to reject these backgrounds, the missing (neutrino) momentum

$$\mathbf{p}_{\rm miss} = \mathbf{P}_{\rm L} - \mathbf{p}_1 - \mathbf{p}_2 \ , \tag{42}$$

the missing energy $E^{\pi\pi}_{\rm miss} = E_{\rm L} - E_1 - E_2$, and the invariant mass $M_{\pi\pi}$ in the pion-pion hypothesis are calculated using the track momenta $\mathbf{p}_{1,2}$ at the $K_L$-candidate vertex.

In the left panel of figure 11, the invariant mass $M_{\pi\pi}$ is shown as a function of the missing momentum.

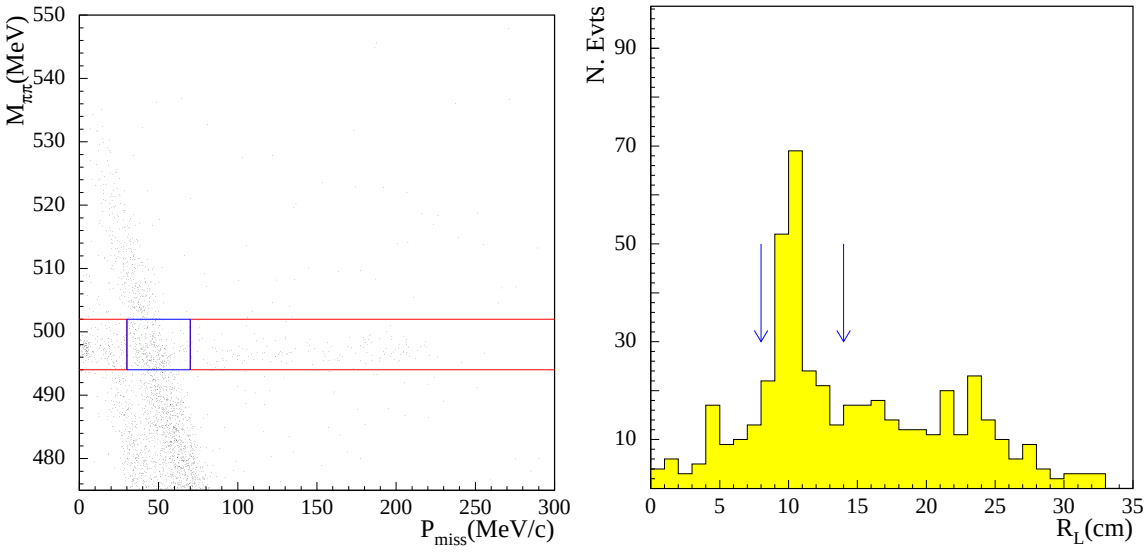


Figure 11: In the left panel, the pion-pion invariant mass is plotted as a function of the missing momentum at the vertex, for $K_S \to \pi^+\pi^-$ selected events in which a $K_L$-candidate vertex is selected before the DC wall. Vertices with invariant mass around the $K^0$ mass are partly due to regenerated $K_S \to \pi^+\pi^-$ or $K_L \to \pi^+\pi^-$ decays: those with missing momentum either less than 30 MeV or greater than 70 MeV are directly rejected. For vertices in the remaining $P_{\rm miss}$ interval, the distance to the IP is calculated (right panel). Events lying within the arrows are due to $K_S$ regenerated on the beam pipe ($R = 10$ cm) material and are rejected.

The two structures in which $M_{\pi\pi}$ and $P_{\rm miss}$ are anticorrelated, are due to $K_L \to \pi\mu\nu$ decays (at lower $P_{\rm miss}$) and to $K_S \to \pi e\nu$ decays. The invariant mass peak around the $K^0$ mass is due to $K_L \to \pi^+\pi^-$ decays (low-$P_{\rm miss}$ region), or to $K_S$ regeneration (in the tail at larger missing momenta). Hence, vertices with invariant mass in the range (red box in Fig. 11)

$$494 \text{ MeV} < M_{\pi\pi} < 502 \text{ MeV} \tag{43}$$

are directly rejected if

$$\{P_{\rm miss} < 30 \text{ MeV OR } P_{\rm miss} > 70 \text{ MeV}\} \, . \tag{44}$$

In the remaining interval of missing momentum (30 MeV $< P_{\rm miss} <$ 70 MeV), regenerated $K_S$ decays are kinematically overlapped with $K_L \to \pi e\nu$ decays. For these events, the distance of the vertex from the IP is also considered (right panel of figure 11); only the region around the beam pipe wall

$$8 \text{ cm} < \sqrt{x_{\rm v}^2 + y_{\rm v}^2 + z_{\rm v}^2} < 14 \text{ cm}, \tag{45}$$

where regeneration takes place, is rejected. For the vertices surviving these cuts, the missing momentum is plotted as a function of the missing energy $E_{\rm miss}^{\pi\pi}$ in the left panel of figure 12.

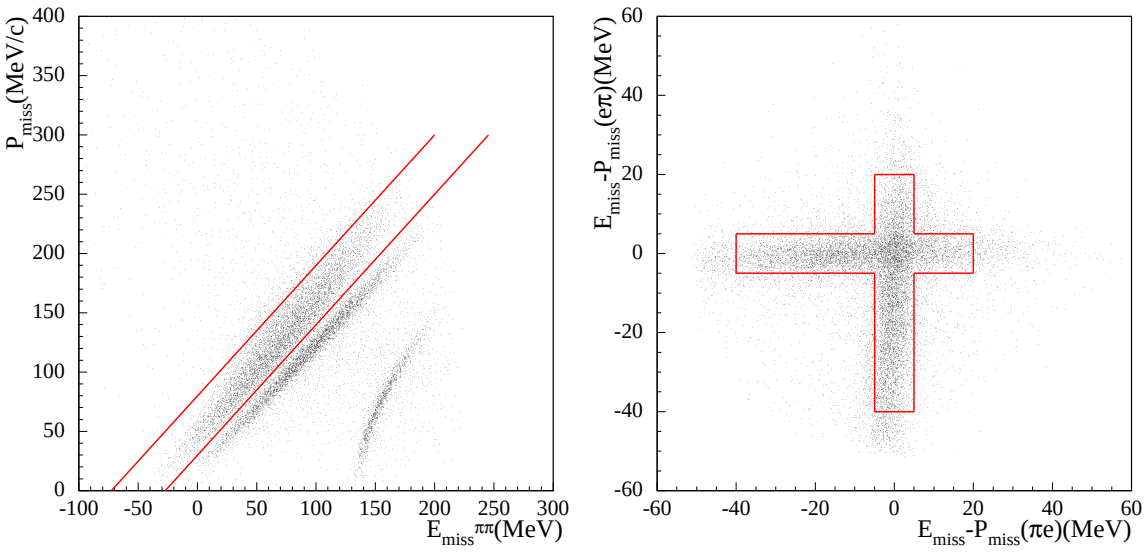


Figure 12: In the left panel, the missing momentum is plotted as a function of the missing energy for $K_L$-candidate vertices surviving the cuts of Eqs. 43–45. For vertices lying within the solid lines, the difference $E_{\rm miss} - P_{\rm miss}$ is calculated using both pion-electron and electron-pion hypotheses (right panel). The region within the "cross" ultimately constitutes a $K_L \to \pi e\nu$ sample with a contamination lower than $3 \times 10^{-3}$.

Going from low to higher missing energies, three structures are visible, due to $K_L \to \pi e\nu$, $K_L \to \pi\mu\nu$, and $K_L \to \pi^+\pi^-\pi^0$ decays. The region defined as

$$30\,\text{MeV} + 1.1E_{\rm miss}^{\pi\pi}\,[\,\text{MeV}] < P_{\rm miss} < 80\,\text{MeV} + 1.1E_{\rm miss}^{\pi\pi}\,[\,\text{MeV}] \tag{46}$$

(within the solid lines in figure 12), is due to $K_L \to \pi e\nu$ decays and is selected. Finally, in order to suppress a residual background due to $K_L \to \pi\mu\nu$ decays, the difference $E_{\rm miss} - P_{\rm miss}$ is evaluated under both possible choices for the particle masses, assuming one to be an electron and the other a pion, and vice versa. These differences are plotted in the right panel of figure 12. This difference should be around zero in a $K_L \to \pi e\nu$ decay, when the mass assumption is correct. Therefore, the region within the "cross" in figure 12 is accepted. It is defined as:

$$\begin{aligned} |E_{\rm miss}\,(\pi_{1,2}, e_{2,1}) - P_{\rm miss}| &< 5 \text{ MeV} \\ -40 < E_{\rm miss}\,(e_{1,2}, \pi_{2,1}) - P_{\rm miss} &< 20 \text{ MeV} \end{aligned} \tag{47}$$

Monte Carlo studies show that these cuts reduce the contamination in the selected sample to below 0.3%. In order to avoid any bias in the $K_L$ sample induced by the trigger or

the $t_0$ conditions, these are required to be satisfied by the $K_S$-pion clusters. In this way, clusters associated to the $K_L$ tracks are free to (not) fire a trigger sector and to (not) produce a $t_0$ cluster. A spatial separation is also imposed between the impact points of the $K_L$ tracks and the centroids of the $K_S$ clusters.

In order to implement the above requirements, all clusters inside (outside) one meter ray spheres centered at the $K_L$ tracks' impact points are assigned to the $K_L$ ($K_S$).
The trigger and $t_0$ requirements are imposed by using $K_S$ clusters and not considering sectors hit by $K_L$ clusters. Events with a not clean separation of $K_S$ clusters and $K_L$ tracks are rejected: specifically these are the events in which the $K_S$ clusters are in the same calorimeter modules hit by the $K_L$ tracks.

### 5.2 Single $\pi$ and $\mu$ tracks from $K_S \to \pi^+\pi^-$ and $\phi \to \pi^+\pi^-\pi^0$ decays

$K_S \to \pi^+\pi^-$ events are selected starting from a $K_{\rm crash}$-tagged sample using the algorithm described in Sec. 4. Additional cuts are applied here in order to select a sample of pion (or muon, according to the definition given in Sec. 3.2) tracks in which any possible bias due to the $t_0$ or trigger conditions has been removed. This sample is then used to estimate single-track TCA, $t_0$, and trigger-sector efficiencies, as discussed in Sec. 6.2.

The $1^{\rm st}(2^{\rm nd})$ $K_S$ track is selected if:

- the $2^{\rm nd}(1^{\rm st})$ track is associated to a golden-$t_0$ cluster satisfying Eq. (15);
- sectors fired by clusters associated to the $2^{\rm nd}(1^{\rm st})$ track, together with those from the $K_{\rm crash}$ satisfy the calorimeter trigger conditions; in evaluating this condition, all of the sectors fired by clusters within a 100-cm sphere centered around the impact point of the $1^{\rm st}(2^{\rm nd})$ track are not taken into account;
- a minimum distance between the point of impact of the $1^{\rm st}(2^{\rm nd})$ track and all of the other known clusters of the event is required, equivalent to 12 EmC cells in the direction transverse to the fibers (20 cm).

In order to obtain the efficiencies cited above for the region of high transverse momentum ($p_{\rm t} > 250$ MeV) populated by the $K_S \to \pi e\nu$ decay, a sample of $\phi \to \pi^+\pi^-\pi^0$ decays has been also selected. This is done by identifying a vertex reconstructed from $\pi^+$ and $\pi^-$ tracks and a pair of photon clusters, as described in detail in [22]. The selection is briefly summarized here:

1. the initial sample is the $\rho\pi$ stream [15];
2. the cut on the missing mass $M^{\pi\pi}_{\rm miss}$ at the $\phi$ vertex is hardened: $|M^{\pi\pi}_{\rm miss} - M_{\pi^0}| < 15\,{\rm MeV}$;
3. using the calculated $\pi^0$ momentum, a pair of photon (prompt) clusters is selected cutting on the $\gamma$-$\gamma$ opening angle $\phi^*$ in the $\pi^0$ rest frame: $\phi^* > 170^\circ$

As above, pion track 1(2) is selected if:

- pion track 2(1) is associated to an EmC cluster(s);
- this pion cluster and the two $\gamma$ clusters satisfy the T0 and calorimeter trigger conditions. As above, trigger sectors hit by clusters lying in a 100 cmsphere around the track 1(2) impact point are not considered;
- the smallest distance between the impact point of track 1(2) and any of the other known clusters in the event is greater than 20 cm.

### 5.3 Single $e$ (or $\pi$) tracks from $K_L \to \pi e\nu$ decays

$K_L \to \pi e\nu$ events, selected as explained in Sec. 5.1, have also been used to obtain a sample of electron(pion) tracks incident on the calorimeter. These are used to estimate single particle electron(pion) efficiencies, as explained in Sec. 6.2.

Once the $K_L$ decay vertex is identified, a single electron(pion) *candidate* track can be selected *without requiring association to an EmC cluster*, either by using DC variables, or by identifying the other (*tagging*) track as a pion(electron) through a time of flight technique. The bias due to the trigger (or $t_0$) conditions is then removed, in the manner described in the previous section.

In order to have a clean measurement of the absolute time, which is useful for the time of flight identification of a single track, the global $t_0$ has to be correctly fixed. This is done by associating both pion tracks from the $K_S \to \pi^+\pi^-$ decay to EmC clusters, and by using in Eq. (17) a "pion" time of flight:

$$t_{\rm t0}^{\rm TOF} = \frac{L}{c \cdot \beta_\pi}, \tag{48}$$

where $L$ is the total track length from the $K_S$ vertex to the calorimeter, and $\beta_\pi$ is the velocity calculated using the track momentum and the pion mass hypothesis. If the global $t_0$'s obtained from the two pions are different, the event is rejected.

For each $K_L$ track of momentum $p$ associated to an EmC cluster of time $T_{\rm CL}$, two variables are then calculated: (a) The squared mass $M^2$ of the particle, obtained from the total track length $L$ (from the $K_L$ vertex to the calorimeter) and from the estimated $K_L$ time of flight $T_{\rm KL}$:

$$M^2 = p^2 \cdot \left(\frac{1}{\beta^2} - 1\right) \tag{49a}$$

$$\beta = \frac{L}{c\,(T_{\rm CL} - T_{\rm KL})} \tag{49b}$$

(b) The difference between the cluster energy and the track momentum $\delta E = E_{\rm CL} - p$. These variables are plotted in figure 13 for $K_L \to \pi e \nu$-identified events in year 2000 data. Two regions are visible, due to pion and electron tracks. The pion-tagging tracks are then selected by applying the following condition:

$$\left(\frac{M^2 - 22\,000\ {\rm MeV}^2}{10\,000\ {\rm MeV}^2}\right)^2 + \left(\frac{\delta E + 70\ {\rm MeV}}{60\ {\rm MeV}}\right)^2 \leq 1 \tag{50}$$

An analogous elliptic cut would be applied if tagging electron tracks were to be selected:

$$\left(\frac{M^2}{5\,000\ {\rm MeV}^2}\right)^2 + \left(\frac{\delta E + 10\ {\rm MeV}}{50\ {\rm MeV}}\right)^2 \leq 1 \tag{51}$$

If different $t_0^G$ values are obtained using $K_S$ pion tracks, or if the $K_L$ pion(electron) cluster is not found, the $|E_{\rm miss} - P_{\rm miss}|$ variable can provide the particle identification as well. As in Eq. (47), both pion-electron assignments are compared. The correct one can be identified only if (see figure 12):

$$|E_{\rm miss}\,(e_{1,2}, \pi_{2,1}) - P_{\rm miss}| < 10\ {\rm MeV} \tag{52a}$$

$$|E_{\rm miss}\,(e_{2,1}, \pi_{1,2}) - P_{\rm miss}| > 10\ {\rm MeV} \tag{52b}$$

If this condition is satisfied, the correct mass assumption is identified as that which gives the value of $E_{miss} - P_{miss}$ closer to zero.

If a pion(electron) tagging track is identified with either of the two methods, the $t_0$ and trigger conditions are then required to be satisfied using the $K_S$ pion clusters and the $K_L$ pion(electron) cluster only. A sample of unbiased electron(pion) candidate tracks is thus obtained.

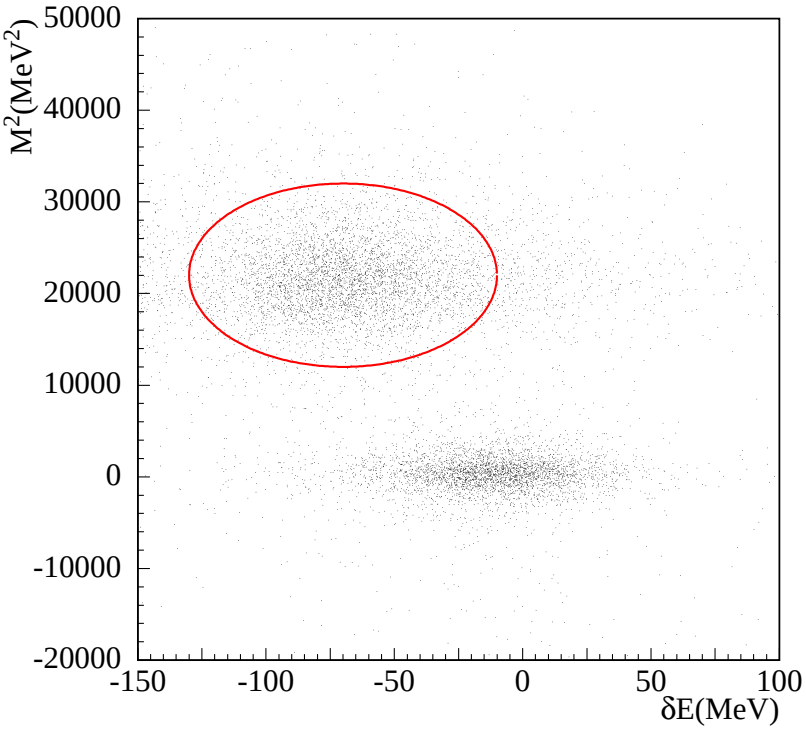


Figure 13: The squared mass $M^2$ is plotted as a function of the difference $\delta E$ between cluster energy and track momentum, for $K_L$ tracks associated to clusters. The ellipse which defines the "pion region" is superimposed.

### 5.4 $K_L \to \pi e\nu$ prompt decays in $K_S \to \pi^0\pi^0$ events

This sample has been used to estimate the vertex efficiency for $K_S \to \pi e\nu$ decays [7] (Sec. 6.1). Therefore the identification of $K_L \to \pi e\nu$ decays is performed by using information from $K_L$ tracks and clusters, without requiring a reconstructed $K_L$ vertex.

#### *5.4.1 Selection of $K_S \to \pi^0\pi^0$ events*

Events output of the *ksneut* [14] algorithm are considered. Tighter cuts are applied here to select a well reconstructed sample. Each photon cluster from $K_S$ is required to satisfy the following conditions:

The cluster is not associated to any track by the official TCA algorithm [19] (53a)

$$\text{Polar angle of the cluster position: } \left|\frac{z_{\rm CL}}{r_{\rm CL}}\right| \leq \cos 21^\circ \tag{53b}$$

$$\text{Cluster energy: } E_{\rm CL} \geq 10 \text{ MeV} \tag{53c}$$

$$\text{Cluster "velocity": } 0.9 \leq \frac{r_{\rm CL}}{c \cdot T_{\rm CL}} \leq 1.2 \tag{53d}$$

Only events with four such clusters are retained. In order to reject events with actually three $\gamma$'s entering the calorimeter and one photon cluster split in two, a cut is applied on the minimum mutual distance $r_{\rm ij}^{\rm min}$ between a pair of prompt clusters:

$$r_{\rm ij}^{\rm min} \geq 20\,{\rm cm} \tag{54}$$

[7] The selection of $K_S \to \pi^0\pi^0$ decays guarantees the presence, in each event, of only two tracks coming from the IP, exactly as in $K_S \to \pi e\nu$-$K_{\rm crash}$ events. $K_L \to \pi e\nu$ prompt decays in $K_S \to \pi^+\pi^-$ events should have lower vertex efficiency, due to a higher multiplicity of tracks from the IP.

For each cluster pair (ij), energies and positions are used to calculate the invariant mass:

$$M_{\gamma\gamma}^{ij} = 2E_{CL}^{i}E_{CL}^{j}\left(1 - \mathbf{r}_{CL}^{i}\cdot\mathbf{r}_{CL}^{j}\right) \tag{55}$$

The $K_S$ invariant mass $M_S$ is also computed. The following cuts have to be satisfied:

$$\left|M_{\gamma\gamma}^{12,34} - M_{\pi^0}\right| < 40\,\mathrm{MeV} \tag{56a}$$

$$|M_S - M_{K^0}| < 100\,\mathrm{MeV} \tag{56b}$$

*5.4.2 Preliminar selection of charged $K_L$ decays*

The identification is performed requiring two tracks coming from IP associated to EmC clusters. $K_L$ particles are then identified through a time of flight technique.

For each track, the acceptance cuts of Eqs. 21 and (23a)–(23c) are imposed [8]. The tracks are also extrapolated backward toward the IP, and are required to intersect the DC inner wall in some point of the extrapolated path. In order to reject tracks badly reconstructed or due to machine background, tracks with lenght greater than 60 cm and with more than 20 hits are considered.

Only events with a single pair of oppositely charged tracks satisfying the above requirements and associated to calorimeter clusters are considered [9]. If one of the tracks is in the low-$p_t$, low $p_z$ region

$$P_t < 165 \text{ MeV AND } |p_z| < 50 \text{ MeV}$$

the event is rejected.

*5.4.3 Rejection of the residual background from $\phi \not\to K_SK_L$ events*

The selection applied to select $K_S \to \pi^0\pi^0$ events is significantly contaminated by background events. This is shown by the distribution of the transverse distance $\rho_v$ from the origin of the charged vertices in the selected events (Fig. 14). Vertices from $K_L$ decays are expected to be almost flatly distributed within the drift chamber wall. Therefore, the peak for $\rho_v < 2\,\mathrm{cm}$ is due to a residual background of prompt decays.

The velocity of the charged particles in these events is around $0.8c$, as obtained from cluster and track information, thus ruling out a possible $e^{\pm}$ contribution from $\pi^0$ Dalitz decay. The missing mass obtained from the two charged particles is greater than the $\pi^0$ mass, thus excluding a contribution from $\phi \to \pi^+\pi^-\pi^0$ decays. $\phi \to \eta\gamma$ decays (followed by $\eta \to \pi^+\pi^-\pi^0$) are rejected *ad hoc* by the *ksneut* algorithm, which only select events with prompt clusters of energy below 300 MeV.

The continuum process $e^+e^- \to \omega\pi^0 \to \pi^+\pi^-\pi^0\pi^0$ seems to fit with the observed background kinematics. The clusters are paired to obtain the best $\pi^0$ masses and the estimated laboratory $\pi^0$ energies $E_{\pi 0}$ are shown in the left panel of figure 15, calculated for different slices of the $\rho_v$ variable. The higher histogram (blu line) is obtained for events with $\rho_v < 2\,\mathrm{cm}$ (due both to signal and background). The other two histograms, for $2\,\mathrm{cm} < \rho_v < 4\,\mathrm{cm}$ and $4\,\mathrm{cm} < \rho_v < 6\,\mathrm{cm}$ are due to background-free $\phi \to K_SK_L$ decays. After the contribution of $\phi \to K_SK_L$ decays has been subtracted, the distribution of $E_{\pi 0}$ is shown in right panel of figure 15. The peak for $E_{\pi 0} \sim 220$ MeV corresponds to the monochromatic $\pi^0$ produced together with the $\omega$.

[8] At present we are computing acceptance efficiency *given* the vertex reconstruction whereas we should do the opposite. This can also be done in the future, but we are planning to completely relax the vertex requirement.

[9] If the pair of tracks is associated to the same EmC cluster, the event is rejected; these cases are usually due to the same particle which backscatters after hitting the calorimeter.

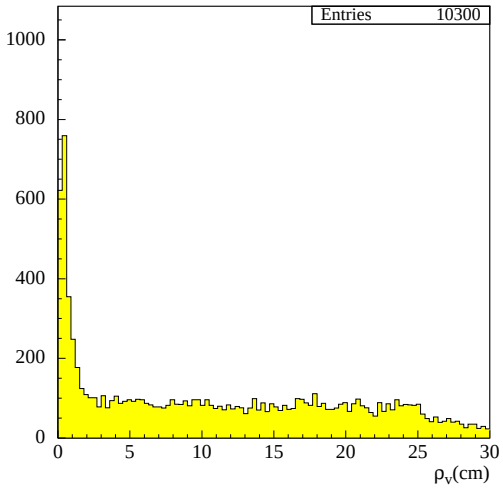


Figure 14: Distribution of the transverse distance $\rho_{\rm v}$ of charged vertices in events passing the $K_S \to \pi^0\pi^0$-selection described above.

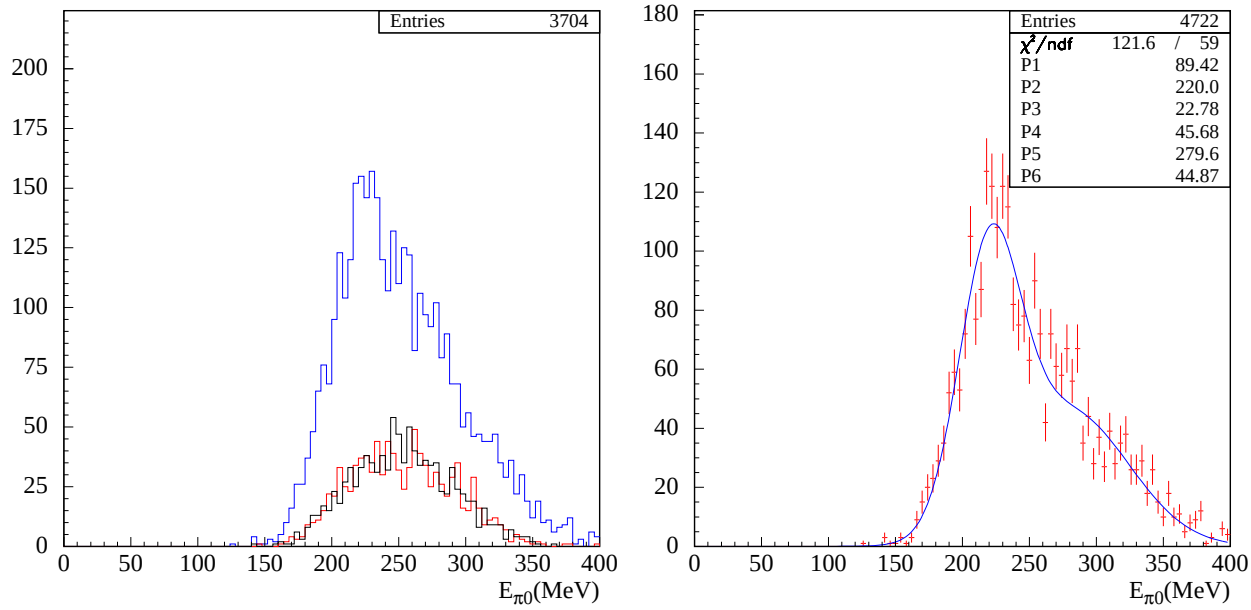


Figure 15: Left: laboratory energy of each $\pi^0$, for events with a vertex of transverse position $\rho_{\rm v} < 2\,{\rm cm}$ (higher histogram) and $2\,{\rm cm} < \rho_{\rm v} < 4\,{\rm cm}$, $4\,{\rm cm} < \rho_{\rm v} < 6\,{\rm cm}$ (lower histograms). These latter histograms represent the contribution of $\phi \to K_S K_L$ decays present in the former, and are subtracted from this. The right panel shows the background only.

The invariant mass $M_\omega$ is calculated by using the two charged pion momenta and the momentum of each of the two $\pi^0$'s in turn. Both masses are shown in figure 16, calculated again in slices of $\rho_v$ (left panel) and after the signal subtraction (right panel). Again a peak can be observed around the $\omega$ mass.

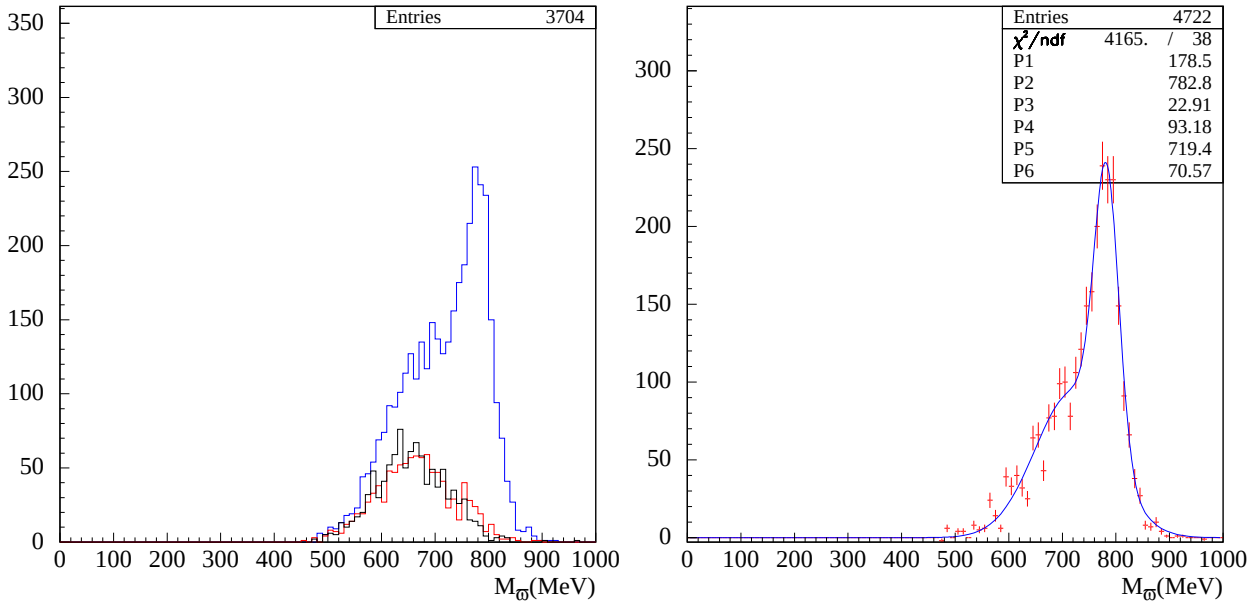


Figure 16: Left: invariant mass of the $\pi^+\pi^-\pi^0$-system, calculated in events with a vertex of transverse position $\rho_v < 2$ cm (higher histogram) and 2 cm $< \rho_v <$ 4 cm, 4 cm $< \rho_v <$ 6 cm (lower histograms). There are two entries per event, one for each $\pi^0$ in the final state. The right plot shows the background only.

The number of background events can be roughly obtained by assuming $\rho_v$ to be flatly distributed for the signal events. The average number of (mainly $\phi \to K_S K_L$) events in a 2-cm slice at $\rho_v > 2\,\mathrm{cm}$ ($N_K$) is subtracted from the number of those with $\rho_v < 2\,\mathrm{cm}$ ($N_P$). The ratio of background and $K_S K_L$ events is $(N_P - N_K)/N_K \sim 3.3$.

An expected value for this ratio can be calculated by using the cross section of production for this process, $\sigma \sim 7\,\mathrm{nb}$ [24], and by calculating the number of $\phi \to K_S K_L$ events in which the $K_L$ decays to charged particles within 2 cm from the IP, and the $K_S$ decays to two $\pi^0$'s. The result is:

$$R \sim \frac{7\mathrm{nb}}{3000\,\mathrm{nb} \times 1/3 \times 1/3 \times 0.8 \times 0.006} = 4.4$$

in a rough agreement with the observed ratio.

In order to reject these events, the following cut is applied:

$$|p_1| + |p_2| < 450\,\mathrm{MeV}, \tag{57}$$

where $p_i$ is the momentum of the $i^{th}$ charged track. The total momentum of the two $\pi^0$'s is also calculated. This is expected to be around 110 MeV for kaon decays. The observed distribution is shown in figure 17, as usual separately for different $\rho_v$-slices (left panel), and for the background (signal-subtracted, right panel). Events with total momentum greater than 140 MeV are rejected.

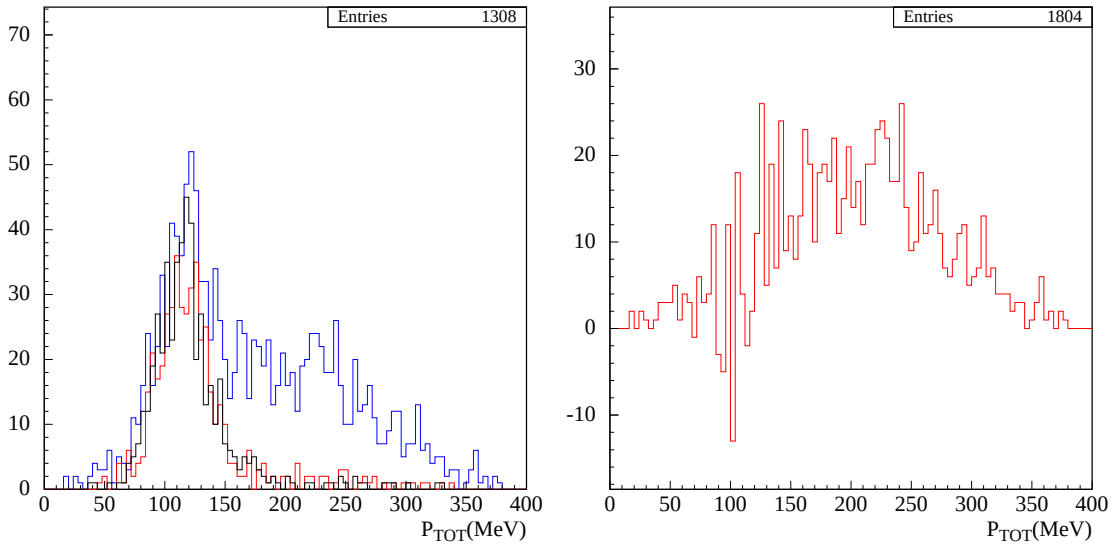


Figure 17: Left: total momentum of the $\pi^0\pi^0$-system, calculated in events with a vertex of transverse position $\rho_v < 2\,\text{cm}$ (higher histogram) and $2\,\text{cm} < \rho_v < 4\,\text{cm}$, $4\,\text{cm} < \rho_v < 6\,\text{cm}$ (lower histograms). The right plot shows the background distribution, after the signal has been subtracted.

*5.4.4 Final selection of $K_L \to \pi e\nu$ decays*

At the end, $K_L \to \pi e\nu$ events are identified among the $\phi \to K_S K_L$ sample. Since vertex information cannot be used, for each track the point of closest approach to the IP is used as starting point. The difference between measured and expected flight times is then computed for both tracks:

$$\delta T = T_{\text{CL}} - L_{\text{TRK}}/\beta c$$

where the total flight path $L_{\text{TRK}}$ is the sum of the track length, the length of the extrapolated path from the last hit to the calorimeter surface and from the first hit backward to the point of closest approach to the IP.

The variables $D\delta T$ of Eqs. (32), (33) are plotted in the left panel of Fig. 18 for both the mass hypotheses ($\pi$-$e$ vs. $e$-$\pi$). Events lying in the regions within the solid lines are selected.

At this level of the selection, residual background events contaminate the $K_L \to \pi e\nu$ sample, mainly $\omega\pi^0$, $K_L \to \pi\mu\nu$, and $K_L \to \pi^+\pi^-\pi^0$ final states.

Although the $D\delta T$ variable allows the most powerful identification of $e^\pm$ and $\pi^\mp$ tracks, other discriminating quantities has been used to reject the residual background:

- The difference between the cluster energy and the track momentum is shown in the central panel of Fig. 18, for the particle identified as an $e^\pm$, as a function of the $D\delta T$ value closest to zero. Events outside the superimposed ellipse are rejected.
- For each track, a $K_L$ flight path is estimated as the distance of closest approach of the track to the origin. The $K_L$ flight time is then subtracted from the time of the associated cluster, and the velocity $\beta$ of the particle is estimated. The $\beta$ value obtained for the track identified as an electron is shown as a function of that for the pion track in the right panel of Fig. 18.

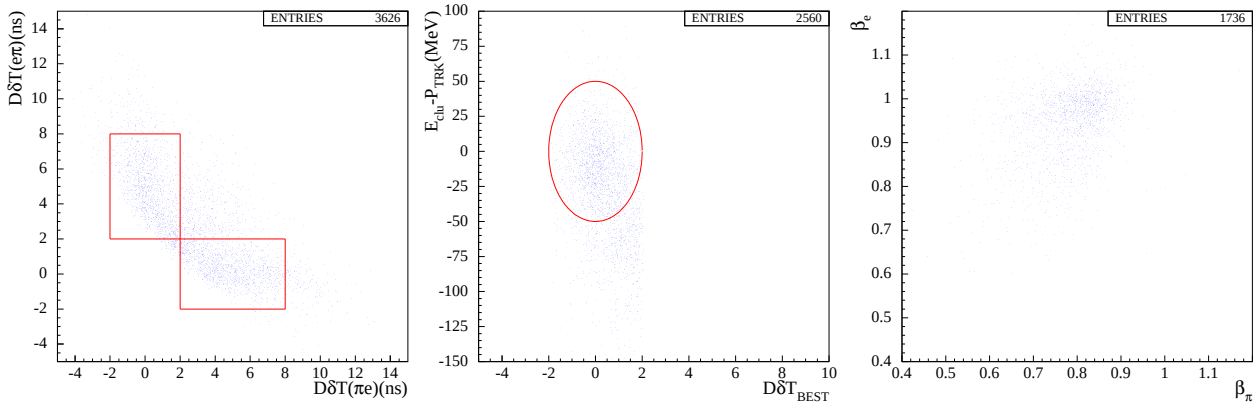


Figure 18: Right: $D\delta T$ variables for $\pi$-$e$ vs. $e$-$\pi$ assignments. Boxes delimiting the selected regions are superimposed. Center: difference between cluster energy and track momentum for the electron track, as a function of the lower $D\delta T$. Right: velocity estimated for the electron as a function of that for the pion.

## 6 Selection efficiency for $K_S \to \pi e \nu$ events

The total efficiency is expressed as a product of conditional probabilities:

$$\varepsilon_{\rm tot}^{\pi e\nu} = \varepsilon_{\rm crash}(E_{\rm cut}) \cdot \varepsilon_{\rm DCpre}^{\pi e\nu} \cdot \varepsilon_{\rm Extrap}^{\pi e\nu} \cdot \varepsilon_{\rm TCAT0trg}^{\pi e\nu} \cdot \varepsilon_{\rm TOF}^{\pi e\nu} \cdot \varepsilon_{\rm tag}^{\pi e\nu} \cdot \varepsilon_{\rm veto}^{\pi e\nu} \tag{58}$$

The logic scheme of the signal selection and of the efficiency estimate are sketched in figure 19. Contributions to the tagging and selection inefficiencies due to purely geometrical

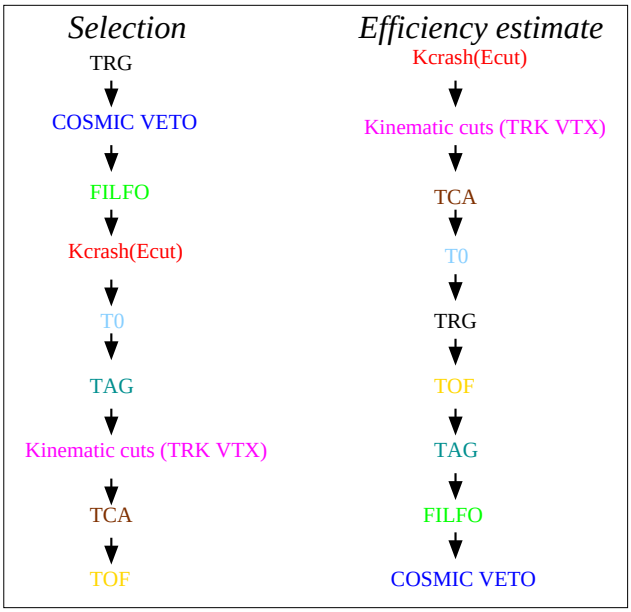


Figure 19: Logic scheme of the $K_S \to \pi e \nu$ selection and of the relative efficiency estimate.

effects have been estimated using MC simulation, while data have been used to estimate the corrections for tracking and trigger inefficiencies. The corrections for vertex reconstruction and time-of-flight $\pi$-$e$ identification inefficiencies have also been evaluated using data.

The efficiency $\varepsilon_{\rm DCpre}$ to satisfy the DC preselection cuts is discussed in the following section. Efficiencies to trigger the event, to have a golden $t_0$ cluster, and to have both tracks extrapolated to the calorimeter and associated to EmC clusters are estimated as discussed in Sec. 6.2.

## 6.1 Efficiency of the drift chamber preselection

In this section, the estimate of the probability of satisfying the DC preselection cuts defined in Sec. 3.1 is discussed.

The efficiency is calculated for events with a $K_{\rm crash}$ cluster. The main correlation between the efficiencies for the DC-preselection and for the $K_{\rm crash}$-tag arises from the position of the $K_L$ decay: the efficiency for reconstructing $K_S$ tracks and vertices is lower (by a few percent [13]) if the $K_L$ decays into charged particles close to the IP. These topologies are absent if a $K_{\rm crash}$ cluster is found in the event; in this case, either the $K_L$ interacts/decays in the calorimeter material, or it decays in flight in the outermost region of the chamber.

The MC is used to compute the efficiency after application of the fiducial cuts, since these are fundamentally geometrical. The result is:

$$\varepsilon_{\rm DCpre}\,({\rm MC}) = (62.4 \pm 0.3)\,\% \tag{59}$$

Data- and MC-extracted tracking and vertex efficiencies are used to estimate scale corrections to the previous value:

$$\varepsilon_{\rm DCpre} = \varepsilon_{\rm DCpre}\,({\rm MC}) \cdot \langle C_{\rm 2tracks}\rangle \cdot \langle C_{\rm vertex}\rangle \cdot \langle C_{M_{\pi\pi}{\rm cut}}\rangle\,. \tag{60}$$

The estimates of the correction factors $\langle C\rangle$ are discussed in the following sections [Eqs. (62), (63), and (64)]. The final result for the efficiency of the DC preselection is:

$$\boxed{\varepsilon_{\rm DCpre} = (60.58 \pm 0.30_{\rm stat} \pm 0.90_{\rm syst})\,\% = (60.58 \pm 0.95)\,\%} \tag{61}$$

### *6.1.1 Tracking efficiency*

The efficiency to reconstruct the tracks of charged particles has been estimated, as discussed in detail in [9], for pion tracks *coming from the IP* [namely satisfying the cuts of Eqs. (37), (38), (23a), and (23b)], in $K_S \to \pi^+\pi^-$ decays. Events with a $K_S \to \pi^+\pi^-$ decay and an identified $K_{\rm crash}$ cluster can be indeed cleanly selected requiring *at least* one reconstructed $\pi^\pm$ track. The momentum of the *not observed* $\pi^\mp$ can be estimated by closing the kinematics at the $K_S$ vertex. The ratio of data and Monte Carlo tracking efficiencies is shown in the left panels of figure 20, as a function of the estimated polar angle $\theta$ of emission. Due to the presence of spurious hits in the innermost layer of the chamber, the plateau value of the data/MC efficiency ratio is sensitive to the value of the cut on the transverse position of the first hit [Eq. (37)], used in the track selection of the $K_S \to \pi^+\pi^-$ sample. This dependence is shown in the right panel of figure 20. For this reason, this cut has been applied in the selection of $K_S \to \pi e\nu$ decays as well as in that of $K_S \to \pi^+\pi^-$ events.

For a fixed particle momentum, the tracking efficiency is not expected to be much different for electron or pion tracks [10].

[10] The contribution of the multiple scattering is actually dependent on the particle type (through the velocity). Nevertheless, for velocities $\beta > 0.7$ the (pion) tracking efficiency has been observed not to vary, at the percent level, if the multiple scattering contribution is not taken into account at all in the fit.

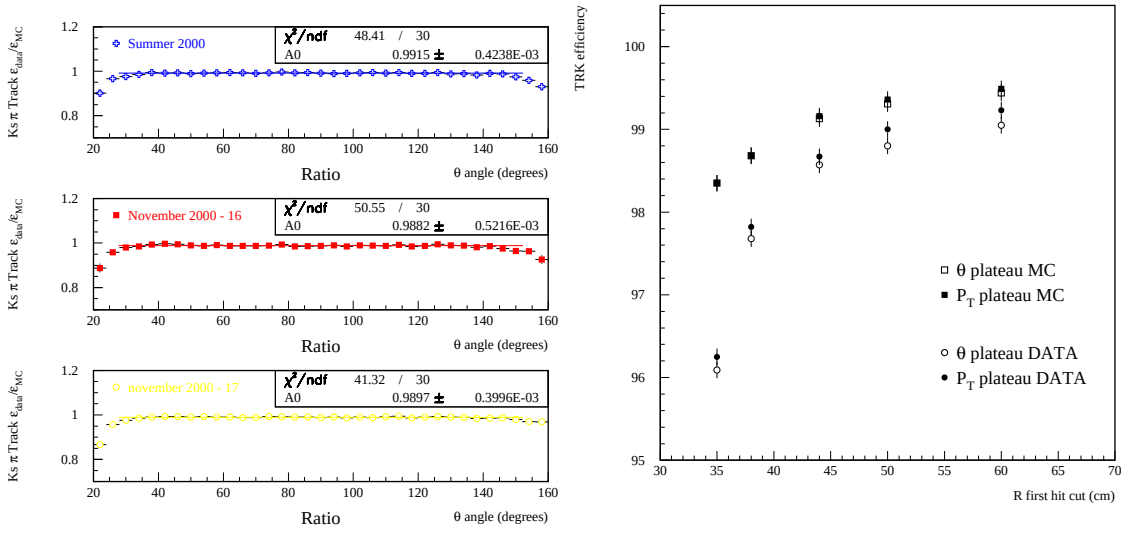


Figure 20: The ratio of data and Monte Carlo tracking efficiencies is shown as a function of the polar angle for $\pi^{\pm}$ tracks (left panels). The plateau value is estimated through a fit to a costant. In the right panel, the plateau-value of the $\theta$ and $p_{\rm t}$ projections is shown as a function of the cut on the transverse position of the first hit in the drift chamber ($R_{\rm first}$), for summer 2000 data (circles) and for Monte Carlo (squares). Both the $p_{\rm t}$ (open symbols) and $\theta$ (full symbols) plateau-values are shown: the data/MC efficiency ratio diminishes as the $R_{\rm first}$ cut is tightened, because of the reduced cell efficiency in the inner layers of the chamber.

The ratio data/Monte Carlo of the tracking efficiencies is seen to be dependent on the track transverse momentum or the polar angle of emission, only in the the low-$p_{\rm t}$ (low-$\theta$) region. This region is more populated in $K_S \to \pi e\nu$, by the $e^{\pm}$ tracks, than in $K_S \to \pi^+\pi^-$ decays. The contribution of this kinematical region remains still to be accurately studied [11].

The data/MC ratio of efficiencies is applied as a correction for both the $\pi^{\pm}$ and $e^{\pm}$ tracks. The plateau value of this efficiency ratio is $(99.0 \pm 0.1_{\rm stat})\%$. For $e^{\pm}$ tracks, the 1% difference from unity is taken as a conservative estimate of the systematic error. For $\pi^{\mp}$ tracks, the statistical error is used. The correction factor of Eq. (60) is:

$$\langle C_{2\rm tracks} \rangle = \underbrace{(99.0 \pm 0.1)\,\%}_{\pi^{\pm}\ \text{tracks}} \cdot \underbrace{(99 \pm 1)\,\%}_{e^{\mp}\ \text{tracks}} = (98 \pm 1)\,\% \qquad (62)$$

*6.1.2 Vertex efficiency*

Data and MC vertex efficiencies are estimated by using the sample of $K_L \to \pi e\nu$-$K_S \to \pi^0\pi^0$ events selected as explained in Sec. 5.4. The fraction $\varepsilon_{\rm vtx}$ of the selected events in which a vertex is reconstructed is the estimated efficiency. These estimates are obtained **integrating over all $K_L \to \pi e\nu$ events, which are flatly distributed within the DC wall.**

Although $K_S \to \pi e\nu$ and $K_L \to \pi e\nu$ decays are expected to have exactly the same kinematics, the flatness of the $K_L$ spatial distribution affects the angular distribution of

[11] Radiative Bhabha events, with an emitted photon of relevant energy could be used as source of low-$p_{\rm t}$ $e^{\pm}$ from the origin to study this problem.

the tracks which enter the chamber: the higher is the distance of the decay point from the IP, the smaller is the minimum $\theta$ (or $p_t$) value of the fitted tracks. This affects the value of $\varepsilon_{\rm vtx}$ more for data than for Monte Carlo, as shown in Fig. 21. Monte Carlo and data efficiencies are compared as a function of the minimum polar angle $\theta_{\rm min}$ of the two tracks (left panel). The data/MC efficiency ratio decreases with $\theta_{\rm min}$ (right panel). For

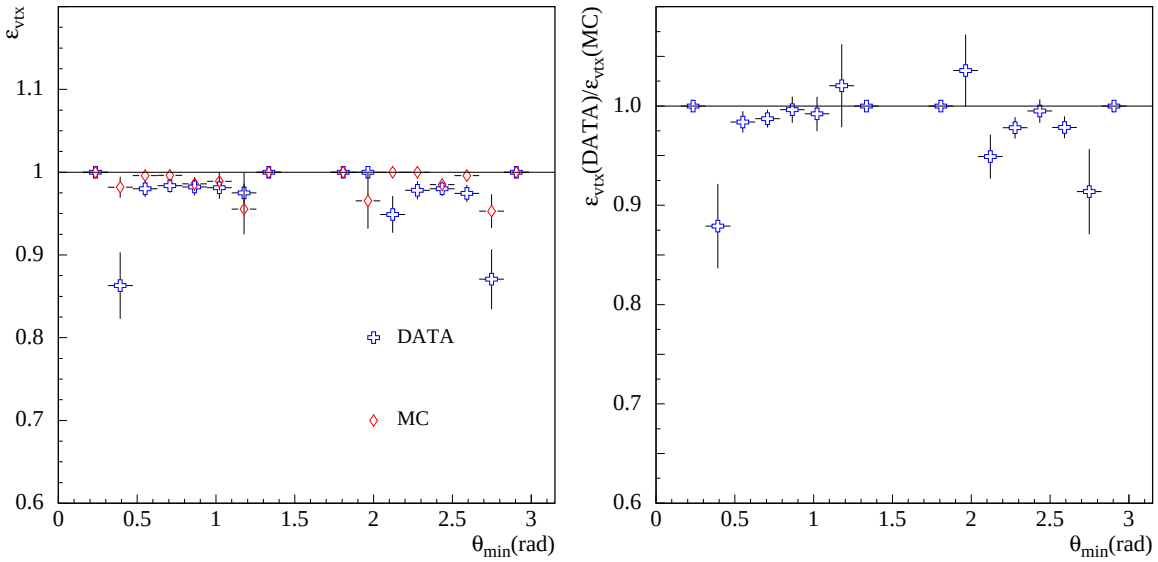


Figure 21: Data and MC vertex reconstruction efficiencies (left panel), and their bin-by-bin ratio (right panel) are shown as a function of the polar angle of the more beam-collinear track.

this reason, an additional angular cut is applied, which requires each $K_L$ track to lie in the same $\theta$ interval used for the $K_S \to \pi e \nu$ selection [this interval is effectively fixed by the cut of Eq. (23b)].

In order to make sure that the dependence of $\varepsilon_{\rm vtx}$ on the $K_L$ decay position can be neglected, the data distribution of the *found* vertices is scaled for the $K_L$ spatial distribution from the selected MC events. The ratio $N_{\rm vtx}^{\rm DATA}/N_{\rm true}^{\rm MC}$ is plotted in the left panel of Fig. 22, as a function of the transverse position $\rho_{\rm vtx}$ of the decay vertex. This can be considered as $\varepsilon_{\rm vtx}$ for data in arbitrary units, if the data and MC distributions of the $K_L$ decay position *before the vertex is reconstructed* coincide. No evident dependence of $N_{\rm DATA}/N_{\rm MC}$ on $\rho_{\rm vtx}$ is present, as the superimposed linear fit shows. [12)]

As an alternative way, the depencence of $\varepsilon_{\rm vtx}$ on the $K_L$ decay position for the selected events *before the vertex is reconstructed* has been studied by calculating a "raw" estimate of the vertex position. The momenta of the $K_L$ track pair are extrapolated to the point of mutual closest approach in the transverse plane. $\varepsilon_{\rm vtx}$ is plotted in the right panel of Fig. 22, as a function of the transverse position $\rho_{\rm raw}$ of this raw vertex. Events with badly reconstructed tracks can have values of $\rho_{\rm raw}$ as a high as 30–60 cm, despite of the fact that each $K_L$ track is required to start from within the DC wall. Therefore, a negative correlation between $\rho_{\rm raw}$ and $\varepsilon_{\rm vtx}$ is to be expected. The Monte Carlo efficiency

[12)] The bin for $\rho_{\rm vtx} < 1$ cm should not be taken into account. It is seldom populated by MC events, due to the Gaussian distribution of the $\phi$ decay vertex around the origin. It is much more populated for data, due to the spatial resolution of the reconstructed vertices.

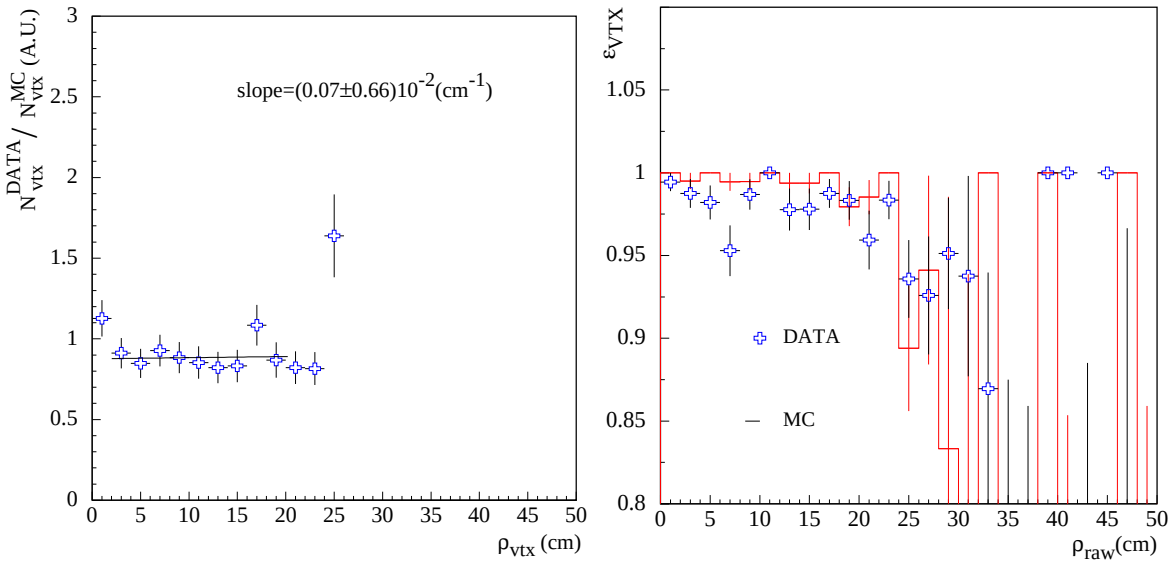


Figure 22: The data distribution of the found vertices corrected for the MC $K_L$ decay population is shown in the left panel, as a function of the transverse position $\rho_{\rm vtx}$ of the $K_L$ vertices. The result from a linear fit is superimposed. The vertex reconstruction efficiency is shown in the right panel, as a function of the trasverse position $\rho_{\rm raw}$ of the "raw" $K_L$ vertex.

is actually reasonably independent of $\rho_{\rm raw}$,

$$\varepsilon_{\rm vtx}({\rm MC}) = (98.8 \pm 0.2_{\rm stat})\,\%.$$

The correlation for real data is instead shown by calculating the data efficiency in the region $\rho_{\rm raw} < \rho_{\rm max}$ for various $\rho_{\rm max}$ values (Fig. 23). The central value and the half width of the interval spanned by $\varepsilon_{\rm vtx}$ as $\rho_{\rm max}$ varies are the estimated efficiency and systematic error, respectively:

$$\varepsilon_{\rm vtx}({\rm DATA}) = (97.8 \pm 0.3_{\rm stat} \pm 1.0_{\rm syst})\,\%.$$

Combining the previous results, the scale correction factor of Eq. (60) is obtained:

$$\langle C_{\rm vertex} \rangle = (99 \pm 1)\,\% \tag{63}$$

The above systematic error also takes into account the effect of a residual background from $K_L \to \pi\mu\nu$ decays in the selected sample. This contamination results to be of $\sim 18\%$, as determined using the Monte Carlo. The presence of $K_L \to \pi\mu\nu$ events is shown by the distribution of electron velocities $\beta_{\rm e}$, shown in the left panel of Fig. 24. $K_L \to \pi\mu\nu$ decays populate the region $\beta < 0.9$. Poorly reconstructed electron velocities (due to the PCA approximation used in the $\beta$ calculation) can populate this region, as well. The dependence of $\varepsilon_{\rm vtx}$ on $\beta$ is shown in the right panel of Fig. 24. Differences at level of 1–2% are observed comparing the average efficiencies calculated in $\beta$ slices: the efficiency is higher in the electron-region ($\beta \sim 1$) than in the low-$\beta$ region. Assuming that this effect is completely determined by $K_L \to \pi\mu\nu$ contamination, we estimate an error of 0.4% on the $K_L \to \pi e\nu$ vertex efficiency.

*6.1.3 Correction for the inefficiency of the $M_{\pi\pi}$ cut*

Another possible systematic effect on the MC estimate of Eq. (59) could derive from the kinematical cuts which are applied in both the invariant mass $M_{\pi\pi}$ and the

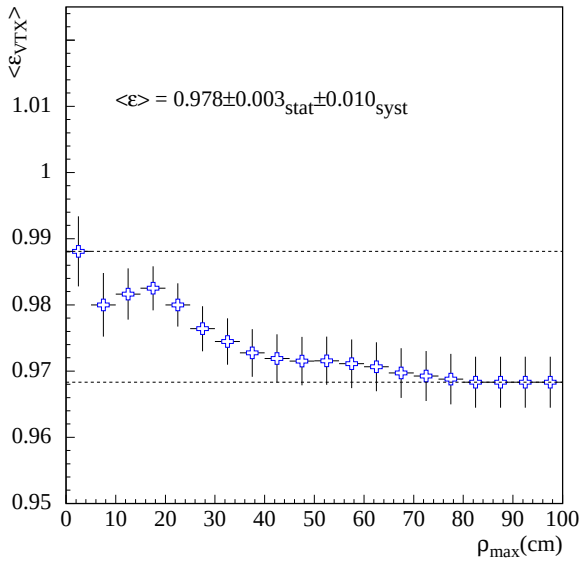


Figure 23: The data vertex reconstruction efficiency in the region $\rho_{\rm raw} < \rho_{\rm max}$ is plotted as a function of the cut position $\rho_{\rm max}$. The dashed lines delimit the interval spanned by $\varepsilon_{\rm vtx}$. The central value and the half width of this interval are the estimated efficiency and systematic error, respectively.

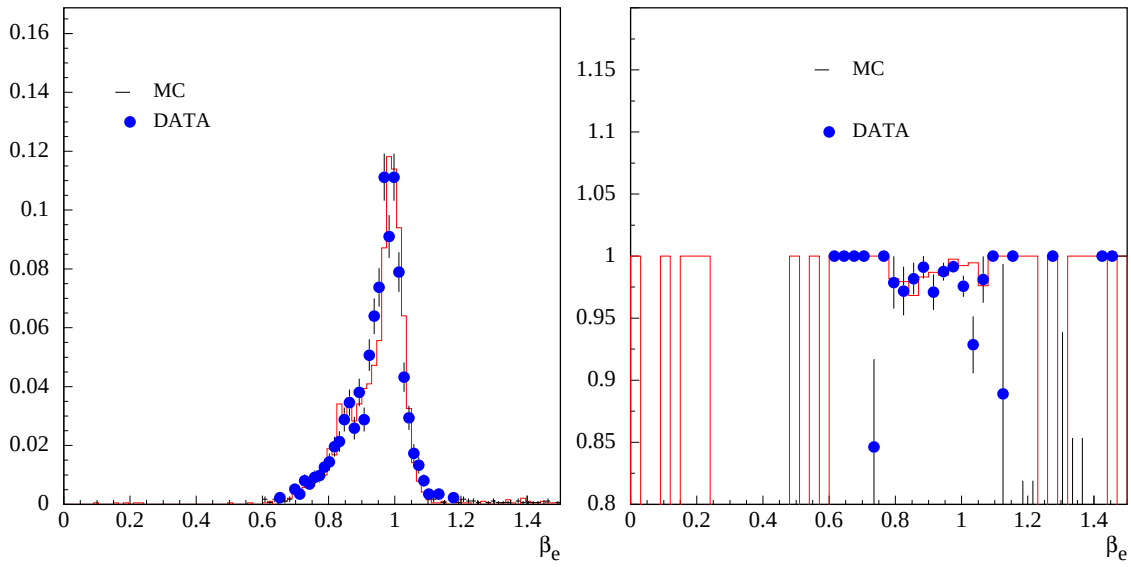


Figure 24: Left: distribution of the velocity ($\beta$) for $e^{\pm}$ tracks in events selected as $K_L \to \pi e \nu$ for data (dots) and Monte Carlo (solid line). Right: vertex efficiency calculated in slices of $\beta$, for data (dots) and Monte Carlo (solid line).

$K_S$ momentum $P_S$ (Fig. 5). Different resolutions in these variables for data and Monte Carlo lead to a systematic error in the Monte Carlo efficiency estimate. Actually, the efficiency only depends on the upper threshold of the $M_{\pi\pi}$ cut, while it is practically independent of the positions of the other boundaries. The representativeness of the Monte Carlo invariant-mass resolution has been checked by comparing the widths of the $K_S$ mass peaks for $K_S \to \pi^+\pi^-$ data and Monte Carlo events: these are 940 KeV and 800 KeV, respectively. The $M_{\pi\pi}$ distribution from $K_S \to \pi e\nu$ Monte Carlo events is essentially a Gaussian with a standard deviation of $\sim$50 MeV. The variation in the efficiency observed when a Gaussian smearing is applied is negligible:

$$\langle C_{M_{\pi\pi}\mathrm{cut}} \rangle \sim 1 - 1 \cdot 10^{-4} \tag{64}$$

### 6.2 Extrapolation, TCA, $t_0$, and trigger efficiencies

$\varepsilon_{\mathrm{extrap}}$ is the probability for having both $K_S$ tracks satisfying the conditions of Eqs. (23a)–(23c) when extrapolated to the calorimeter. It is expressed as the product

$$\varepsilon_{\mathrm{extrap}} = \varepsilon_{\mathrm{toEmC}} \cdot \varepsilon_{\mathrm{categ}} \tag{65}$$

of the probabilities

1. $\varepsilon_{\mathrm{toEmC}}$ to extrapolate the first (or second, for the *Kink* category) track segment to the calorimeter, and
2. $\varepsilon_{\mathrm{categ}}$ to have both tracks of the *Golden* or *Kink* categories [the condition of Eq. (23c)].

All of the categories are used when performing the extrapolation, including the *Other* category; so $\varepsilon_{\mathrm{toEmC}}$ becomes a purely geometrical acceptance and is estimated by directly using the Monte Carlo. The result is:

$$\varepsilon_{\mathrm{toEmC}} = (51.1 \pm 0.2_{\mathrm{stat}})\,\% \tag{66}$$

The second quantity has been estimated together with the TCA, $t_0$, and trigger efficiencies both by directly using the $K_L \to \pi e\nu$ sample selected as described in Sec. 5.1, and by plugging the single-track efficiencies derived from the samples of Secs. 5.2 and 5.3 into the Monte Carlo. These approaches are referred to as "method 1" and "method 2" in the following and are discussed in the following two sections.

In both methods, the trigger efficiency *given the* $t_0$ is actually calculated by combining the probability $\varepsilon_{\mathrm{S|T0}}(\geq 1)$ for the $K_S$ to fire one or more trigger sectors with the probability $\varepsilon_{\mathrm{L|T0}}(\geq 2)$ for the $K_{\mathrm{crash}}$ to fire two or more sectors: [13)]

$$\varepsilon_{\mathrm{TRG|T0}} = \varepsilon_{\mathrm{L}}(\geq 2) + \varepsilon_{\mathrm{L}}(1)\,\varepsilon_{\mathrm{S|T0}}(1) \tag{67}$$

$\varepsilon_{\mathrm{S|T0}}(\geq 1)$ is estimated by applying either method 1 and 2, while $\varepsilon_{\mathrm{L|T0}}(\geq 2)$ has been estimated by using $K_S \to \pi^0\pi^0$ events as discussed in detail in ref. [9] ($\varepsilon_{\mathrm{L|T0}}(\geq 2) \sim 40\%$).

The results from the two methods are discussed and compared in Sec. 6.2.3

#### *6.2.1 Method 1: prompt $K_L \to \pi e\nu$ decays*

In method 1, direct use is made of the unbiased $K_L \to \pi e\nu$, $K_S \to \pi^+\pi^-$ sample. The efficiencies associated with a cut are estimated as the fraction of events passing it (on a sample in which the previous cuts are satisfied). The efficiency estimates follow the

[13)] Remember that the $K_{\mathrm{crash}}$ always fires at least one trigger sector on the barrel; so it is sufficient to estimate the probabilities for the $K_S$ to fire at least one sector, and for the $K_L$ to fire at least two.

chosen order of Fig. 19. TCA efficiency is obtained counting the fraction of selected events with two associated $K_L$ tracks. The presence of kinks is handled as in the selection of $K_S \to \pi e\nu$ events (Sec. 3.2). Given TCA, we count the fraction of events with at least one of the two associated clusters satisfying the $t_0$ cluster condition. Finally, we count how many times at least one calorimeter trigger sector is fired by a cluster from $K_L \to \pi e\nu$. This last step is performed rejecting events with $K_S$ and $K_L$ clusters contributing to the same trigger sector. The results are listed in table 4.

*6.2.2 Method 2: single particle efficiencies and MC convolution*

In method 2, the single-particle efficiencies $\rho_{\rm TCA}$ for associating a track to an EmC cluster are extracted from the samples described in Secs. 5.2 and 5.3. These efficiencies are then are histogrammed in the transverse and longitudinal momentum of the tracks. Separate histograms are created for tracks hitting the barrel and endcap calorimeters, as well as for *Golden* ($\pi^+$, $\pi^-$) and *Kink* ($\mu^+$, $\mu^-$) tracks of each sign of charge, and for *Golden* electron tracks.[14] Some of these efficiencies are plotted in figure 25.

A similar treatment has been applied to estimate the efficiencies $\rho_{\rm T0}$ for producing a golden-$t_0$ cluster (expressed as a function of the momentum $P$ of the track at first hit and of the cosine of the impact angle with respect to the normal to the calorimeter) and $\rho_{\rm Sett|T0}$ ($\rho_{\rm Sett|\overline{T0}}$) for firing a trigger sector having (not having) found the $t_0$ cluster (as a function of $P$ and of the coordinate of the impact point along the fibers, $Z/Y$ for barrel/endcap).

The separate treatment of endcap/barrel efficiencies is motivated by the fact that, for a fixed $p_{\rm t}$ $p_{\rm z}$ couple, the hit detector depends by the decay vertex position; this is uniformly distributed for the $K_L \to \pi e\nu$ control sample needed to estimate the electron efficiencies, while it is peaked close to the IP in $K_S$ or $\phi$ decays. Besides, barrel and endcap "sector" efficiencies have to be separated, since the thresholds profiles are different. Actually, trigger efficiencies are also divided for the endcap into the 3 threshold zones (hot, warm, and cold) defined in ref. [7].

$t_0$ and sector efficiencies are plotted in figures 26 and 27 for *Golden* pion tracks.

The above efficiencies are then used to weight the Monte Carlo simulated $K_S \to \pi e\nu$ decays. For a single MC event passing the DC preselection, $K_S$ tracks are extrapolated toward the calorimeter by using the method of Sec. 3.2. Pions and electrons are identified from the Monte Carlo truth. *For a single MC event,* the joint probability for associating both tracks to clusters, for having at least a golden-$t_0$ cluster, and for firing at least one trigger sector are then calculated:

$$\varepsilon_{\rm TCA}\,(\text{event}) = \rho^{\pi,\mu}_{\rm TCA} \cdot \rho^{\rm e}_{\rm TCA} \tag{68a}$$

$$\varepsilon_{\rm T0TCA}\,(\text{event}) = \rho^{\pi,\mu}_{\rm TCA} \cdot \rho^{\rm e}_{\rm TCA} \cdot (\rho^{\pi,\mu}_{\rm T0} + \rho^{\rm e}_{\rm T0} - \rho^{\pi,\mu}_{\rm T0} \cdot \rho^{\rm e}_{\rm T0}) \tag{68b}$$

$$\varepsilon_{\rm SettT0TCA}\,(\text{event}) = \rho^{\pi,\mu}_{\rm TCA} \cdot \rho^{\rm e}_{\rm TCA} \cdot \left(\rho^{\pi,\mu}_{\rm T0}\rho^{\pi,\mu}_{\rm Sett|T0} + \rho^{\rm e}_{\rm T0}\rho^{\rm e}_{\rm Sett|T0} - \rho^{\pi,\mu}_{\rm T0}\rho^{\pi,\mu}_{\rm Sett|T0} \cdot \rho^{\rm e}_{\rm T0}\rho^{\rm e}_{\rm Sett|T0} + \ldots\right) \tag{68c}$$

where "..." indicates terms involving the probability for a track to fire a trigger sector without giving a $t_0$ cluster, which are not written here. Finally, the efficiencies are

[14] Different energy release are indeed observed in the calorimeter for $\pi^+$ and $\pi^-$ tracks of a given momentum, so the particle charge is taken into account. The pion and muon efficiencies are obtained by combining three samples: $K_S \to \pi^+\pi^-$, $\phi \to \pi^+\pi^-\pi^0$, and single pion tracks from $K_L \to \pi e\nu$ decays.

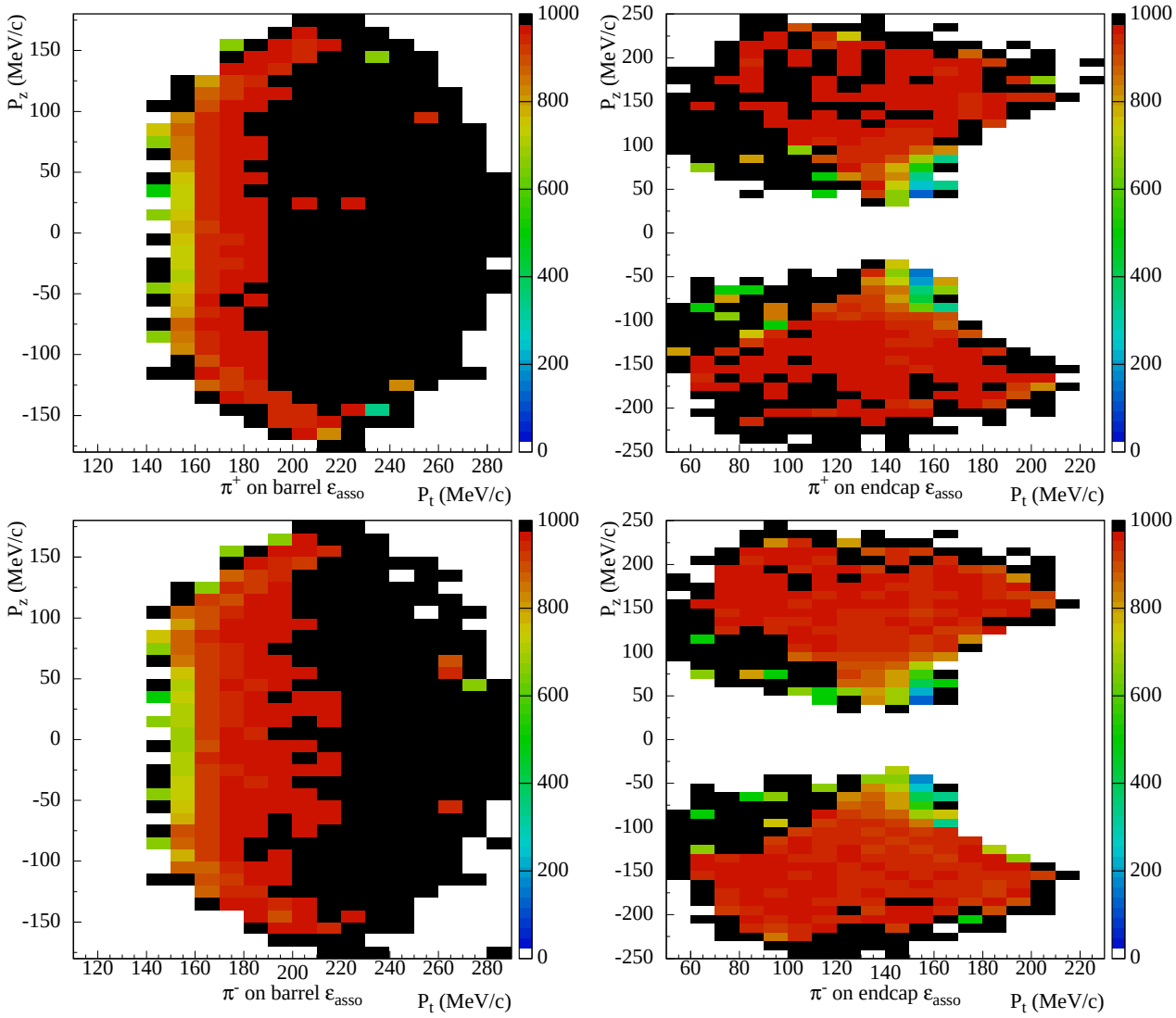


Figure 25: Efficiencies for associating a single $\pi^+$ ($\pi^-$) track are plotted in the upper (lower) panels as a function of the longitudinal ($p_z$) and transverse ($p_t$) momentum (the $z$ axis is in units of $10^3$). Tracks entering the barrel (left panels) and endcap (right panels) calorimeters are distinguished.

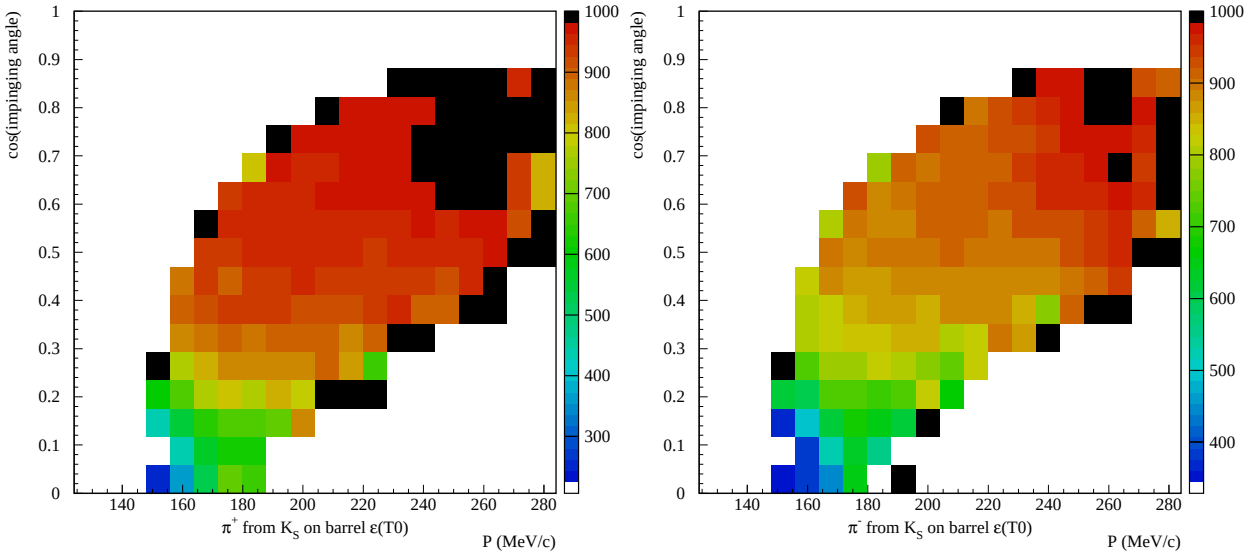


Figure 26: T0 efficiency as a function of the cosine of the impact angle of the track and of the track momentum, for $\pi^+$ (left) and $\pi^-$ (right) on the barrel calorimeter.

calculated by averaging over the Monte Carlo events, as follows:

$$\varepsilon_{\mathrm{TCA}} = \langle \varepsilon_{\mathrm{TCA}}\,(\mathrm{event}) \rangle \tag{69a}$$

$$\varepsilon_{\mathrm{T0|TCA}} = \frac{\langle \varepsilon_{\mathrm{T0TCA}}\,(\mathrm{event}) \rangle}{\langle \varepsilon_{\mathrm{TCA}}\,(\mathrm{event}) \rangle} \tag{69b}$$

$$\varepsilon_{\mathrm{S|T0}}(\geq 1) = \frac{\langle \varepsilon_{\mathrm{SettT0TCA}}\,(\mathrm{event}) \rangle}{\langle \varepsilon_{\mathrm{T0TCA}}\,(\mathrm{event}) \rangle} \tag{69c}$$

*6.2.3 Results and comparison of method 1 and 2*

The results from methods 1 and 2 are compared in table 4. The trigger efficiency is calculated by applying Eq. (67). The agreement between the methods is very good. The final efficiency estimates are obtained as the error-weighted average of the results

| Efficiency | Method 1 | Method 2 |
|---|---|---|
| $\varepsilon_{\mathrm{categ}}$ | $95.6 \pm 0.3$ | $95.9 \pm 0.1$ |
| $\varepsilon_{\mathrm{TCA}}$ | $92.0 \pm 0.5$ | $93.1 \pm 0.2$ |
| $\varepsilon_{\mathrm{T0\|TCA}}$ | $99.83 \pm 0.07$ | $99.6 \pm 0.1$ |
| $\varepsilon_{\mathrm{TRG\|T0TCA}}$ | $92.7 \pm 0.5$ | $92.3 \pm 0.5$ |
| $\varepsilon_{\mathrm{TCAT0TRG}}$ | $85.1 \pm 0.5$ | $85.6 \pm 0.5$ |

Table 4: Efficiency results from Method 1 and 2 are compared.

from both methods and the systematic error is given by the absolute difference. The efficiency for assigning tracks to any of the categories used in the analysis is $\varepsilon_{\mathrm{categ}} = (95.87 \pm 0.09)\,\%$. Combining this value with the efficiency $\varepsilon_{\mathrm{toEmC}}$ of Eq. (66), the final extrapolation probability is obtained:

$$\boxed{\varepsilon_{\mathrm{extrap}} = (48.99 \pm 0.20_{\mathrm{stat}} \pm 0.16_{\mathrm{syst}})\,\%} \tag{70}$$

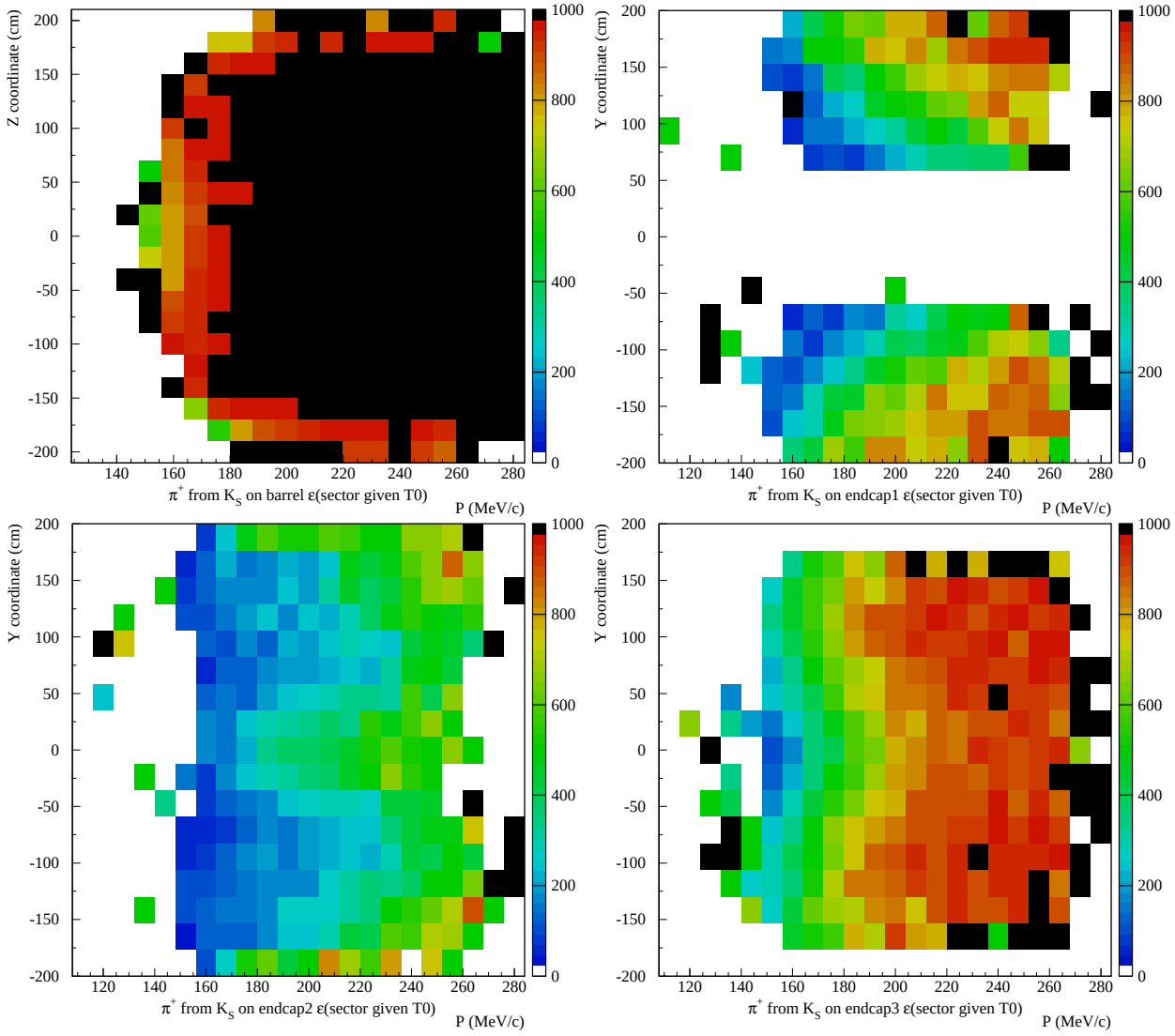


Figure 27: Sector efficiencies for $\pi^+$ tracks satisfying the golden-$t_0$ requirement [Eq. (15)]. $Z$-coordinate vs momentum for track on the barrel (up left), $Y$-coordinate vs momentum for track on the endcap for hot (up right), warm (down left), and cold (down right) trigger sector zones. The different effective-threshold profiles are visible.

The final efficiency for track to cluster association, $t_0$, and trigger is:

$$\boxed{\varepsilon_{\mathrm{TCAT0TRG}} = (85.35 \pm 0.35_{\mathrm{stat}} \pm 0.50_{\mathrm{syst}})\,\%} \tag{71}$$

A detailed discussion of the systematic errors associated with each of the two methods is given in the following two sections.

*6.2.4 Systematic errors: method 1*

The efficiency estimates are obtained directly from the sample of selected $K_L \to \pi e\nu$ decays before the DC wall (method 1). The systematic errors on the results listed in table 4 are discussed in this section.

Each efficiency $\varepsilon$ has been estimated as an average over the selected sample:

$$\varepsilon_{\mathrm{A}} = \frac{N_{\mathrm{sele}}\,(A)}{N_{\mathrm{sele}}} = \frac{\#\text{ Selected events in which A is true}}{\text{Total }\#\text{ of selected events}} \tag{72}$$

where the condition A is either the requirement that both tracks are associated to EmC clusters (TCA), or that there is at least one $t_0$ cluster ($t_0$), or finally that at least one trigger sector is fired by a $K_S$ cluster (Sett).

A first source of systematic deviation is the contamination in the selected $N_{\mathrm{sele}}$ events, mainly due to $K_L \to \pi\mu\nu$ decays. This is estimated to be as low as 0.3% using the Monte Carlo. The fractional contribution to the systematic error is then at most equal to this value.

All of the estimated efficiencies are observed to depend on the track momenta, as can been seen in figures 25, 26, and 27, which refer to single pion tracks. Hence, a second type of systematic error arises if the distribution of kinematic variables from the $N_{\mathrm{sele}}$ $K_L \to \pi e\nu$ events is different from that of true $K_S \to \pi e\nu$ events. This kinematic bias, in turn, could either be induced by the selection cuts, or be an effect of the distribution of $K_L$ vertices, which is practically flat within the DC wall.

The error on $\varepsilon_{\mathrm{TCA}}$ has been estimated as follows. The distributions of the transverse ($P_{\mathrm{t}}$) and longitudinal ($P_{\mathrm{z}}$) track momenta from $K_L \to \pi e\nu$ (data) and $K_S \to \pi e\nu$ (Monte Carlo) events *before the track-to-cluster association is required* have been compared. This comparison is made separately for pions and electrons. The distributions shown in figure 28 are obtained as follows:

- Monte Carlo $K_S \to \pi e\nu$ events are selected by requiring the $K_{\mathrm{crash}}$ tag, the DC preselection cuts (Sec. 3.1), and the extrapolation cuts of Eqs. (23a)–(23c) to be satisfied. Distributions of electron and pion momenta are then obtained according to the Monte Carlo truth.
- The data $K_L \to \pi e\nu$ sample has been selected without requiring the track-to-cluster association, but TCA is necessary in order to identify pion and electron tracks. Let $d_{\pi(\mathrm{e})}\,(\mathrm{i},\mathrm{j})$ be the number of events in the bin i, j of the $P_{\mathrm{t}} \otimes P_{\mathrm{z}}$ plane for pion(electron) tracks identified by requiring TCA and by applying a TOF technique. The corresponding population $D_{\pi(\mathrm{e})}\,(\mathrm{i},\mathrm{j})$ *before the TCA is required* is obtained by correcting for the single-particle association efficiency $\varepsilon_{\pi(\mathrm{e})}\,(\mathrm{i},\mathrm{j})$, computed as discussed for method 2:

$$D_{\pi(\mathrm{e})}\,(\mathrm{i},\mathrm{j}) = \frac{d_{\pi(\mathrm{e})}\,(\mathrm{i},\mathrm{j})}{\varepsilon_{\pi(\mathrm{e})}\,(\mathrm{i},\mathrm{j})} \tag{73}$$

Some difference between the data and Monte Carlo distributions can be observed in figure 28, especially in the low-$P_{\mathrm{t}}$ region. The associated systematic error $\Delta\varepsilon_{\mathrm{TCA}}$ is calculated as the quadrature sum of the contributions from pions and electrons. These, in

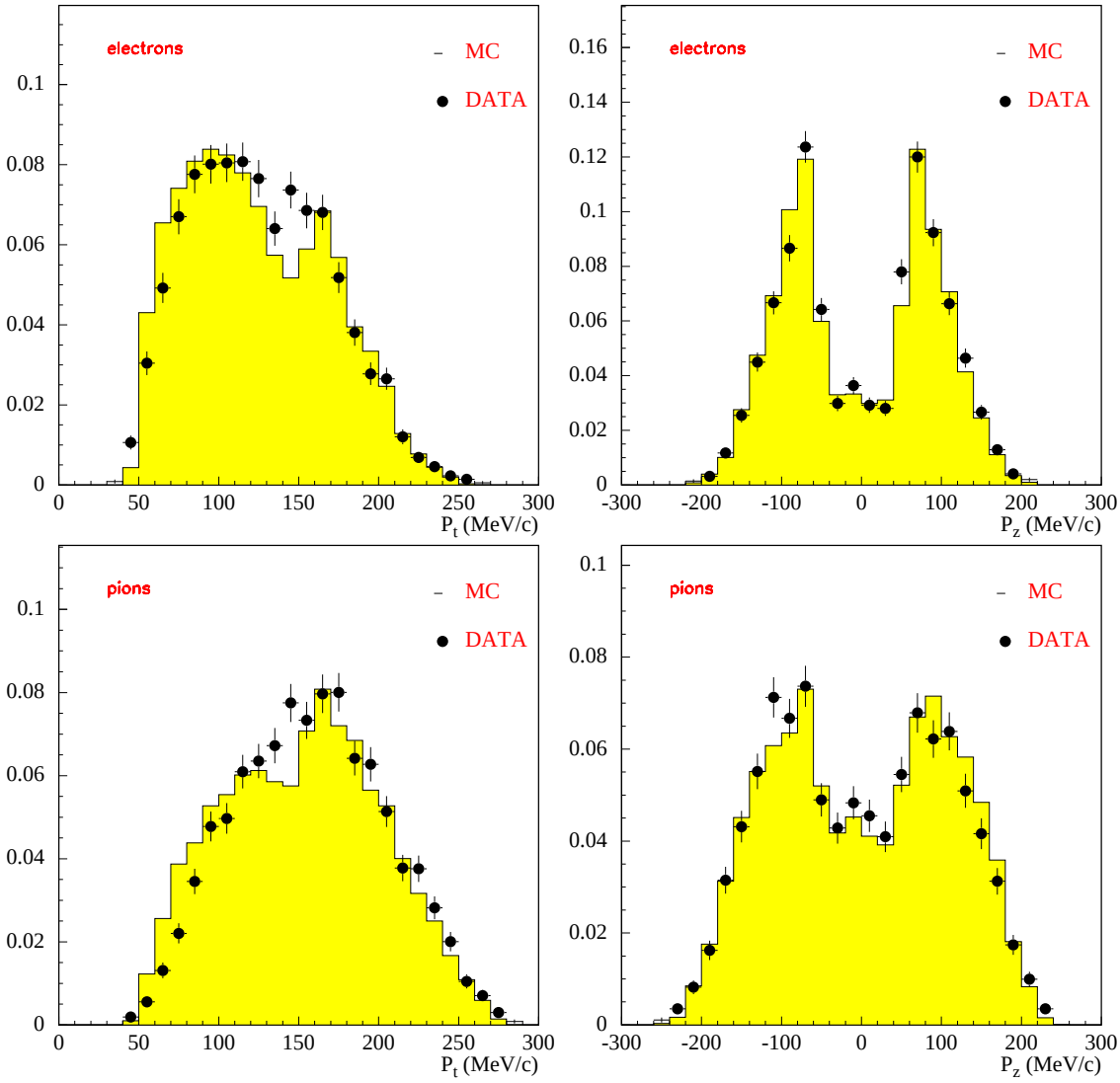


Figure 28: Distributions of transverse (left panels) and longitudinal (right panels) momenta for electron (top panels) and pion (bottom panels) tracks from $K_L \to \pi e\nu$ data (solid circles) and $K_S \to \pi e\nu$ Monte Carlo (solid line) events before TCA is required. All of the distributions are normalized to unity.

turn, are obtained by weighting the difference between data $[D_{\pi(\mathrm{e})}(i,j)]$ and Monte Carlo $[M_{\pi(\mathrm{e})}(i,j)]$ distributions with the single-particle TCA efficiency $\varepsilon_{\pi(\mathrm{e})}(i,j)$, and summing over the bins $i,j$ of the $P_\mathrm{t} \otimes P_\mathrm{z}$ plane:

$$\delta\varepsilon_{\pi(\mathrm{e})} = \sum_{i,j} \varepsilon_{\pi(\mathrm{e})}(i,j) \cdot \Big[ M_{\pi(\mathrm{e})}(i,j) - D_{\pi(\mathrm{e})}(i,j) \Big] \tag{74a}$$

$$\delta\varepsilon_{\mathrm{TCA}} = \sqrt{\delta\varepsilon_\pi^2 + \delta\varepsilon_\mathrm{e}^2} \tag{74b}$$

The following values have been obtained:

$$\begin{array}{c} \delta\varepsilon_\mathrm{e} = (2.1 \pm 3.5_{\mathrm{stat}}) \times 10^{-3} \\ \delta\varepsilon_\pi = (-1.0 \pm 4.5_{\mathrm{stat}}) \times 10^{-3} \end{array} \tag{75a}$$

$$\Delta\varepsilon_{\mathrm{TCA}} = (2.3 \pm 3.7_{\mathrm{stat}}) \times 10^{-3} \tag{75b}$$

*6.2.5 Systematic errors: method 2*

Three types of systematic uncertainties have been considered.

**1.** The efficiency $\varepsilon_{\mathrm{categ}}$ to have both tracks from $K_S \to \pi e\nu$ belonging to the *Golden* or *Kink* categories has been estimated from Monte Carlo. The effectiveness of the Monte Carlo in reproducing the populations of *Golden* or *Kink* categories for real events has been checked using a $K_S \to \pi^+\pi^-$ sample, as explained in Sec. 3.2.1. The uncertainty in the MC estimate of the inefficiency is as low as 0.4% (Table 2).

**2.** The efficiencies $\varepsilon_\mathrm{A}$ are obtained by averaging functions of the single particle efficiencies $\rho$ over Monte Carlo events [Eqs. (68) and (69)]. The efficiencies $\rho$ are binned in terms of DC kinematical variables. Two sources of error are then present: the statistical fluctuation in the population of each event configuration and the systematic error due to the uncertainties on the efficiencies $\rho$ plugged into the Monte Carlo. These errors are treated as follows.

Each Monte Carlo $K_S \to \pi e\nu$ event is defined by the set of variables used to parametrize the efficiencies $\rho$. For each track, the following variables are used:

$$\Big(\text{ particle type }\Big) \otimes \Big(\text{ barrel/endcap }\Big) \otimes \Big(\ P_\mathrm{t}, P_\mathrm{z}\ \Big) \otimes \Big(\ P, \cos\alpha_{\mathrm{impact}}\ \Big) \otimes \Big(\ P, z_{\mathrm{impact}}\ \Big) \tag{76}$$

The event configuration is fixed by the set of such variables for each of the 2 tracks. The estimated efficiencies can be expressed as an average over the event configurations:

$$\langle \varepsilon_\mathrm{A}(\text{event}) \rangle = \frac{\sum_{\{i\}} x_i \epsilon_i}{\sum_{\{i\}} x_i} \tag{77}$$

where $i$ runs over the event configuration space and $x_i$ is the Monte Carlo population of the configuration. The error on the efficiency is then calculated by propagating two contributions: first, the statistical error $\sigma_i = \sqrt{x_i}$ on the Monte Carlo populations, and second, the error $\delta_i$ on the event efficiency $\epsilon_i$ due to the finite statistics of the data samples used to estimate the single particle efficiencies. The total error is:

$$\delta\varepsilon^2 = \sum_{\{i\}} \left( \frac{\epsilon_i - \langle\varepsilon\rangle}{N} \right)^2 \sigma_i^2 + \sum_{\{i\}} \left( \frac{x_i}{N} \right)^2 \delta_i^2 \ , \tag{78}$$

where $N = \sum_{\{i\}} x_i$ is the total number of events. While the first term is linear in $x_i$ and can be easily summed event by event, the second one is quadratic in $x_i$, and can be calculated only after computation of the populations $x_i$.

The above formula has been actually applied separately for TCA, T0 and trigger sector efficiencies, in order to reduce the configuration space needed for the evaluation to a dimension lower than that in Eq. (76). The total relative error has been obtained as the quadrature sum of the separate contributions:

$$\left(\frac{\delta\varepsilon_{\rm TCAT0TRG}}{\varepsilon_{\rm TCAT0TRG}}\right)^2 = \left(\frac{\delta\varepsilon_{\rm TCA}}{\varepsilon_{\rm TCA}}\right)^2 + \left(\frac{\delta\varepsilon_{\rm T0|TCA}}{\varepsilon_{\rm T0|TCA}}\right)^2 + \left(\frac{\delta\varepsilon_{\rm TRG|T0TCA}}{\varepsilon_{\rm TRG|T0TCA}}\right)^2 \tag{79}$$

**3.** The $\rho$ efficiencies for electrons and positrons are estimated from $K_L \to \pi e\nu$ decays, selected as in Sec. 5.3. An error in the identification of particles therefore leads to a systematic error in the estimation of these efficiencies.
To estimate the contamination of pions in the electron sample, we exploit the two methods of particle-ID illustrated in Sec. 5.3. The first uses using only one clustering information (the $M^2$ and $\delta E$ variables of Fig. 13) and performs a particle-ID by using only the cluster of the *tagging* particle. The second uses the missing energy and momentum at the $K_L$ vertex, compares the two possible choices for the particles masses (Fig. 12), and can be only applied outside the overlapping region of the $E_{\rm miss} - P_{\rm miss}$ plane [defined in Eq. (52b)].

In order to count the fraction of wrongly identified particles, we used the first method to cross check the second and viceversa. In the left panel of Fig. 29, the variable $E_{\rm miss} - P_{\rm miss}$ is plotted (i: horizontal axis) as calculated using the pion identification obtained with the $M^2$-vs-$\delta E$ method and (ii: vertical axis) with the opposite choice of masses. The presence of events within the horizontal stripe ($-5\,{\rm MeV} < E_{\rm miss} - P_{\rm miss} < 5\,{\rm MeV}$) points to a misidentification of the $M^2$-vs-$\delta E$ method. The fraction of events at more than 10 MeV and less than $-10$ MeV in the right panel of Fig. 29 gives the probability to misidentify an $e^\pm$ using the $M^2$-vs-$\delta E$ method, and is $\sim 3\%$.

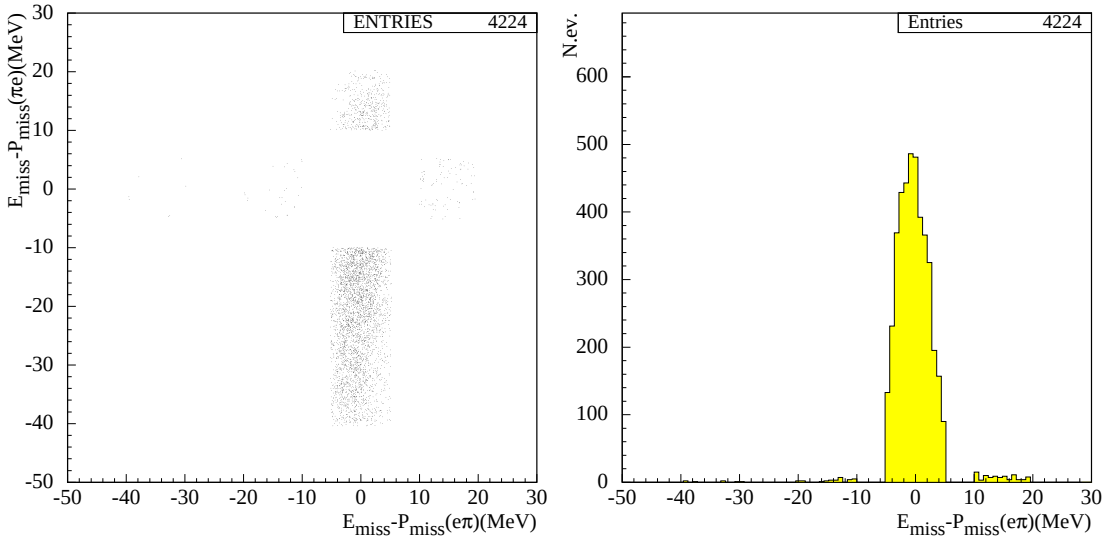


Figure 29: (Left) $E_{\rm miss} - P_{\rm miss}$ using the particle-ID from $M^2$-vs-$\delta E$ method (abscissa) compared with the opposite choice (ordinate). (Right) X-axis projection of the left plot.

On the same footing, we identify $\pi^\pm$ and $e^\mp$ first by using $E_{\rm miss} - P_{\rm miss}$, and then we plot the $M^2$ variable for the particle recognized as a pion with that for the other particle, assumed to be an electron (left panel of Fig. 30). Events correctly identified lie around $(0\,{\rm MeV}^2, 20\,000\,{\rm MeV}^2)$, while those with wrong particle assignements lie around

$(20\,000\,\mathrm{MeV}^2, 0\,\mathrm{MeV}^2)$. The fraction of events with $M^2\,(e) > 10\,000\,\mathrm{MeV}^2$ in the right panel of Fig. 30 (right) gives the probability to misidentify an $e^\pm$ using the $E_{\mathrm{miss}} - P_{\mathrm{miss}}$ method, and is $\sim 3.5\%$.

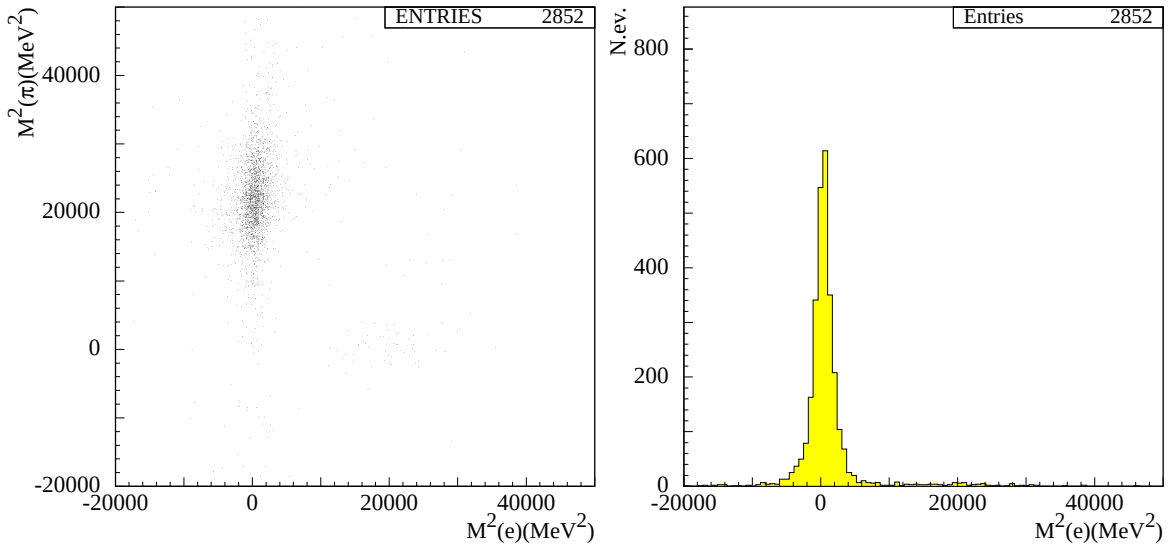


Figure 30: (Left) $M^2$ distribution for "pions" as function of $M^2$ for "electrons," both identified using $E_{\mathrm{miss}} - P_{\mathrm{miss}}$ at the vertex. (Right) X-axis projection of the left plot.

The systematic error is finally estimated. The two methods contribute approximately 50% each to the event selection. The difference in TCA efficiency between pions and electrons is $\sim$6%. This leads to the following error for TCA electron efficiency:

$$\delta\epsilon^{\mathrm{TCA}}_{\mathrm{SYST}}(e) = 0.06\,(0.5 \times 0.03 + 0.5 \times 0.035) = 0.20\%$$

Likewise, the difference in $t_0$ efficiency is 7.5% and this leads to the following uncertainty in the $t_0$ electron efficiency:

$$\delta\epsilon^{\mathrm{T0}}_{\mathrm{SYST}}(e) = 0.075\,(0.5 \times 0.03 + 0.5 \times 0.035) = 0.24\%$$

### 6.3 Time of flight particle id

The probability of satisfying the TOF cuts defined by Eq. (34) is estimated directly using the $K_L \to \pi e \nu$ sample. In figure 31, the distributions of the $D\delta T$ variables are shown. Since this efficiency has to be estimated *given the trigger condition*, two probabilities actually have to be derived from the $K_L \to \pi e \nu$ sample:

1. The probability $\varepsilon_{\mathrm{TOF|S\geq 1}}$ of satisfying the TOF cuts, given one or more trigger sectors fired by the $K_S$ clusters.
2. The probability $\varepsilon_{\mathrm{TOF|S=0}}$, given that no sectors are fired by the $K_S$.

The final result for the TOF efficiency is obtained by weighting these efficiencies with the relative probability for each of the two cases to occur:

$$\varepsilon_{\mathrm{TOF}}\,(\mathrm{data}) = \frac{\varepsilon_{\mathrm{S}}(0)\,\varepsilon_{\mathrm{L}}(\geq 2)\,\varepsilon_{\mathrm{TOF|S=0}} + \varepsilon_{\mathrm{S}}(\geq 1)\,\varepsilon_{\mathrm{TOF|S\geq 1}}}{\varepsilon_{\mathrm{S}}(0)\,\varepsilon_{\mathrm{L}}(\geq 2) + \varepsilon_{\mathrm{S}}(\geq 1)} \tag{80a}$$

$$\boxed{\varepsilon_{\mathrm{TOF}}\,(\mathrm{data}) = (82.0 \pm 0.7_{\mathrm{stat}})\,\%} \tag{80b}$$

The Monte Carlo value is $(83.5 \pm 0.4_{\mathrm{stat}})\,\%$. The discrepancy between data and Monte Carlo is basically due to different resolutions on the $D\delta T$ variables: the standard deviation of the $D\delta T$ distribution is of 440 ps for data and $\sim$ 300 ps for Monte Carlo events.

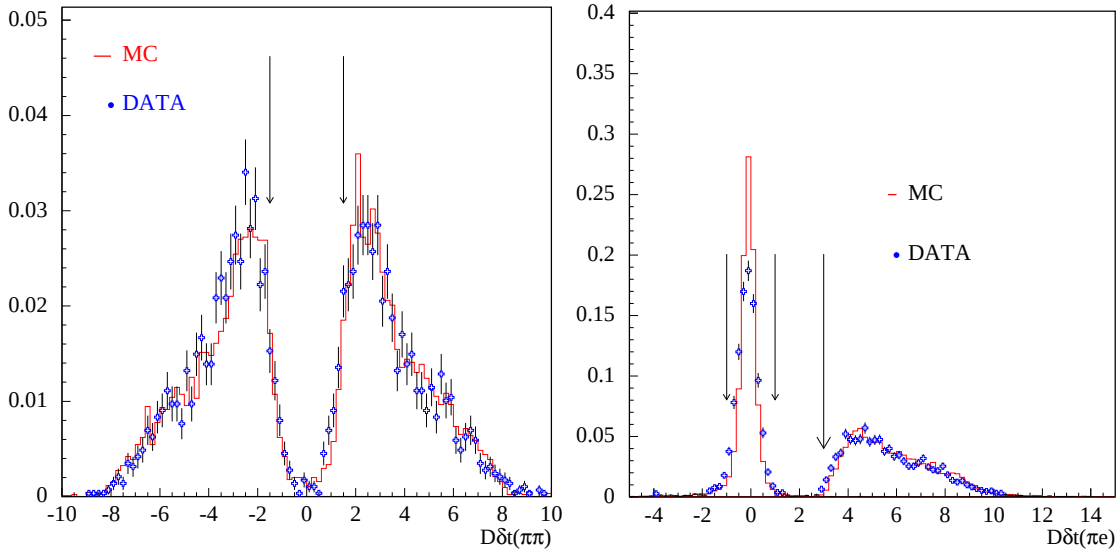


Figure 31: $D\delta t\,(\pi\pi)$ (left panel) and $D\delta t\,(\pi e)$ (right panel) distributions for $K_L \to \pi e\nu$ data and $K_S \to \pi e\nu$ Monte Carlo events. The arrows show the applied cuts, Eqs. (31) and (34).

### 6.4 Tag bias induced by the global $t_0$ estimate

In principle, the $K_L$-crash identification efficiency cancels out in the ratio of the number of selected $K_S \to \pi e\nu$ and $K_S \to \pi^+\pi^-$ events [Eq. (5)]. In practice, since the event $t_0$ is obtained from the $K_S$ [Eq. (17)] and the $K_L$ is recognized by its time of flight [the $\beta^*$ variable of Eq. (18)], there is a small dependence of the $K_L$-crash identification efficiency on the $K_S$ decay mode.

The probability of satisfying the $K_{\rm crash}$ tag depends basically on the difference between the estimated ($t_0^G$) and correct ($t_0^{\rm ref}$) global $t_0$'s,

$$t_0^{\rm ref} - t_0^G\Big|_i = \sum_{n=-n_{\rm max}}^{n_{\rm max}} p_n^i \times nT_{\rm bunch}, \tag{81}$$

where the weight $p_n^i$ stands for the fraction of events with a $t_0$ difference of $n$ units of $T_{\rm bunch}$ for the $i^{\rm th}$ $K_S$ decay channel (one of $K_S \to \pi^+\pi^-$ or $K_S \to \pi e\nu$ decays).

The weights $p_n$ have to be measured for every value of $n$ and for both channels involved in the ratio. In Secs. 6.4.1 and 6.4.2, the methods used to estimate the $p_n$'s for $K_S \to \pi^+\pi^-$ and $K_S \to \pi e\nu$ events are described. The tag efficiency ratio is then calculated as explained in Sec. 6.4.3.

#### *6.4.1 $K_S \to \pi^+\pi^-$ $t_0$ error distribution*

The distribution of weights $p_i^{\pi\pi}$ is obtained using events $K_S$-tagged by means of the identification of $K_L \to \pi^+\pi^-\pi^0$ decays.

The tagging-algorithm requirements are summarized below.

Charged vertices reconstructed in the fiducial volume

$$30\,{\rm cm} \le \sqrt{x^2+y^2} \le 180\,{\rm cm} \ \text{AND} \ |z| \le 130\,{\rm cm}$$

by two oppositely charged tracks are considered. The angle $\alpha$ between the vertex position vector and the $\phi$ nominal momentum $P_\phi$ are used to calculate the $K_L$ momentum $P_L$:

$$aP_L^4 + bP_L^2 + c = 0, \text{ where} \tag{82a}$$

$$a = \gamma^4 \left(1 - \beta^2 \cos^2\alpha\right)^2 \tag{82b}$$

$$b = 2\left[\gamma^2\left(1 + \beta^2\cos^2\alpha\right)\left(\gamma^2\beta^2 M_K^2 - P^{*2}\right) - 2\beta^2\gamma^2 M_K^2\cos^2\alpha\right] \tag{82c}$$

$$c = \left(\beta^2\gamma^2 M_K^2 - P^{*2}\right)^2 \tag{82d}$$

In the above formulae, the $\phi$ velocity ($\beta$) and boost intensity ($\gamma$) are calculated using nominal values of $\mathbf{P}_\phi$ and $\sqrt{s}$; $M_K$ is the kaon mass and $P^*$ is the $K_L$ momentum in the $\phi$ rest frame.

The missing mass, energy, and momentum at the vertex are then calculated using the momentum $\mathbf{p}_i$ of the charged tracks, which are assumed to be pions:

$$E_{\rm miss} = \sqrt{P_{\rm L}^2 + M_K^2} - \sqrt{\mathbf{p}_1^2 + M_\pi^2} - \sqrt{\mathbf{p}_2^2 + M_\pi^2} \tag{83a}$$

$$\mathbf{P}_{\rm miss} = \mathbf{P}_L - \mathbf{p}_1 - \mathbf{p}_2 \tag{83b}$$

$$M_{\rm miss} = \frac{E_{\rm miss}^2 - P_{\rm miss}^2}{\sqrt{|E_{\rm miss}^2 - P_{\rm miss}^2|}} \tag{83c}$$

The selection cuts

$$|M_{\rm miss} - M_{\pi^0}| < 20\,{\rm MeV} \text{ AND } P_{\rm miss} < 90\,{\rm MeV} \tag{84}$$

aim at identifying events with a missing $\pi^0$, and at rejecting the copious background due to vertices uncorrectly reconstructed from split tracks (fake-vertices). Since these vertices have almost back-to-back tracks, the missing momentum is close to the $K_L$ momentum ($\sim 110$ MeV).

Finally, the photons of the $\pi^0 \to \gamma\gamma$ decay are identified. The energy, velocity, and boost intensity of the missing $\pi^0$,

$$\begin{array}{rl} E_{\pi^0} = & \sqrt{P_{\rm miss}^2 + M_{\pi^0}^2} \\ \beta_{\pi^0} = & P_{\rm miss}/E_{\pi^0} \\ \gamma_{\pi^0} = & E_{\pi^0}/M_{\pi^0}, \end{array} \tag{85}$$

are used to calculate the relative emission angle $\phi^*$ in the $\pi^0$ rest frame of each pair of clusters not associated to any track. Only centroid-positions are involved in this calculation. The time difference between the clusters of the pair is also considered:

$$\delta T_{ij} = \left(T_{\rm CL}^i - \frac{\Delta R^i}{c}\right) - \left(T_{\rm CL}^j - \frac{\Delta R^j}{c}\right), \tag{86}$$

where $\Delta R^{i,j}$ are the distances between cluster $i, j$ of the pair and the selected $K_L$-vertex. At least a couple of photon clusters must satisfy:

$$|\delta T_{ij}| < 2\,{\rm ns} \text{ AND } \phi^* > 170^\circ \tag{87}$$

This selection doesn't explicitly use the global-$t_0$ estimate. Nevertheless, some correlation between the selection efficiency and the $t_0$ value could remain, since the times of the DC hits are also reconstructed using a global-$t_0$ value. It has however to be underlined that the selection of the $t_0$ cluster to be used for the hit-time calculation is much looser than that applied to have a $K_{\rm crash}$ tag [Eq. (15)]. The extent of this correlation has however to be checked.

The idea is then to estimate the true global-$t_0$ ($t_0^{\rm ref}$) event by event, using the cluster times $T_{\rm CL}^{i,j}$ of the $K_L$ photons. Hence, after the $K_S \to \pi^+\pi^-$ selection of Sec. 4 has been applied, the difference of $t_0^{\rm ref}$ with respect to the global $t_0$ obtained from $K_S$-cluster times is calculated.

The $t_0$ is calculated from the $i^{\rm th}$ photon cluster time $T_{\rm CL}^i$ through the equation

$$t_0^i = \delta_{\rm cable} - {\rm Nint}\left[\frac{\delta_{\rm cable} - T_{\rm CL}^i + t_{\rm TOF}^i}{T_{\rm bunch}}\right] \times T_{\rm bunch}, \tag{88}$$

where the time of flight $t_{\rm TOF}^i$ is calculated adding $K_L$ and photon times of flight ($\beta_L$ is the $K_L$ velocity):

$$t_{\rm TOF}^i = \frac{R_L}{\beta_L c} + \frac{\Delta R_i}{c} \tag{89}$$

Two other requirements are then imposed:

1. Both $t_0$ estimates have to be equal: $t_0^{i=1} = t_0^{i=2}$. The golden-$t_0$ condition [Eq. (15)] have to be satisfied by at least one of the photon clusters, too.
2. $K_L$ tracks are associated to clusters. In order to avoid biases on the $K_S$ clusters distributions, the calorimeter trigger conditions are required to be satisfied using the trigger sectors fired by the $K_L$-clusters (photons and pions).

The effectiveness of the global $t_0$ estimate obtained from $K_L$ photons can be studied in events selected as $K_S \to \pi^0\pi^0$. In these events, the value $t_0^{00}$ obtained from $K_S$ photons is correct at the $2 \times 10^{-3}$ level, as results from the anlysis of $\sim 10^4$ Monte Carlo events. Hence, at this level, the difference $t_0^i - t_0^{00}$ measures the accuracy of the $K_L$-estimate. The difference turns to be 0 at the same cited level, so that one can conclude from this study that the estimate $t_0^i$ is accurate at the $2 \times 10^{-3}$ level.

Finally, the $K_S \to \pi^+\pi^-$ selection algorithm is applied and $t_0^G$ is calculated using the sample of clusters complementary to the $K_L$-clusters. The cluster with lowest time among those satisfying the golden-$t_0$ condition is used, as in Eq. (17). This time, the time of flight is that of a prompt photon [Eq. (16)].

The difference $\Delta{\rm T0} = t_0^{\rm ref} - t_0^G$ is the desired $t_0$ error distribution of Eq. (81) and is plotted in the left panel of Fig. 32.

*6.4.2 $K_S \to \pi e\nu$ $t_0$ error distribution*

The distribution of weights $p_i^{e\pi}$ is obtained using $K_L \to \pi e\nu$, $K_S \to \pi^+\pi^-$ events. These are selected by means of the cuts illustrated in Sec 5.1 *and of the additional TOF cuts [Eq. (34)].*

In each event, the true global T0 ($t_0^{\rm ref}$) is fixed by using pion clusters from the $K_S \to \pi^+\pi^-$ decay: only events in which the same $t_0$ value is obtained from both $K_S$ pions are considered. This global $t_0$ is subtracted from the $K_L$ cluster times.

In $K_L \to \pi e\nu$ events, the $K_L$ time of flight contributes to the $K_L$-cluster times more than the $K_S$ does in $K_S \to \pi e\nu$ events. In order to correct this discrepancy, in place of the reconstructed $K_L$ vertex, a $K_S$-like vertex is "simulated" along the same flight direction, but at a different distance from the $\phi$ decay point (Fig. 33). This distance is randomly sampled from an exponential distribution with decay length equal to that of the $K_S$, $\lambda = 0.6$ cm. From the simulated $K_S$ vertex, new fictitious tracks are then extrapolated to the calorimeter (dashed curve in the picture) using the track momenta for the $K_L$ (solid curve in the picture). For each track, a new cluster time $T_{\rm CL}^{\rm new}$ is calculated by correcting

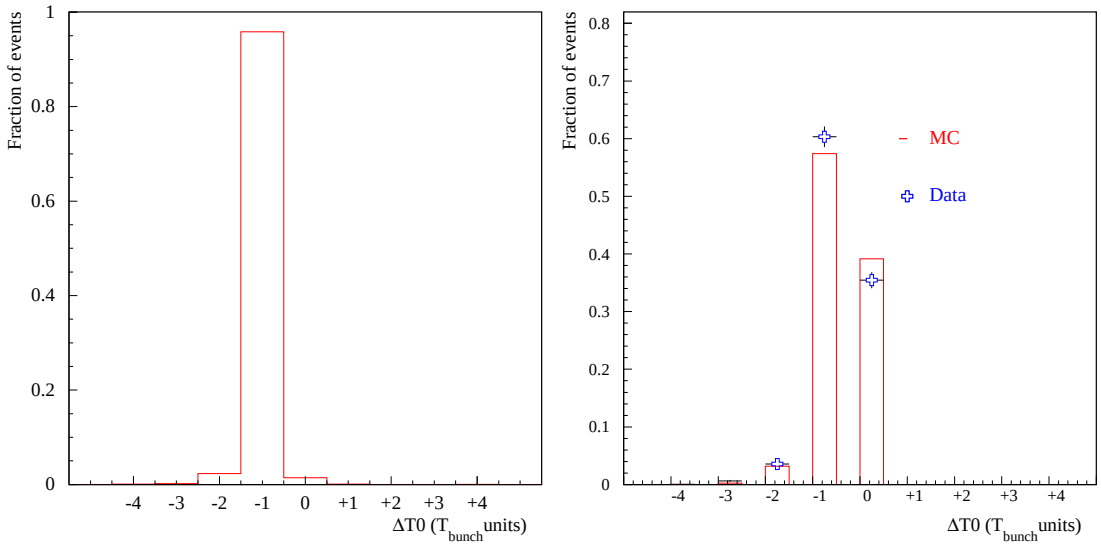


Figure 32: The difference ΔT0 between the correct $t_0$ and that estimated using the fastest cluster as a prompt photon is shown for $K_S \to \pi^+\pi^-$ (left) and $K_S \to \pi e\nu$ (right) events. These are the results of a calculation performed using data samples of $K_S$'s tagged through the identification of $K_L \to \pi^+\pi^-\pi^0$ decays (for the left plot) and $K_{\rm L} \to \pi e\nu$ decays before the DC wall (for the right plot). The distribution obtained in $K_S \to \pi e\nu$ Monte Carlo events is superimposed in the right plot.

the measured cluster time $T_{\rm CL}^{\rm old}$:

$$T_{\rm CL}^{\rm new} = T_{\rm CL}^{\rm old} + \frac{L_{\rm S} - L_{\rm L}}{\beta_{\rm L} \times c} + \frac{L'_{\rm TRK} - L_{\rm TRK}}{\beta \times c} \tag{90}$$

where $L_{\rm L}$ and $L_{\rm TRK}$ are the measured $K_L$ flight path and the length of a real $K_L$ track; $L_{\rm S}$ and $L'_{\rm TRK}$ are the "simulated" $K_S$ path length and the length of the fictitious $K_S$-like track from the simulated $K_S$ vertex to the calorimeter.

A new position for the associated cluster has to be calculated taking into account the new impact point of the track. This is done by considering distance from the old (true) impact point. The distance of the cluster centroid from the old (true) impact point is projected onto three directions: orthogonal to the calorimeter surface, along the fibers, and orthogonal to the fibers and laying on the calorimeter surface. The new cluster position is computed using this projections and starting from the new track impact point. This procedure is very useful especially when the old impact point is on barrel while the new is on the end-cap.

The fastest cluster among those satisfying the $t_0$ requirements is then identified using the corrected times $T_{\rm CL}^{\rm new}$ ($t_0$-cluster).

In Fig. 34 (left and center panels) the estimated pion and electron cluster time distributions are compared with those directly obtained from $K_S \to \pi e\nu$ Monte Carlo events [15]. In Fig. 34 (right panel) the distribution of $T_{\rm CL} - R_{\rm CL}/c$ for the $t_0$-cluster is shown. In both cases, the good agreement indicates the effectiveness of the corrections applied to the $K_L$ cluster times and positions.

[15] In Monte Carlo events, the real $t_0$ is estimated using time of flight of pions from $K_S$, pion and electron, as in data.

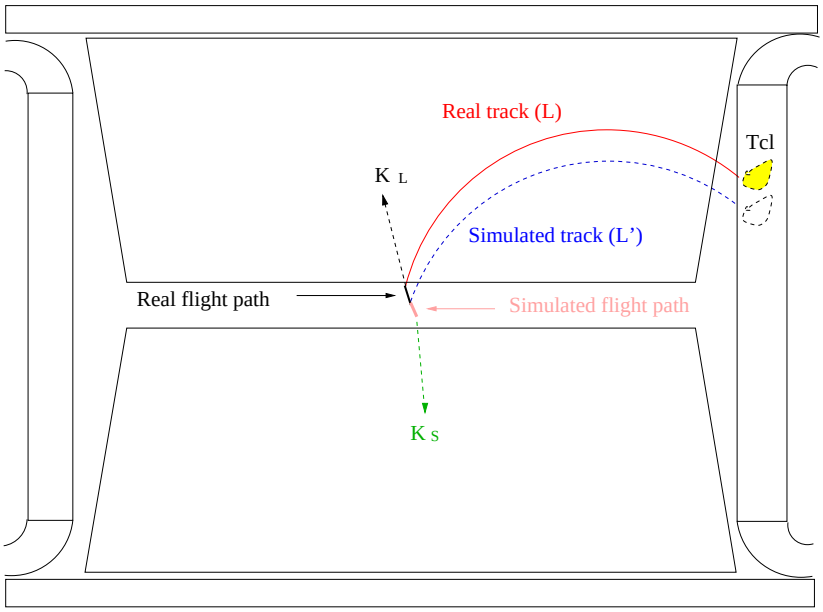


Figure 33: Sketch of the procedure used to simulate $K_S \to \pi e\nu$ cluster times, using an identified $K_L \to \pi e\nu$ event: starting from the $K_L$ reconstructed vertex and the $K_L$ direction estimated from the $K_S \to \pi^+\pi^-$ decay, a $K_S$ path is sampled from an exponential decay distribution. Using the "real" $K_L$ track momentum, a $K_S$ simulated track (dashed curve) is extrapolated to the calorimeter.

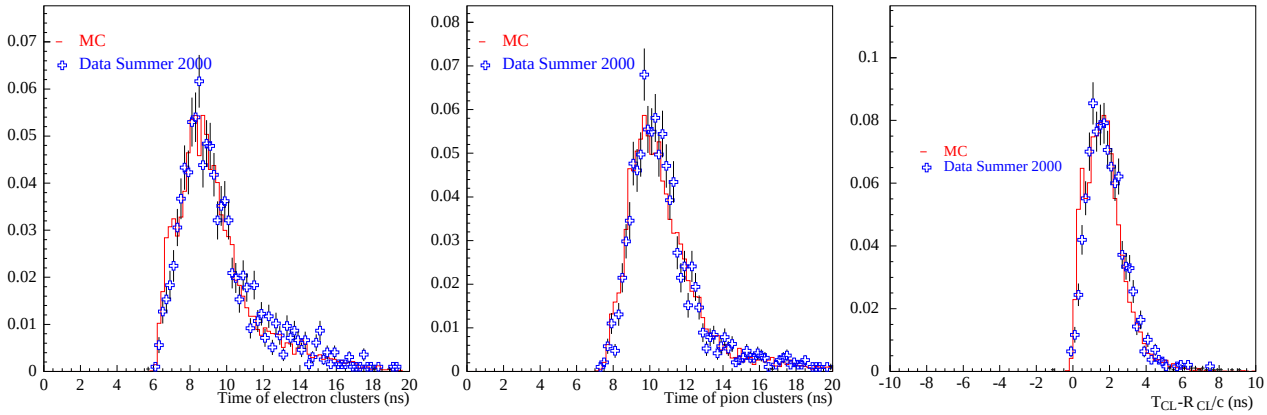


Figure 34: Comparison of the electron (left) and pion (center) cluster time distributions for $K_S \to \pi e\nu$ Monte Carlo (solid line) and $K_L \to \pi e\nu$ data (crosses) events in which the the $K_L$ flight time has been corrected by using [Eq. (90)]. Right panel: distribution of $T_{\rm CL} - R_{\rm CL}/c$ for the $t_0$-cluster.

Finally, the difference between the $t_0$ estimated using a $K_S$-like cluster and the correct one (derived from real $K_S$ pions) is calculated. The result is shown in the right panel of figure 32: it represents the population $\{p\}$ for $K_S \to \pi e\nu$ events. Note that it is significantly different from that obtained from $K_S \to \pi^+\pi^-$ events (left panel). This difference determines the extent of the $R_{\rm tag}$ correction [next section, Eqs. (91) and (94)].

*6.4.3 Tag efficiency ratio*

Finally, having estimated the wheights $p_{\rm n}$ for $K_S \to \pi e\nu$ and $K_S \to \pi^+\pi^-$ events, the tag efficiency $\varepsilon_n$ for the events with a $t_0$-error of $n$ $T_{\rm bunch}$-units has to be calculated for every $n$. It is sufficient to estimate all the $\varepsilon_n$'s *up to a common constant*, since the ratio is computed as:

$$R_{\rm tag} = \frac{\sum_m p_m^{e\pi} \times \varepsilon_m}{\sum_n p_n^{\pi\pi} \times \varepsilon_n} \tag{91}$$

The calculation of the ratio is performed using a $K_S \to \pi^+\pi^-$ sample in which the correct global $t_0$ is fixed by both $K_S$ pion clusters, with a pion-like time of flight:

$$t^{\rm TOF} = \frac{L}{c \cdot \beta_\pi} \tag{92}$$

Then, the $K_{\rm crash}$-search is performed applying an $nT_{\rm bunch}$-shift to all cluster times; let $N_n$ be the number of found events. For each event, the search is repeated varying $n$. The ratio can be calculated as:

$$R_{\rm tag} = \frac{\sum_m p_m^{e\pi} \times N_m}{\sum_n p_n^{\pi\pi} \times N_n} \tag{93}$$

The final result is:

$$\boxed{R_{\rm tag} = 1.023 \pm 0.004_{\rm stat} \pm 0.005_{\rm syst}} \tag{94}$$

The statistical error on this estimate takes into account both the statistical errors on the weights $p_n^i$, and the fluctuations on the number of events $N_n$. The mutual correlation between the $\{N_n\}$ counts, due to the fact that the same event can satisfy the $K_{\rm crash}$-tag for both an $n$ and $m$ $t_0$-shift, is taken into account (see appendix B).

### 6.5 Corrections due to the FILFO-algorithm

The FILFO algorithm [8] is used to recognize and reject Bhabha, machine-background and cosmic-ray events. These tasks are performed using only reconstructed calorimeter information, cell/cluster positions, times and energies; the DC information is used only at the "hit-level" (no space-to-time conversion, nor tracking/vertex fits are used).

The probability that a $K_{\rm crash}$-tagged event identified as $K_S \to \pi^+\pi^-$ or $K_S \to \pi^0\pi^0$ be rejected by the FILFO-algorithm has been estimated using a data sample of FILFO-rejected events and results to be as low as $10^{-4}$. The same study has been repeated using the Monte Carlo simulation, yielding a result compatible within the error. For what concerns the output of the FILFO-algorithm, it is possible to conclude that the Monte Carlo simulation reproduce what is observed in the data at the level of $10^{-4}$.

The probability that a $K_{\rm crash}$-tagged event identified as $K_S \to \pi e\nu$ be rejected by the FILFO-algorithm is less than $10^{-3}$, as directly calculated from the Monte Carlo. The efficiency to survive the FILFO-rejection is then considered the unity for both the signal and the normalization samples.

### 6.6 Corrections due to the cosmic-ray rejection

During the data acquisition, a fast recognition and rejection of the cosmic ray events, which occur with a rate of 2.5 KHz, is provided by the trigger: the presence of two fired "cosmic-sectors" [16] tags a cosmic-ray event [26]. During the data taking of year 2000, a fraction 1/50 of these events have been acquired and reconstructed (downscaled sample).

This veto, however, rejects a small fraction $\rho_{\rm veto}$ of $\phi \to K_S K_L$ events, due essentially to the $K_{\rm crash}$ cluster. Assuming an indicative value of 30 mb for the total cross section of the $K_L$ in the calorimeter, the mean free path is of the order of 10 cm. Hence, the overall calorimeter length corresponds roughly to three interaction lengths. It is then possible that a small fraction of the $K_{\rm crash}$ clusters hits the outermost plane, firing one or two cosmic sectors.

The correction to be applied to the ratio of observed $K_S \to \pi e \nu$ and $K_S \to \pi^+\pi^-$ events is:

$$C_{\rm veto} = \frac{1-\rho_{\rm veto}\left(K_S \to \pi e \nu\right)}{1-\rho_{\rm veto}\left(K_S \to \pi^+\pi^-\right)} \tag{95}$$

The fraction $\rho(K_S \to \pi e \nu)$ of rejected events can be in principle estimated from the downscaled sample, by calculating the fraction $x_{\rm veto}$ of vetoed events among those selected as $K_S \to \pi e \nu$, as follows:

$$\rho_{\rm veto}\left(K_S \to \pi^+\pi^-, K_S \to \pi e \nu\right) = F_{\rm dw} \cdot \frac{x_{\rm veto}}{1+(F_{\rm dw}-1)\cdot x_{\rm veto}}\Bigg|_{K_S \to \pi^+\pi^-, K_S \to \pi e \nu} \tag{96}$$

With a downscaling factor $F_{\rm dw}$ of 50 and a typical $\rho$ value of 5%, the relative statistical accuracy would be worse than 100% (less than 1 vetoed event is expected).[17]

A study performed on the $K_S \to \pi^+\pi^-$ and $K_S \to \pi^0\pi^0$ samples shows that the difference of the $\rho$ inefficiencies between these two channels is small. The correction factor is of $C_{\rm veto}^{\pm/00} = 1.0017 \pm 0.0025$, thus confirming that the cosmic-ray veto inefficieny is dominated by the contribution of the $K_L$ interactions, common to both $K_S$ channels.

A difference of $C$ from unity could arise from different average multiplicities of $K_S$ clusters. In the case considered, these multiplicities are two and four, respectively. For this analysis, signal and normalization samples give instead the same average multiplicity of $K_S$ clusters, so the correction is expected to be even closer to the unity. The correction factor is then assumed to be:

$$\boxed{C_{\rm veto} = 1 \pm 0.0025_{\rm stat}} \tag{97}$$

where the statistical error is actually that obtained in the estimate of $C_{\rm veto}^{\pm/00}$.

## 7 Results and conclusions

In this section, the results of the analysis are summarized. In order to check its stability, the measurement of $BR\left(K_S \to \pi e \nu\right)$ has been performed for each of the four subsamples of table 1. $BR(K_S \to \pi e \nu)$ is obtained from the ratio of the number of signal

[16] A cosmic sector uses calorimeter signals from the outermost EmC plane, from both EmC sides. An effective threshold of $\sim 30$ MeV is applied, equal to the average deposit of a minimum ionizing particle.

[17] A possible technique similar to "method 2" could be implemented, in order to safely estimate the correction and the systematic error. The cosmic-sector probabilities would have to be extracted from the real data, for the single particles: pion, electron, and $K_{\rm crash}$ clusters. The Monte Carlo would then provide the kinematical correlation used to calculate the average probability of veto.

and $K_S \to \pi^+\pi^-$ events, correcting for the total selection efficiencies, and for the ratios of tagging efficiencies and of cosmic-ray veto inefficiencies.

$$\mathrm{BR}(\mathrm{K_S} \to \pi\mathrm{e}\nu) = \frac{N^{\pi e\nu}}{N^{\pi\pi}} \times \frac{\varepsilon^{\pi\pi}_{\mathrm{tot}}}{\varepsilon^{\pi e\nu}_{\mathrm{tot}}} \times \frac{1}{R_{\mathrm{tag}}} \times \frac{1}{C_{\mathrm{veto}}} \times \mathrm{BR}(\mathrm{K_S} \to \pi^+\pi^-) \tag{98}$$

The total selection efficiency for the signal is:

$$\boxed{\varepsilon^{\pi e\nu}_{\mathrm{tot}} = (20.77 \pm 0.24_{\mathrm{stat}} \pm 0.34_{\mathrm{syst}})\,\%} \tag{99}$$

The present experimental value for $BR(K_S \to \pi^+\pi^-)$ is used [2]:

$$\boxed{\mathrm{BR}(\mathrm{K_S} \to \pi^+\pi^-) = (86.61 \pm 0.28)\,\%} \tag{100}$$

The number of signal and $K_S \to \pi^+\pi^-$ observed events, the efficiency for the selection of $K_S \to \pi^+\pi^-$ events, and the measurement of the $K_S \to \pi e\nu$ branching ratio are listed in table 5, for the four periods of year 2000 defined in table 3. Only the statistical errors are shown in the table. The measurements are stable within the errors.

| Running period | $N^{\pi e\nu}$ | $N^{\pi\pi}$ | $\varepsilon^{\pi\pi}_{\mathrm{tot}}$ [units %] | $\mathrm{BR}(\mathrm{K_S} \to \pi\mathrm{e}\nu)$ (units $10^{-4}$) |
|---|---|---|---|---|
| 15/07 → 05/08 | $113 \pm 12$ | 263 158 | $56.4 \pm 0.4_{\mathrm{tot}}$ | $7.84 \pm 0.80_{\mathrm{stat}}$ |
| 30/10 → 15/11 | $242 \pm 17$ | 609 737 | $56.1 \pm 0.4_{\mathrm{tot}}$ | $7.17 \pm 0.52_{\mathrm{stat}}$ |
| 15/11 → 24/11 | $133 \pm 13$ | 382 237 | $56.2 \pm 0.4_{\mathrm{tot}}$ | $6.32 \pm 0.62_{\mathrm{stat}}$ |
| 24/11 → 06/12 | $151 \pm 13$ | 381 472 | $56.2 \pm 0.4_{\mathrm{tot}}$ | $7.15 \pm 0.64_{\mathrm{stat}}$ |
| Weighted average | | | | $7.06 \pm 0.31_{\mathrm{stat}}$ |

Table 5: Summary of the results for the measurement of the $K_S \to \pi e\nu$ branching ratio.

The measurement is finally obtained considering the whole Year 2000 data set. Let $N^{\pi\pi}_i$ and $\varepsilon^{\pi\pi}_i$ be the number of $K_S \to \pi^+\pi^-$ selected events and the efficiency for the $i^{\mathrm{th}}$ sample of year 2000. The following formula is used to estimate the branching ratio:

$$\mathrm{BR}(\mathrm{K_S} \to \pi\mathrm{e}\nu) = \frac{N^{\pi e\nu}_{\mathrm{tot}}}{\varepsilon^{\pi e\nu}_{\mathrm{tot}}} \times \frac{1}{\sum_i N^{\pi\pi}_i/\varepsilon^{\pi\pi}_i} \times \frac{1}{R_{\mathrm{tag}}} \times \frac{1}{C_{\mathrm{veto}}} \times \mathrm{BR}(\mathrm{K_S} \to \pi^+\pi^-) \tag{101}$$

where $N^{\pi e\nu}$ is the total number of $K_S \to \pi e\nu$ events counted in the whole data set:

$$\boxed{N^{\pi e\nu}_{\mathrm{tot}} = 624 \pm 30} \tag{102}$$

The result is:

$$\boxed{\mathrm{BR}(\mathrm{K_S} \to \pi\mathrm{e}\nu) \times 10^4 = (6.91 \pm 0.34_{\mathrm{stat}} \pm 0.15_{\mathrm{syst}}) = 6.91 \times (1 \pm 0.049_{\mathrm{stat}} \pm 0.022_{\mathrm{syst}})} \tag{103}$$

The different contibutions to the total error are disentangled in table 6.

| Source | Fractional error $[10^{-2}]$-units |
|---|---|
| **Statistics of $\mathbf{K_S} \to \pi \mathbf{e} \nu$** | **4.86** |
| Statistics of $K_S \to \pi^+\pi^-$ | 0.08 |
| $K_S \to \pi e \nu$ selection | |
| Tracking efficiency | 1.0 |
| Vertex reconstruction efficiency | 1.1 |
| DC preselection efficiency (MC stat) | 0.5 |
| Extrapolation to EmC (MC stat) | 0.4 |
| Track categories | 0.3 |
| TCA, $t_0$, and Trigger | 0.7 |
| Time of flight cuts | 0.9 |
| $K_S \to \pi^+\pi^-$ selection | |
| Fiducial cuts | 0.2 |
| Tracking | 0.2 |
| $t_0$ and Trigger | 0.3 |
| Ratio of tagging efficiencies | 0.7 |
| Ratio of cosmic veto inefficiencies | 0.3 |
| BR($\mathrm{K_S} \to \pi^+\pi^-$) | 0.4 |
| **Total relative error** | **5.3** |

Table 6: Contributions to the fractional error on $BR(K_S \to \pi e \nu)$.

# 8 Acknowledgments

We want to warmly acknowledge (just to make something different we itemize again):

- First of all, our partners in the semileptonic group: Carlo Forti, Giuseppe Finocchiaro, and Marco Incagli;
- Paolo Valente and Matteo Palutan for overlapping reasons. Moreover, the Method 2 is deeply in debt with them (especially for the spataro.f, debbuged and compiled in static mode by Paolo)
- Cesare Bini, Marco Incagli (again), for a careful reading of this memo
- Antonella Antonelli, for the figure (and kumac) with the error on real part of $x$
- Last, but actually should be FIRST, Fabio Bossi for a tremendous reading of a poorly preliminar version of this funny memo :-)

# A Explicit calculation of $\Gamma\left(K_S \to \pi e \nu\right) / \Gamma\left(K_L \to \pi e \nu\right)$

If the CPT symmetry is not assumed, two mixing parameters are needed to describe the mass eigenstates of the $K^0$-$\overline{K}^0$ system:

$$|K_{S,L}\rangle = \frac{\left(1+\epsilon_{\mathrm{S,L}}\right)|K^0\rangle \pm \left(1-\epsilon_{\mathrm{S,L}}\right)\left|\overline{K}^0\right\rangle}{\sqrt{2\left(1+\left|\epsilon_{\mathrm{S,L}}\right|^2\right)}}\ , \tag{104}$$

The mixing parameters $\epsilon_{\mathrm{S,L}}$ are related to the elements of the mass and width matrices $M$ and $\Gamma$. Their difference $\Delta$ describes the CPT-violation in the mass matrix:

$$\epsilon_{\mathrm{S,L}} = \epsilon_{\mathrm{M}} \pm \frac{\Delta}{2} \tag{105a}$$

$$\Delta = \frac{1}{2}\frac{M_{11} - M_{22} - \frac{i}{2}\left(\Gamma_{11} - \Gamma_{22}\right)}{\mathrm{Re}M_{12} + \frac{i}{2}\mathrm{Re}\Gamma_{12}} \tag{105b}$$

Four independent matrix elements describe the semileptonic decay amplitudes of $K^0$ and $\overline{K}^0$. These are usually written as:

$$_{\mathrm{out}}\left\langle \pi^- e^+ \nu_e \right| \hat{H}_{\mathrm{weak}} \left|K^0\right\rangle \equiv a + b \tag{106a}$$

$$_{\mathrm{out}}\left\langle \pi^+ e^- \overline{\nu}_e \right| \hat{H}_{\mathrm{weak}} \left|\overline{K}^0\right\rangle \equiv a^* - b^* \tag{106b}$$

$$_{\mathrm{out}}\left\langle \pi^+ e^- \overline{\nu}_e \right| \hat{H}_{\mathrm{weak}} \left|K^0\right\rangle \equiv c + d \tag{106c}$$

$$_{\mathrm{out}}\left\langle \pi^- e^+ \nu_e \right| \hat{H}_{\mathrm{weak}} \left|\overline{K}^0\right\rangle \equiv c^* - d^* \tag{106d}$$

The transitions in Eqs. (106a) and (106b) are allowed by the $\Delta S = \Delta Q$ rule, while the remaining two, with $\Delta S = -\Delta Q$, are suppressed. The amplitudes $c$ and $d$ are expected to be of fourth order in the weak coupling. The CPT symmetry requires the amplitudes $b$ and $d$ to vanish.

The squared amplitude $\Gamma_{\mathrm{S}}^+$ ($\Gamma_{\mathrm{S}}^-$) for the transition $K_S \to \pi^- e^+ \nu_e$ ($K_S \to \pi^+ e^- \overline{\nu}_e$) is obtained from Eqs. (104) and (106a)–(106d):

$$\Gamma_{\mathrm{S}}^+ = \left| \frac{a + b + c^* + d^* + \epsilon_{\mathrm{S}}\left(a + b - c^* + d^*\right)}{\sqrt{1+\left|\epsilon_{\mathrm{S}}\right|^2}} \right|^2 \tag{107a}$$

$$\Gamma_{\rm S}^{-} = \left| \frac{a^* - b^* + c + d + \epsilon_{\rm S}\left(-a^* - b^* + c + d\right)}{\sqrt{1+\left|\epsilon_{\rm S}\right|^2}} \right|^2 \tag{107b}$$

Adding both charge states, one obtains:

$$\begin{aligned}\frac{\Gamma_{\rm S}^{+} + \Gamma_{\rm S}^{-}}{2\left|a\right|^2} =& 1 + 2{\rm Re}\left(\frac{c^*}{a} - \frac{b^*}{a}\frac{d^*}{a^*}\right)\frac{1-\left|\epsilon_{\rm S}\right|^2}{1+\left|\epsilon_{\rm S}\right|^2} \\ &+ 4{\rm Re}\left(\epsilon_{\rm S}\right){\rm Re}\left(\frac{b^*}{a} + \frac{d^*}{a}\frac{c}{a^*}\right) \\ &- 4{\rm Im}\left(\epsilon_{\rm S}\right){\rm Im}\left(\frac{c}{a^*} - \frac{d}{a^*}\frac{b}{a}\right) \\ &+ \left|\frac{b}{a}\right|^2 + \left|\frac{c}{a}\right|^2 + \left|\frac{d}{a}\right|^2\end{aligned}$$

The analogous expression for the $K_L$ transitions can be obtained with the replacements: $\epsilon_{\rm S} \to \epsilon_{\rm L}$, $c \to -c$, and $d \to -d$. Terms of the second order in the quantities $b/a$, $c/a$, $d/a$, $\varepsilon_{\rm S,L}$, and $\Delta$ can be safely neglected [see below, Eqs. (111)], thus yielding:

$$\frac{\Gamma_{\rm S}^{+} + \Gamma_{\rm S}^{-}}{\Gamma_{\rm L}^{+} + \Gamma_{\rm L}^{-}} = 1 + 4{\rm Re}\left(\frac{c^*}{a}\right) \tag{108}$$

The following definitions are usually made:

$$x = \frac{A\left(\overline{K}^0 \to \pi^- e^+ \nu_e\right)}{A\left(K^0 \to \pi^- e^+ \nu_e\right)} = \frac{c^* - d^*}{a + b} \tag{109a}$$

$$\bar{x} = \frac{A\left(\overline{K}^0 \to \pi^+ e^- \overline{\nu}_e\right)}{A\left(\overline{K}^0 \to \pi^+ e^- \overline{\nu}_e\right)} = \frac{c^* + d^*}{a - b} \tag{109b}$$

$$y = -\frac{b}{a} \tag{109c}$$

The $x$ ($\bar{x}$) parameter represents a violation of the $\Delta S = \Delta Q$ rule in the decay to positive (negative) leptons, while $y$ represents a CPT violation in a $\Delta S = \Delta Q$ decay. The following combinations are also defined:

$$x_+ = \frac{x + \bar{x}}{2} = \frac{\frac{c^*}{a} - y\frac{d^*}{a}}{1+y^2} \sim \frac{c^*}{a} \tag{110a}$$

$$x_- = \frac{x - \bar{x}}{2} = \frac{\frac{c^*}{a}y - \frac{d^*}{a}}{1+y^2} \sim -\frac{d^*}{a}, \tag{110b}$$

The approximated equalities follow by neglecting second order violation terms and allow the interpretation of $x_+$ ($x_-$) as a $\Delta S = \Delta Q$-violation parameter in a CPT conserving (violating) decay. One can then conclude that the ratio of $K_S$ and $K_L$ semileptonic decay partial widths is a measurement of ${\rm Re}(x_+)$ (or, assuming the $CPT$ symmetry in the $\Delta S = \Delta Q$-violating amplitude, of ${\rm Re}(x)$).

The following parameters have been measured by the CPLEAR experiment studying the semileptonic decay time distribution of strangness-tagged $K^0$ and $\overline{K}^0$ beams. Neglecting second order terms, they obtain [27]:

$$\begin{array}{c} \mathrm{Im}\,(x_+) = (-2.0 \pm 2.7) \times 10^{-3} \\ \mathrm{Re}\,(x_-) = (-0.5 \pm 3.0) \times 10^{-3} \\ 2\mathrm{Re}\,(\Delta) = (2.4 \pm 2.8) \times 10^{-4} \\ 2\mathrm{Im}\,(\Delta) = (2.4 \pm 5.0) \times 10^{-5} \\ \mathrm{Re}\,(\epsilon_{\mathrm{M}}) = (1.649 \pm 0.025) \times 10^{-3} \\ \mathrm{Re}\,(y) = (0.3 \pm 3.1) \times 10^{-3} \end{array} \tag{111}$$

Besides, **neglecting linear terms in $d/a$ with respect to those in $c^*/a$** and second order terms, the following measurement is also obtained [3]:

$$\mathrm{Re}\,(x_+) = (-1.8 \pm 4.1_{\mathrm{stat}} \pm 4.5_{\mathrm{syst}}) \times 10^{-3} \tag{112}$$

# B Error on the $t_0$-bias estimate

The ratio of tagging efficiency for $K_S \to \pi e \nu$ vs $K_S \to \pi^+\pi^-$ decays has been estimated by calculating

$$R_{\mathrm{tag}}^{\mathrm{ke3}/\pm} = \frac{\sum_n p_n^{e\pi} \times N_n}{\sum_m p_m^{\pi\pi} \times N_m} = \frac{\langle p^{e\pi} \rangle}{\langle p^{\pi\pi} \rangle} \tag{113}$$

where $N_n$ is the number of $K_S \to \pi^+\pi^-$ events in which the $K_{\mathrm{crash}}$-tag is satisfied being the pion-like $t_0$ shifted by $n \times T_{\mathrm{bunch}}$ units. Since the same event is repeatedly shifted for all the possible values of $n$, the $\{N_n\}$ are all statistically dependent one each other. Each event can be described as a sequence of digits

$$q\,(\mathrm{Event}) = (\mathrm{d}_1, \mathrm{d}_2, \ldots \mathrm{d}_{\mathrm{m}}) \tag{114}$$

where $d_{\mathrm{i}} = 0/1$ if the $K_{\mathrm{crash}}$ tag is/isn't satisfied, applying a shift of $\mathrm{i} \times T_{\mathrm{bunch}}$-units to the pion-like $t_0$. In place of summing over the events, it is also possible to sum over the event-configurations:

$$N_n = \sum_{\{q\}} f_n(q) F(q) \tag{115a}$$

$$R_{\mathrm{tag}}^{\mathrm{ke3}/\pm} = \frac{\sum_n \sum_{\{q\}} p_n^{e\pi} \times f_n(q) F(q)}{\sum_m \sum_{\{q\}} p_m^{\pi\pi} \times f_m(q) F(q)} \tag{115b}$$

where $\{q\}$ stands for all the possible configurations, $F(q)$ is the number of events with a configuration $q$, and $f_n(q) = 0/1$ if in the combination $q$ the $K_{\mathrm{crash}}$ tag isn't/is obtained shifting by $n$-units (it is a projector). The countings $F(q)$ are statistically independent, so it is possible to calculate the error as:

$$\delta R_{\mathrm{stat}} = \sqrt{\sum_{\{q\}} \left( \frac{\mathrm{d}R}{\mathrm{d}F(q)} \right)^2 \sigma_{F(q)}^2} \tag{116a}$$

$$\frac{\mathrm{d}R}{\mathrm{d}F(q)} = \sum_n \frac{(p_n^{e\pi} - p_n^{\pi\pi} R_{\mathrm{tag}}) \times f_n(q)}{\sum_m p_m^{\pi\pi} \times N_m} \tag{116b}$$

From the equality $\sigma^2_{F(q)} = F(q)$, and using Eqs. (115a) and (113), the error can be written as a linear sum over the events, as follows:

$$\delta R^2_{\text{stat}} = \sum_{\text{evt}} \left\{ \left( \frac{\sum_n p_n^{e\pi} f_n(q)}{\langle p^{e\pi} \rangle} \right)^2 + \left( \frac{\langle p^{e\pi} \rangle \sum_n p^{\pi\pi} f_n(q)}{\langle p^{\pi\pi} \rangle^2} \right)^2 - \right. \\ \left. -2 \frac{\langle p^{e\pi} \rangle}{\langle p^{\pi\pi} \rangle^3} \left[ \sum_n p_n^{e\pi} f_n(q) \right] \left[ \sum_n p_n^{\pi\pi} f_n(q) \right] \right\}, \tag{117}$$

where $f_n(q)$ is determined event by event.

## References


[1] G. D'ambrosio, G. Isidori and A. Pugliese, *The second DAΦNE physics handbook*, **Volume I:63-95**, 1995.

[2] 2001 web update of the Particle Listing, http://pdg.lbl.gov

[3] A. Angelopoulos et al., *Phys. Lett.* **B 444:38-42**, 1998.

[4] R. Akhmetshin et al., *Phys. Lett.* **B 456:90-94**, 1999.

[5] G. Cabibbo and T. Spadaro, *Klcrash tag related studies*, KLOE **memo 210** (2000).

[6] G. Cabibbo and T. Spadaro, *Klcrash tag efficiency studies*, KLOE **memo 224** (2000).

[7] A. Aloisio, *et al.* (the KLOE collaboration), *The KLOE Trigger System. Addendum to the KLOE Technical Proposal.*, LNF Report **(LNF-96/043)**.

[8] C. Bini et al., *Rejection of cosmic rays and* Bhabha *background with the electromagnetic calorimeter*, KLOE **memo 126** (1997); B. Golosio et al., *Rejection of machine background in the KLOE experiment*, KLOE **memo (172)** (1998); G. Finocchiaro and A. Menicucci, *Cosmic rays rejection in KLOE*, KLOE **memo 203** (1999).

[9] M. Palutan, T. Spadaro and P. Valente *Measurement of* $\Gamma(K_S \to \pi^+\pi^-)/\Gamma(K_S \to \pi^0\pi^0)$ *with KLOE 2000 data*, KLOE **memo 253** (2001).

[10] F. Ambrosino *et al.*, *Current status of the track reconstruction using the KLOE drift chamber*, KLOE **memo 177** (1999); A. Antonelli *et al.*, *Short description of the track reconstruction with the KLOE drift chamber*, KLOE **memo 194** (1999).

[11] M. Adinolfi *et al.*, *The KLOE Electromagnetic Calorimeter*, **LNF-01/017 (P)** (2001); C. Bini *et al.*, *Reconstruction of time and position in the KLOE calorimeter*, KLOE **memo 205** (2000).

[12] G. Pirozzi *et al.*, *The Event Classification procedures*, KLOE **memo 225** (2000).

[13] S. Di Falco, *The K Long tagging algorithm*, KLOE **memo 173** (1998).

[14] G. Pirozzi *et al.*, *Current version of the* $K_S \to \pi^0\pi^0$ *ECL filter*, KLOE **memo 220** (2000).

[15] C. Bini and P. Gauzzi, *Event classification of non-K phi decays*, KLOE **memo 171** (1998).

[16] G. Finocchiaro, C. Forti and A. Menicucci, *Ks semileptonic tag*, KLOE **memo 239** (2001).

[17] G. Finocchiaro et al., *First observation of the* $K_S \to \pi e \nu$ *decay in KLOE*, KLOE **memo 240** (2001).

[18] C. Gatti and T. Spadaro, *Offline TCA library*, KLOE memo in preparation.

[19] M.Antonelli, *et al.*, *The Track to Cluster association program*, KLOE **memo 129** (1996).

[20] F. Ambrosino et al., *Details of the track fit procedure using the drift chamber of the KLOE experiment*, KLOE **memo 141** (1999).

[21] R. J. Barlow and C. Beeston, Fitting using finite monte carlo samples, *Comput. Phys. Commun.* **77**, 219–228 (1993).
[22] S. Miscetti and T. Spadaro *Photon detection efficiency*, KLOE memo in preparation.
[23] M. Incagli *et al.*, *The Event Classification procedures*, KLOE **memo 225** (2000).
[24] R.R. Akhmetshin *et al.*, *Phys.Lett.* **B415 445**, 2000.
[25] F. Bossi, G. Cabibbo and M. Palutan, *Trigger efficiency determination on $K_S$ decays*, KLOE **memo 223** (2000).
[26] M. Palutan, CP *Violation Study at DAFNE: the Trigger of the KLOE Experiment.* PhD thesis, Università degli Studi di Roma Tor Vergata, 1999.
[27] A. Apostolakis et al., *Phys. Lett.* **B 456:297-303**, 1999.